UNIVERSIDADE DE LISBOA
FACULDADE DE CIÊNCIAS
DEPARTAMENTO DE QUÍMICA E BIOQUÍMICA

STUDIES ON CYTOTOXIC ACTIVITY OF ORGANOMETALLIC COMPLEXES OF Mo(II) WITH α-DIIMINES

Soraia Raquel Maciel Martins

Dissertação
Mestrado em Bioquímica
Área de especialização em Bioquímica
2012

UNIVERSIDADE DE LISBOA
FACULDADE DE CIÊNCIAS
DEPARTAMENTO DE QUÍMICA E BIOQUÍMICA

STUDIES ON CYTOTOXIC ACTIVITY OF ORGANOMETALLIC COMPLEXES OF Mo(II) WITH α-DIIMINES

Soraia Raquel Maciel Martins

Dissertação orientada por:
Prof. Doutora Margarida Meireles
Prof. Doutora Maria José Calhorda

Dissertação
Mestrado em Bioquímica
Área de especialização em Bioquímica
2012

ABSTRACT

Five molybdenum(II) complexes, [MoBr(η^3-C_3H_5)$(CO)_2${1,4-(4-**X**)phenyl-2,3-naphthalenediazabutadiene}], X = H (**C1**), Me (**C2**), OMe (**C3**), Cl (**C4**) and COOH (**C5**), were synthesized and characterized by FTIR and ^{1}H NMR spectroscopy. Their redox properties were studied by cyclic voltammetry and strong oxidation waves and less intense reduction waves were observed in the cyclic voltammograms. The difference between the oxidation and reduction potentials ($\Delta E = E_p^{ox} - E_p^{red} > 0.059$) indicated irreversible processes, namely Mo(II) to Mo(III) oxidations and reductions occurring at the ligand. The cytotoxic activity of **C1 – C5** was studied *in vitro* against several cancer cell lines (HeLa, MCF-7, MDA-MB-231, SW480 and Caco-2), using a colorimetric assay, MTT (3-(4,5-dimethyl-thiazol-2-yl)-2,5-diphenyltetrazolium bromide). All the complexes display a powerful cytotoxic activity *in vitro* against HeLa (with IC_{50} values ranging from 3.2 to 27.1 μM) and a smaller antitumoral effect against MDA-MB-231 and Caco-2 cells (IC_{50} > 100 μM). **C3** is the most cytotoxic complex, with lowest IC_{50}, while **C5** has the highest IC_{50} value, in all cell lines tested. The interaction of these molybdenum(II) complexes with CT DNA was studied, using absorption titration spectroscopy, in order to elucidate their mechanism of action. The absorption spectra of **C1 – C5** showed a decrease in the intensity of the absorbance (hypochromism), accompanied by a small red-shift (batochromism) with increasing CT DNA concentration, which indicates an interaction of the complexes with CT DNA. The intrinsic binding constant values (K_b) show that **C3** and **C5** bind strongly to the CT DNA (K_b = 4.47 x 10^4 M^{-1} and 6.53 x 10^4 M^{-1}, respectively) and **C2** has the weakest interaction with CT DNA (K_b = 2.11 x 10^4 M^{-1}). These results support the capability of these molybdenum(II) complexes for potential application in chemotherapy.

Keywords: molybdenum, cancer, cytotoxic activity, interaction with DNA, chemotherapy

RESUMO

De acordo com a Organização Mundial de Saúde (OMS), milhões de pessoas vivem com o diagnóstico de cancro e esta é uma das doenças que causa mais mortes, a nível mundial (cerca de 8 milhões de mortes por ano). Se esta tendência não for invertida, estima-se que em 2030, 12 milhões de pessoas morram devido ao cancro. A investigação nesta área tão importante é, inquestionavelmente, necessária. Foram identificados mais de 200 tipos diferentes de cancro, todos caracterizados pelo crescimento e proliferação descontrolados de células anormais. Atualmente, a quimioterapia, radioterapia e cirurgia são os principais tipos de tratamento do cancro, sendo a quimioterapia a opção mais comum e com mais resultados favoráveis. Os fármacos usados na quimioterapia possuem, cada vez mais, alvos biológicos específicos, como proteínas e enzimas ou o DNA de células cancerígenas, tentando não afetar as células normais e saudáveis.

Na segunda metade do século XX, houve um grande avanço na história da quimioterapia com a descoberta da cisplatina que, ainda hoje em dia, juntamente com os seus análogos são os fármacos mais utilizados no tratamento de tumores sólidos, devido à sua elevada eficácia. No entanto, estes compostos de platina apresentam diversas limitações, nomeadamente resistência das células tumorais aos compostos e elevada toxicidade destes. Contudo, a descoberta da cisplatina levou à investigação da atividade anti-tumoral de outros compostos com centros metálicos, como o molibdénio, ruténio, ouro, ferro, entre outros. Foram feitos vários estudos citotóxicos com compostos contendo molibdénio, tendo sido comprovadas as suas propriedades anti-tumorais. No entanto, o seu mecanismo de ação encontra-se ainda por esclarecer.

Este trabalho teve como objetivo o estudo das propriedades anti-tumorais de cinco complexos organometálicos de molibdénio(II), [Mo(η^3-C_3H_5)Br$(CO)_2${1,4-**X**-fenil-2,3-naftalenodiazobutadieno}], com X = H (**C1**), Me (**C2**), OMe (**C3**), Cl (**C4**) e COOH (**C5**) (**Figura 1**). Estes complexos foram sintetizados por reação do precursor de molibdénio(II) [Mo(η^3-C_3H_5)Br$(CO)_2$(MeCN)] (**P0**) com diferentes ligandos bidentados azotados da família das α-diiminas (**L1 – L5**) e foram caracterizados por FTIR e ^{1}H NMR.

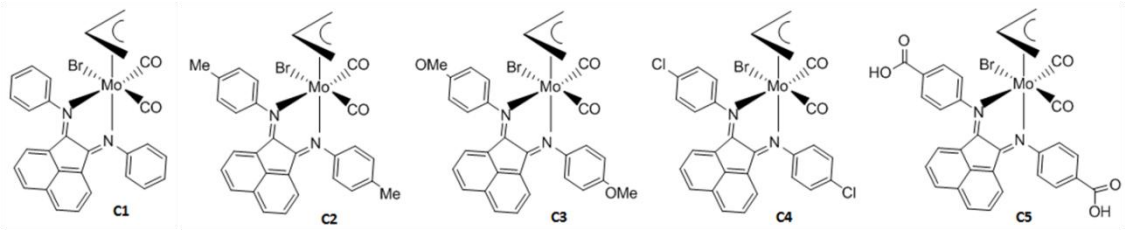

Figura 1 – Estrutura dos complexos organometálicos [Mo(η^3-C_3H_5)Br(CO)$_2${1,4-**X**-fenil-2,3-naftalenodiazobutadieno}] com X = H (**C1**), Me (**C2**), OMe (**C3**), Cl (**C4**) e COOH (**C5**).

Realizaram-se ensaios de voltametria cíclica para estudar as propriedades de oxidação/redução dos complexos **C1 – C5**. Nos voltamogramas cíclicos obtidos para cada complexo, foram observadas ondas de oxidação de maior intensidade e uma onda de redução de menor intensidade. As oxidações estão associadas ao processo de oxidação de Mo(II) a Mo(III) e as reduções ocorrem no ligando, de acordo com a composição das HOMOs e LUMOs dos complexos calculadas por DFT (do inglês, *Density Functional Teory*). Os complexos apresentam em geral um comportamento de oxidação irreversível, comprovado pela diferença (ΔE) de potencial de oxidação (E_p^{ox}) e potencial de redução (E_p^{red}), $\Delta E = E_p^{ox} - E_p^{red} > 0.059$.

Realizaram-se estudos de citotoxicidade destes compostos em diversas linhas celulares tumorais humanas: HeLa (células endoteliais do cancro do colo do útero), MCF-7 e MDA (células epiteliais do cancro da mama), SW480 e Caco-2 (células epiteliais do cancro do cólon) utilizando o ensaio de viabilidade celular MTT (brometo de 3-(4,5-dimetiltiazol-2-il)-2,5-difeniltetrazólio). Os resultados de IC_{50} obtidos (concentração necessária para inibir metade do crescimento celular) mostram que estes complexos têm uma elevada atividade citotóxica *in vitro* nas linhas tumorais estudadas, com valores de IC_{50} a variar entre 3,2 e 27,1 µM em células HeLa. Nas células SW480 obtiveram-se valores de IC_{50} entre 0,6 e 50 µM e para as células MCF-7, IC_{50} a variar entre 25 e 98,4 µM. Observou-se uma possível resistência das linhas celulares MDA-MB-231 e Caco-2 células aos compostos, traduzido por um menor efeito anti-tumoral, e refletido em valores de IC_{50} maiores que 100 µM. O complexo **C3** é o mais citotóxico, uma vez que apresenta o menor valor de IC_{50}, dos cinco compostos, em todas as linhas celulares estudadas. Por outro lado, o complexo **C5** é o que tem o maior valor de IC_{50} em todas as linhas celulares testadas, sendo o que tem um efeito anti-tumoral mais baixo.

Uma vez que a maioria dos complexos organometálicos têm como alvo o DNA das células tumorais, foram feitos ensaios de titulação de *calf thymus* DNA (CT DNA) usando espectrofotometria de UV-Vis para detetar a interação destes complexos de molibdénio(II) com o DNA, de modo a tentar elucidar o seu mecanismo de ação. Os espectros obtidos para cada complexo mostraram uma diminuição da intensidade da absorvência dos complexos (hipocromismo), acompanhada de um desvio para o vermelho (batocromismo), medidos a um determinado comprimento de onda, após a adição (e consequente aumento de concentração) de CT DNA. Isto indica uma interação dos compostos de molibdénio(II) com o CT DNA. Foram calculados os valores da constante de ligação intrínseca (K_b) entre o CT DNA de cada complexo, obtendo-se maiores valores de K_b para os complexos **C3** e **C5** (K_b = 4.47 x 10^4 M^{-1} e 6.53 x 10^4 M^{-1}, respetivamente) e o menor valor para o complexo **C2** (K_b = 2.11 x 10^4 M^{-1}). Assim sendo, os complexos **C3** e **C5** interagem mais fortemente com o DNA e o complexo **C2** apresenta a interação mais fraca com esta molécula biológica.

Os resultados obtidos neste trabalho permitiram a identificação de complexos organometálicos de molibdénio(II) como potenciais agentes anti-tumorais, a partir dos estudos de atividade citotóxica em diferentes linhas celulares, e o esclarecimento de um dos possíveis mecanismos da sua ação em células cancerígenas, através da interação destes com o DNA, levando à inibição do crescimento das células tumorais e, consequente morte celular. Muitos mais estudos teriam de ser realizados para compreender melhor a interação destes compostos, não só com o DNA, mas com os outros constituintes celulares (enzimas, proteínas, membranas, etc), de modo a poder investigar a potencialidade destes compostos **C1** a **C5** em quimioterapia. Este fato pode trazer novas perspetivas a esta área de investigação, de modo a ultrapassar as limitações existentes nos fármacos atualmente usados na quimioterapia. Com efeito, estes compostos organometálicos de Mo(II) apresentam propriedades químicas diferentes das dos complexos em fases mais avançadas de desenvolvimento ou mesmo em utilização clínica. A utilização destes ligandos bidentados azotados da família das α-diiminas e a possibilidade de combinar outros novos ligandos ao molibdénio constituem uma mais valia no tratamento no cancro.

Palavras-chave: molibdénio, cancro, atividade citotóxica, interação com o DNA, quimioterapia

Index

INDEX OF FIGURES

INDEX OF SCHEMES

INDEX OF TABLES

ABBREVIATIONS

Abs – Absorbance

ALL – Acute Lymphoblastic Leukaemia

AML – Acute Myeloid Leukemia

C1 – [$MoBr(\eta^3\text{-}C_3H_5)(CO)_2${1,4-phenyl-2,3-naphthalenediazabutadiene}]

C2 – [$MoBr(\eta^3\text{-}C_3H_5)(CO)_2${1,4-(4-methyl)phenyl-2,3-naphthalenediazabutadiene}]

C3 – [$MoBr(\eta^3\text{-}C_3H_5)(CO)_2${1,4-(4-methoxy)phenyl-2,3-naphthalenediazabutadiene}]

C4 – [$MoBr(\eta^3\text{-}C_3H_5)(CO)_2${1,4-(4-chloro)phenyl-2,3-naphthalenediazabutadiene}]

C5 – [$MoBr(\eta^3\text{-}C_3H_5)(CO)_2${1,4-(4-carboxylato)phenyl-2,3-naphthalenediazabutadiene}]

Caco-2 – Human colorectal adenocarcinoma cell line

$CDCl_3$ – Deuterated Chloroform

δ – Chemical shift

CMF – Cyclophosphamide, Methotrexate and Fluorouracil

CT DNA – Calf Thymus DNA

CV – Cyclic Voltammetry

DFT – Density Functional Theory

DMEM – Dulbecco's Modified Eagle's Medium culture medium

DMF – Dimethylformamide

DMSO – Dimethyl Sulfoxide

Doxorubicin – [(7S,9S)-7-[(2R,4S,5S,6S)-4-amino-5-hydroxy-6-methyloxan-2-yl]oxy-6,9,11-trihydroxy-9-(2-hydroxyacetyl)-4-methoxy-8,10-dihydro-7H-tetracene-5,12-dione]

DNA – Desoxyribonucleotic Acid

DRC – Dose-response Curve

E – Potential

ΔE – difference between the oxidation potential (E_p^{ox}) and reduction potential (E_p^{red})

Ehtidium Bromide – 3,8-diamino-5-ethyl-6-phenylphenanthridinium bromide

FBS – Fetal Bovine Serum

FDA – Food and Drug Administration

ν – Frequency

FTIR – Fourier Transform Infrared Spectroscopy

^{1}H NMR – Proton Nuclear Magnetic Ressonance

HeLa – Human cervical adenocarcinoma cell line

HOMO – Highest Occupied Molecular Orbital

IC_{50} – Half maximal inhibitory concentration

IR - Infrared

K_b – Intrinsic binding constant

L1 – 1,4-phenyl-2,3-naphthalenediazabutadiene

L2 – 1,4-(4-methyl)phenyl-2,3-naphthalenediazabutadiene

L3 – 1,4-(4-methoxy)phenyl-2,3-naphthalenediazabutadiene

L4 – 1,4-(4-chloro)phenyl-2,3-naphthalenediazabutadiene

L5 – 1,4-(4-carboxylato)phenyl-2,3-naphthalenediazabutadiene

LUMO – Lowest Unoccupied Molecular Orbital

MCF-7 – Human breast adenocarcinoma cell line

MDA-MB-231 – Human breast adenocarcinoma cell line

MDR – Multidrug Resistance

Mo – Molybdenum

MOPP – Mustargen, Oncovin, Procarbazine and Prednisone

MTT – (3-(4,5-dimethyl-thiazol-2-yl)-2,5-diphenyl tetrazolium bromide)

nm – Nanometers

P0 – $[MoBr(\eta^3\text{-}C_3H_5)(CO)_2(MeCN_2)]$

PBS – Phosphate Buffered Saline

POMP – Purinethol, Oncovin, Methotrexate and Prednisone

ppm – Parts-per-million

Pt – Platinum

RNA – Ribonucleic Acid

ROS – Reactive Oxygen Species

RPMI 1640 – Roswell Park Memorial Institute culture medium

SCE – Saturated Calomel Electrode

SD – Standard Deviation

SW480 – Human colorectal adenocarcinoma cell line

UV-Vis – Ultraviolet–visible

WHO – World Health Organization

1) INTRODUCTION

1.1) Cancer: disease and research

According to the site of World Health Organization (WHO), cancer is one of the world's leading causes of death. Each year globally, around 13 million people find out that they have cancer, and 8 million people die from the disease [1]. Projections reveal that cancer will increase to 22 million new cases each year by 2030, if this tendency is not reversed [1, 2].

More than 200 types of cancer have been identified [3], all characterized by the uncontrolled growth and proliferation of abnormal cells [3, 4]. According to Hanahan and Weinberg, there are six hallmarks of cancer, that is, six essential alterations in the normal cell physiology that collectively dictate malignant growth, and they are: self-sufficiency in growth signals, insensitivity to antigrowth signals, evasion of programmed cell death (apoptosis), unlimited replicative potential, sustained angiogenesis and tissue invasion and metastasis [5]. One decade later, these authors added two new emerging hallmarks; namely reprogramming of energy metabolism and evading immune destruction, and described two enabling characteristics crucial to the acquisition of the hallmarks: inflammation [6, 7] and genome instability [8]. These acquired features of cancer are the main targets for therapy. Nowadays, chemotherapy, radiation therapy and surgery are the main types of treatment against cancer [3, 9], chemotherapy being the most common and effective treatment for several kinds of neoplasias [10]. Although there is an expanding knowledge and remarkable progress in this research area and its therapeutics, it is not yet enough to find an efficiently and effectively cure for all cancer types.

1.2) Chemotherapy

1.2.1) Chemotherapy: state of the art

Chemotherapy kills or stops the proliferation or growth of rapidly dividing cancer cells by targeting specific parts of the cell cycle. However, normal healthy cells, such as fast growing cells like bone marrow cells, digestive tract cells and hair follicles cells, share some of these pathways and are also damaged or killed by this treatment, causing severe side effects [11]. The most important challenge in cancer chemotherapy is the discovery and development of new compounds that selectively kill tumor cells without affecting normal cells.

The history of a systematic therapy of cancer using drugs started only in the middle of the 1960's. Before the 1940-1950 decade, cancer therapy was essentially done by surgery. Radiation therapy became a valuable tool for the control of local tumors after 1960 but, like surgery, could not eradicate metastatic cancers [3, 12]. The beginning of modern era chemotherapy can be traced to the discovery of nitrogen mustard (mechlorethamine), with therapeutic use in 1942, by Louis Goodman and Alfred Gilman [12, 13]. This toxin, similar to sulfur mustards and, initially developed for chemical warfare, was used to treat a patient with non-Hodgkin's lymphoma [14, 15]. Goodman and Gilman observed tumor regression on the patients and, even though the remission lasted only a few weeks, the principle of the systemic administration of drugs to induce tumor regression was established [12]. A few years later, the same investigators studied the molecular action of the nitrogen mustard, describing it as an alkylating agent [16] (**Chapter 1.2.2**). Other improved alkylating agents (such as cyclophosphamide) became standard components used to treat patients with lymphoma, leukaemia and some solid tumors, although Goodman and his collaborators noted that the tumors quickly became resistant to these drugs [12].

A second approach to drug therapy of cancer began with Sydney Farber and his studies on the effects of folic acid and folate analogues (aminopterin and amethopterin, commonly known as methotrexate) on children with acute

lymphoblastic leukaemia (ALL), in 1948. Remissions were observed and it was determined that antifolates could suppress proliferation of malignant cells [17]. It was also shown that methotrexate had an antitumor activity in epithelial cancers and it could cure a rare cancer that originates in placenta's cells (choriocarcinoma). This was the first solid tumor to be cured by drug therapy in humans [12].

In 1950, George Hitchings and Gertrude Elion studied purine analogues such as 6-mercaptopurine and their inhibition of the growth of tumor cells [18]. James Holland, Emil Freireich, and Emil Frei showed, in 1965, that the combination of methotrexate (antifolate), vincristine (plant alkaloid), 6-mercaptopurine (purine analogue) and prednisone (glucocorticoid immunosuppressive drug), known as the POMP regimen, could induce long-term remissions in children with ALL [19]. This finding marked the beginning of modern chemotherapy by using combination chemotherapy against different types of cancers. Furthermore, in 1960, Frank Schabel and Howard Skipper created *in vivo* assays for quantifying drug cytotoxicity, and showed that cytotoxicity was a direct function of drug dose and demonstrated the efficiency of combination therapies in preventing drug resistance [12]. Their work led to the current practice of using high dose chemotherapy, along with bone marrow transplants, to treat patients with lymphoma and leukaemia [12].

In 1965, there was a major breakthrough in the history of chemotherapy with the discovery of the antitumor properties of *cis*-diamminedichloroplatinum(II), known as cisplatin ($Pt(NH_3)_2Cl_2$) (**Figure 1**), by Barnett Rosenberg and collaborators [12, 20]. Nowadays, cisplatin (and its derivative carboplatin), are the most used compounds for the treatment of several human solid carcinomas, namely testicular and ovarian carcinomas [21, 22]. The clinical use of cisplatin (approved by the FDA in 1978) for the treatment of testicular and ovarian cancer, caused unwanted side effects, such as resistance and kidney toxicity to the treated patients [21]. This led to the research of cisplatin based compounds, such as carboplatin (1980) and other analogues (**Figure 1**) [23]. There are still significant negative side effects from the use of these drugs, therefore an emergent research on novel compounds with cytotoxic activity and low toxicity is necessary.

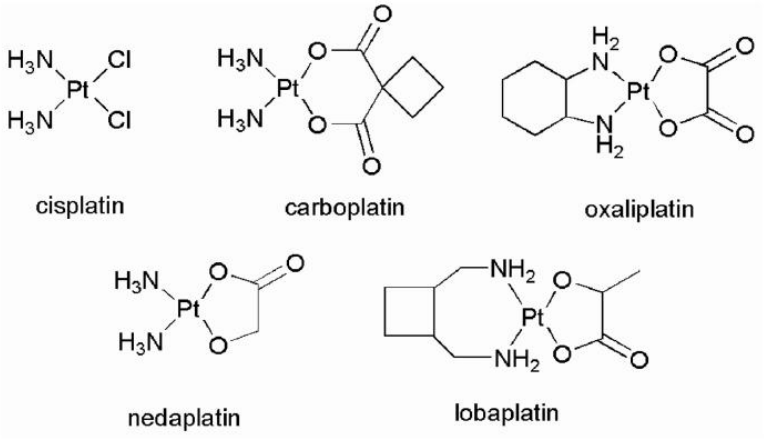

Figure 1 – Structure of the platinum(II) compounds cisplatin and its analogues (adapted from [23]).

In the late 1960s, Vincent DeVita and George Canellos used a new combination chemotherapy known as the MOPP regimen (including nitrogen mustard, vincristine, procarbazine and prednisone) and proved that it could help patients with Hodgkin's and non-Hodgkin's lymphoma [14]. In 1975, Gianni Bonadonna and collaborators used CMF, a combination of cyclophosphamide (nitrogen mustard based alkylating agent), methotrexate (antifolate drug) and fluorouracil (pyrimidine analog), which shown to be effective as adjuvant treatment for patients with breast cancer after a mastectomy procedure [24, 25]. In the early 1980s, the screening approaches did not provide groundbreaking discoveries, so a screen based method was adopted, testing drugs against a panel of 60 human cancer cell lines, covering a broad range of tumor types [26]. Unfortunately, none of the results was successful enough to continue to clinical trials. However the screening methodology itself was improved and a rapid colorimetric assay for cell viability was developed (the MTT assay, described in **Chapter 2.4.3**) [12, 27]. In the 1990 decade, there were innovative molecular and genetic approaches to understanding cell biology that exposed new signaling networks, which control and regulate cellular activities such as proliferation, survival and apoptosis. It was also found that many of these pathways where completely altered in cancer cells. As result, researchers outlined drugs to repair or counteract these specific molecular defects in malignant cells, thus beginning the era of targeted therapy. These new targets included growth factors, signaling molecules, cell-cycle proteins, modulators of apoptosis and molecules that promoted angiogenesis [5, 12].

1.2.2) Classes of drugs used in chemotherapy

In chemotherapy, the era of targeted therapy marked the specificity of drugs to targets that exist on cancer cells. These antitumor compounds can be classified in four major categories, according to their mechanism of action [3, 11, 21, 28] (**Figure 2**):

- Alkylating Agents – form covalent bonds with DNA and prevent DNA replication. These compounds possess an alkyl radical with active end groups, which can bind to different molecules (like DNA). Some agents, such as nitrogen mustard and cyclophosphamide are also active against resting (G0) cells and are used in non-Hodgkin's lymphoma. Cisplatin and carboplatin are also included in this class of drugs and are used in the treatment of ovarian, testicular, lung, bladder and colon cancer.
- Antimetabolites – interfere with protein synthesis by competing for and blocking specific receptors, such as the folic acid analog – methotrexate – used in acute lymphocytic leukemia (ALL). They also include compounds such as the purine antagonist 6-mercaptopurine used against acute myelogenous leukemia (AML) and the pyrimidine antagonist 5-fluorouracil in colorectal and gastric cancers, which interfere with the biosynthesis of purines or pyrimidines, affecting the DNA biosynthesis.
- Plant Alkaloids – these compounds are obtained from plants or microorganisms and they affect the cell cycle and cellular division. For example vincristine inhibits mitosis at metaphase by binding to tubulin (and it is used to treat lymphoma and leukemia) and taxanes which blocks the polymerization of tubulins into microtubules (used in ovarian and breast carcinoma and lung cancer).
- Antitumor Antibiotics – binds to the DNA molecule and/or block the topoisomerase II action, inhibiting DNA and RNA synthesis, like doxorubicin used in Hodgkin's disease; bleomycin causes fragmentation of DNA chains and its applied in cervical cancer; dactinomycin intercalates in DNA, interferes with RNA polymerase and inhibits transcription and its used in nephroblastoma.

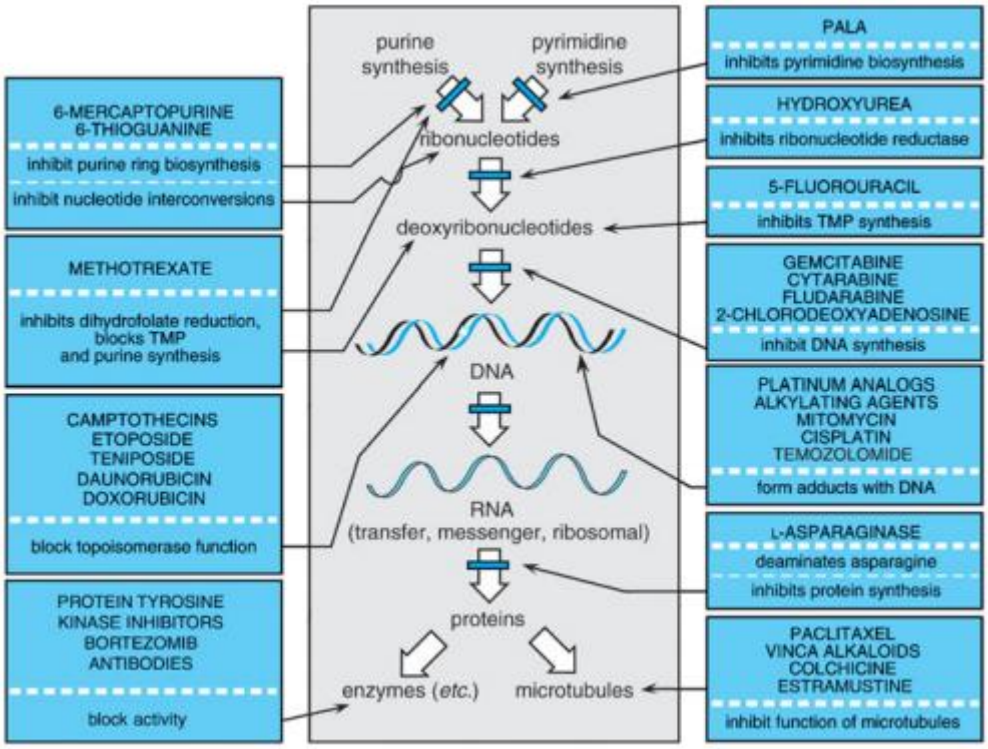

Figure 2 – Summary of the mechanisms and sites of action of some chemotherapeutic agents. PALA=*N*-phosphonoacetyl-L-aspartate; TMP=thymidine monophosphate (adapted from [28]).

These are just a few examples of cytotoxic compounds used in chemotherapy. However, the characteristics of promising anticancer drugs not only have to be determined by their mechanism of action, but they should also include solubility in aqueous medium, metabolic stability, long half-life in humans and a slow rate of metabolism by enzymes, showing a favorable dose dependent response (**Chapter 1.2.4**), with limited or no side effects [29].

1.2.3) Chemotherapy and DNA-binding drugs

Most of the drugs used in chemotherapy have DNA as target [21, 30]. These compounds can interact directly with the DNA molecule or inhibit the DNA synthesis and replication machinery.

As mentioned before, *cis*-diamminedichloroplatinum(II), known as cisplatin ($Pt(NH_3)_2Cl_2$), is considered an alkylating agent (although it has no alkyl groups) since it forms covalent bonds with DNA [28]. Most cisplatin enters the cells through active

transport, but some molecules are passively diffused through the cell membrane. Once inside the nucleus, cisplatin undergoes a hydrolysis reaction, by which each chloride ligand is replaced by a molecule of water (**Figure 3**). The water molecule itself is easily displaced, allowing the platinum fragment to bind to nitrogen atoms in guanine bases, forming an adduct with two consecutive guanine bases within a strand of DNA. This cisplatin-DNA complex bends the DNA molecule and blocks the correct DNA replication and transcription, inducing cell death [21, 30 – 35]. Most cisplatin-DNA complexes bind adjacent guanines or less commonly adenine and guanine (intrastrand). Cisplatin can also form very rare interstrand adducts with bases from two DNA strands. Although these interstrand adducts are improbable, they are thought to be highly cytotoxic [30, 33].

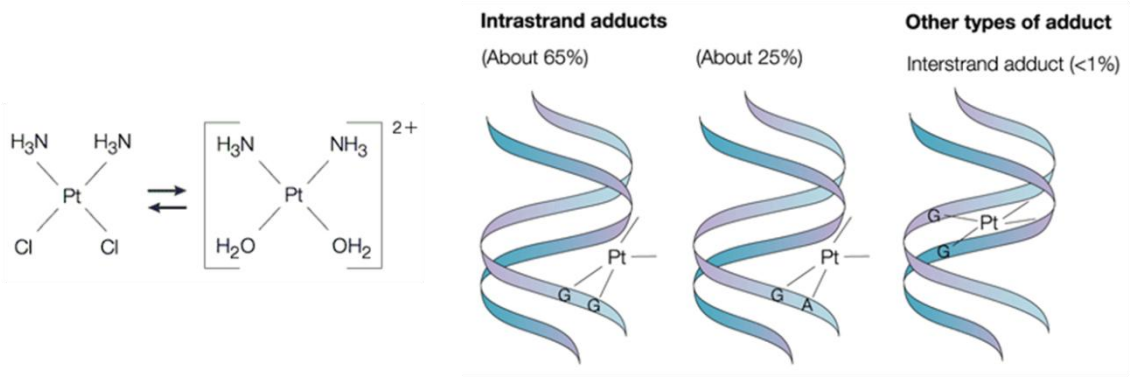

Figure 3 – Structure of cisplatin and water substituted cisplatin molecule (left) and diagrams of intrastrand and interstrand cisplatin-DNA adducts (right) (adapted from [33]).

A classical DNA intercalator is the anthracycline antibiotic [(7S,9S)-7-[(2R,4S,5S,6S)-4-amino-5-hydroxy-6-methyloxan-2-yl]oxy-6,9,11-trihydroxy-9-(2-hydroxyacetyl)-4-methoxy-8,10-dihydro-7H-tetracene-5,12-dione], known as doxorubicin (trade name Adriamycin, **Figure 4**) [35]. The planar aromatic portion of doxorubicin intercalates between two base pairs of the DNA molecule (usually nitrogen atoms of guanine and cytosine), while the daunosamine sugar fits in the minor groove and interacts with nearby base pairs (**Figure 4**) [35 – 39]. These doxorubicin-DNA interstrand adducts [40, 41], and possible inhibition of the enzyme topoisomerase II (which unwinds DNA for transcription), stop the process of DNA replication, resulting in a cell death response [42].

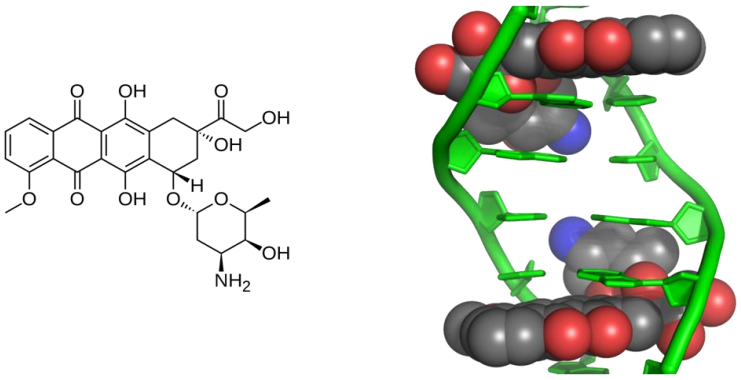

Figure 4 – Structure of the anthracycline doxorubicin (left) and diagram of two doxorubicin molecules intercalating with DNA (right) (adapted from [36]).

Although it is not used in chemotherapy, 3,8-diamino-5-ethyl-6-phenylphenanthridinium bromide, ethidium bromide, is another well-known DNA intercalator. This dye is usually used in nucleic acid staining as a fluorescent tag for DNA and RNA detection in gels [43, 44]. The hydrophobic ring structure of ethidium bromide binds to the double-stranded DNA by inserting itself between the base pairs and forming van der Waals interactions with the hydrophobic interior of the DNA. This intercalation causes elongation of the DNA double helix and distortion of the base pairs, changing their properties and interfering with DNA replication and transcription, making ethidium bromide a potent mutagen (**Figure 5**) [35, 45 – 48].

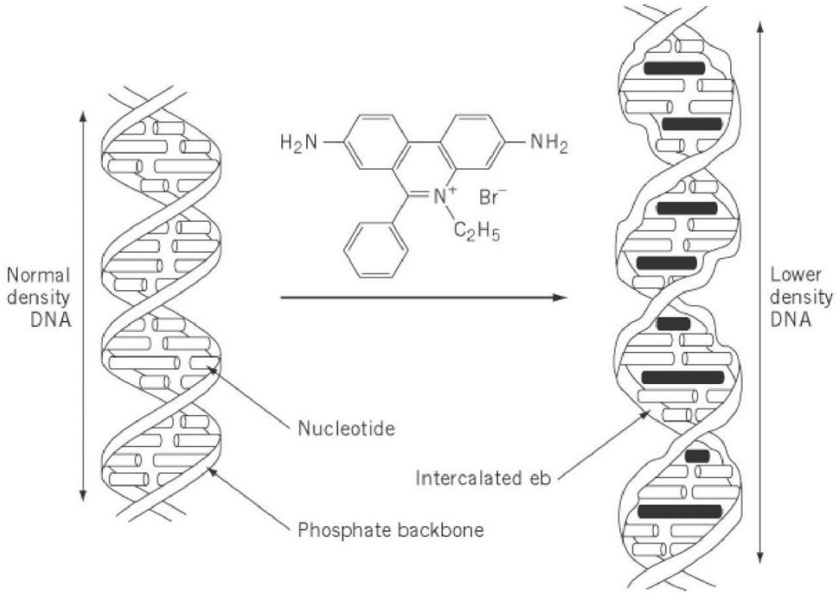

Figure 5 – Scheme of the intercalation of ethidium bromide in the DNA and consequent elongation of the double helix and distortion of the base pairs (adapted from [45]).

The intense fluorescence of ethidium bromide after binding with DNA is probably due to the hydrophobic environment of the base pairs of DNA which forces the ethidium cation to lose its associated water molecules. Since water is an efficient fluorescent quencher (decreasing the fluorescence of a given molecule), this dehydrogenation allows the ethidium-DNA complex to fluoresce more intensively [49].

1.2.4) Limits of chemotherapy

Since Gilman and Goodman introduced nitrogen mustard into clinical treatment of lymphoma, tumor resistance associated with chemotherapy was observed [12]. After an initial regression of the disease, a second lower dose of drug was given (due to its toxicity), with less therapeutic effect. When the third dose was administered, the tumor no longer responded positively to the chemotherapeutic agent [50, 51]. Some authors proposed that resistance mechanisms are reflected in dose-response relationships with log % cell survival *versus* drug dose plots (**Figure 6**) [52, 53]:

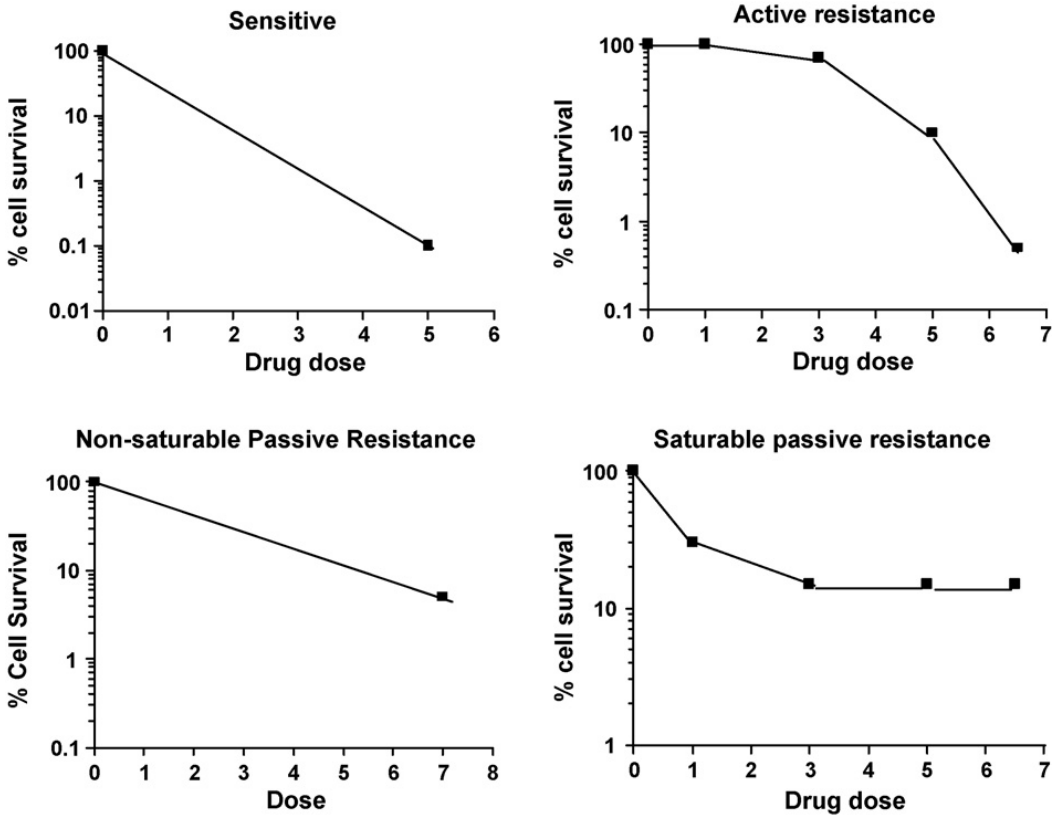

Figure 6 – Dose-response curves and proposed resistance mechanisms (adapted from [52]).

According to dose-response curves (DRC) in **Figure 6**, resistance may be classified as: active if there is a "shoulder" on the DRC, due to a resistance factor, analogous to competitive drug inhibition; non-saturable passive if it is a decreased DRC slope, possibly owing to alteration of the drug transport or activating system, corresponding to a decreased affinity of a drug for its receptor; and saturable passive if the DRC has a terminal plateau, due to the lack of factor required for drug efficacy or cell killing, analogous to the effect of non-competitive drug inhibition [52, 53].

Drug resistance is a major obstacle limiting the efficacy of chemotherapy. Although some tumors may be intrinsically resistant to chemotherapy before the treatment, others, initially sensitive to chemotherapy, can acquire resistance during treatment, becoming insensitive to similar drugs (multidrug resistance – MDR) [54 – 56]. These resistance factors can be divided in two main groups. The first group includes pharmacological and physiological factors and the second group includes cell specific factors [51, 56 – 65]:

- <u>First group</u>:
  - reduced intracellular drug concentration;
  - inadequate route of delivery, distribution and drug access to the tumor;
  - incorrect drug metabolism;
  - reduced drug uptake and enhanced drug efflux.

- <u>Second group</u>
  - cytochrome P450 enzymes are often overexpressed in several solid tumors, which can contribute to drug elimination;
  - altered topoisomerase I and II activity prevents the binding of intercalators to the topoisomerase-DNA complex, allowing the broken DNA strands to be repaired in the tumor cells;
  - the activation of the DNA repair systems originating resistance to many anticancer drugs, such as platinum compounds and alkylating agents;
  - regulation of cell death by evasion of apoptosis, necrosis or evasion of senescence;

- glutathione transferases (GST) are enzymes involved in detoxification and can catalyze and inactivate several anticancer drugs;
- overexpression of membrane proteins such as solute carriers, channels and ATP-binding cassette (ABC) transporters that can excrete drugs from the cell.

All these factors play an important role in drug resistance [51, 55, 59, 61] and although they are mentioned individually in most cases, several factors act simultaneously, resulting in multidrug resistance [55, 61, 65]. To investigate successful chemotherapeutic drugs, it is essential to override these resistance factors in cancer cells and reduce the side effects that damage normal healthy cells.

1.3) Antitumor metal compounds

Medicinal applications of metal complexes as therapeutic drugs have more than 5000 year history, with ancient Chinese using gold compounds [22, 66, 67].

The discovery of antitumor activity of cisplatin (platin, group 10, period 6 in the periodic table) against human carcinomas gave a strong hint that metal compounds may be active as cytostatic drugs, and that other metal compounds might also be used as antitumor agents [22]. This led to a renewed interest in investigating the cytotoxic properties of other metals compounds, namely those closer to the platinum in the periodic table (**Figure 7**).

The major classes of metal-based anticancer drugs include platinum(II), ruthenium(II) and ruthenium(III), gold(I) and gold(III), iron(II) [68] and also molybdenum(II) compounds [69].

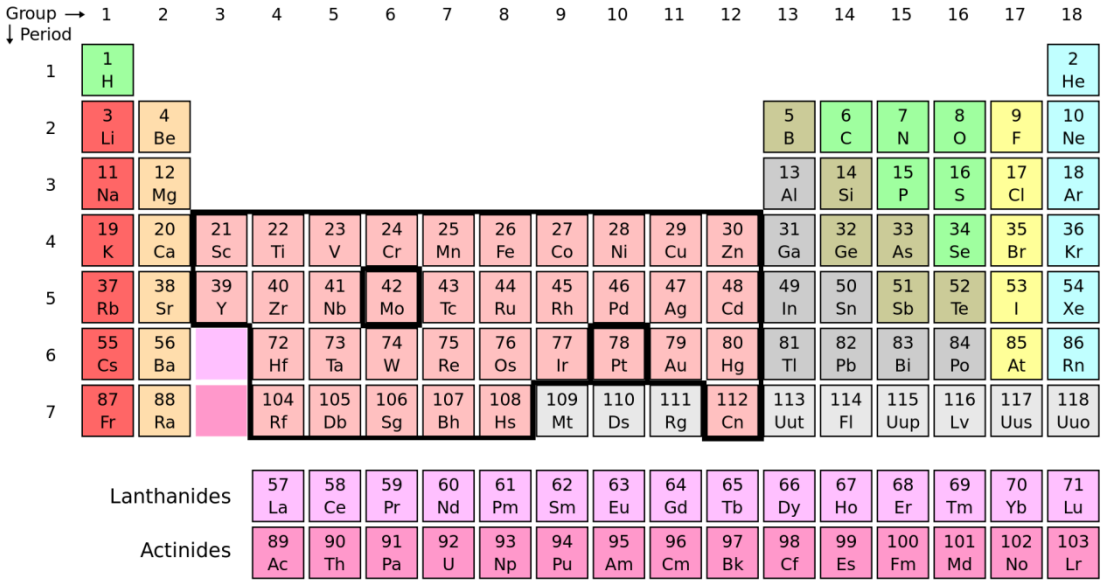

Figure 7 – Periodic table (adapted from [70]).

Metal complexes with ruthenium, which interact with the DNA, present less antitumoral activity when compared with cisplatin, but they are best tolerated *in vivo* [71]. Gold compounds have a great affinity to thiol groups of proteins and enzymes in mitochondria, thioredoxin reductase being their primary target [72 – 74]. Simple ferricenium salts were the first published iron complexes to show cytotoxic activity, through the iron unique redox properties, leading to the formation of reactive oxygen species (ROS) that can oxidize proteins and DNA [75, 76]. In 1979, Köpf and Köpf-Maier reported the antitumor activity of an extensive range of metallocene complexes, including molybdenum [77]. In 2005, Portuguese investigators studied several molybdenum(II) compounds in different cancer cell lines *in vitro*, concluding that the complexes are cytotoxic [78], although the mechanism of action of these complexes is still not fully understood. In 2010, Bandarra and Lopes studied the cytotoxic activity of Mo(II) complexes with 1,10-phenanthroline and 2,2'-bipyridyl, in several cancer lines *in vitro*, obtaining high antitumoral values. These authors, also determined that these Mo(II) complexes can possibly bind to the DNA molecule [69].

1.3.1) Advantages and classes of antitumor metal compounds

Some of the advantages of metal based compounds are the increased possibility of binding with several ligands, creating better complexes to target specific molecules or macrostructures (like DNA or enzymes) [79]. Metal ions exhibit a wide range of coordination numbers and geometries, and the binding of different ligands with their own properties and possible cytotoxic activity, may improve their properties, providing specificity to the target molecules. Besides, the redox potencial of the metal ions can influence the redox state of the cell and change the cells viability through the formation of radical species, activation of apoptosis pathways dependent from oxygen, or increase the toxicity of the drug [80, 81].

The increasing number of metal complexes that have a cytotoxic activity against cancer cells contributed to a general comprehension that the biological activity and mechanism of action of metal compounds could be adjusted by an appropriate choice of the metal, its oxidation state and of the ligands [82, 83]. Therefore a classification of anticancer metal drugs based on their possible mode of action has been suggested [81]. This classification consists on the metal compound itself, rather than their presumed targets (DNA, proteins, enzymes, cellular transduction pathways, etc) [83, 84], since there is great uncertainty in this area.

The five suggested classes are:

- the metal with a functional role – the activity comes from a direct binding of the metal to the biological target;
- the metal with a structural role – the shape of the compound affects the binding to the biological target through non-covalent interactions;
- the metal as a carrier for active ligands that are delivered *in vivo* and/or the metal might also protect the ligands before they reach their biological target;
- the metal compound behaves as a catalyst *in vivo*, through the production of reactive oxygen species (ROS) that cause damages to the cells;
- the metal compound is photoactive and behaves as a photo-sensitizer.

Frequently functional complexes must be activated by reactions of reduction/oxidation or aquation. Consequently, it is important that the active metal species has at least one labile ligand that can be substituted, providing a coordination position available for binding to the target (example: binding of cisplatin to DNA – **Chapter 1.2.3**). Unfortunately, functional compounds have disadvantages since they can react with several biomolecules, rather than with specific cancer targets [81].

In functional compounds, the coordination of the metal to the biological target(s) is the main interaction responsible for the antitumor activity; nevertheless non-covalent interactions may be very important. In structural compounds, the metal does not bind directly to the biological target [81]. For instance, metallo-intercalators are expected to interact non-covalently with DNA in a way more similar to the intercalation of doxorubicin than the covalent DNA adducts formed by cisplatin (**Chapter 1.2.3**). These compounds are usually organometallic and more stable and less toxic than functional compound. For example, ferrocifen proved to be more cytotoxic against breast cancer cells than the commonly used chemotherapeutic drug tamoxifen [85, 86].

In the third class of this classification, the metal is not expected to have an activity itself. The metal acts as a carrier for active ligands and also protects the ligands before they reach their biological target. For example, in complexes of Co(III) with nitrogen mustards, the Co(III) in hypoxic tumor environment is reduced to Co(II), which is more labile and detaches itself from the active ligand, delivering it to its biological target, the DNA [81].

The metal compounds can behave as catalysts *in vivo*, through the production of reactive oxygen species (ROS) that cause cell damage. For example, Ru(II) organometallic complexes act as catalysts for the oxidation of glutathione (GSH) to glutathione disulfide (GSSG). Since GSH is the primary cellular antioxidant, its depletion leads to an increase of ROS levels [87].

The last group of this classification includes photoactive metal compounds which behave as photo-sensitizers. These complexes can be used in photodynamic therapy, where nontoxic photo-sensitizer compounds are exposed selectively to specific wavelengths, usually through lasers, upon which the complexes become toxic to targeted specific tumor cells. For example, Ru(II) complexes with polypyridine

ligands when excited by light can form non-covalent adducts with DNA by groove-binding and/or intercalation [30, 81, 87].

The classification of anticancer metal complexes based on the metals action on their possible mode of action might help in the design of novel compounds and/or lead to the biological studies of metal compounds previously neglected.

1.3.2) Molybdenum: the metal and its biology

The transition element molybdenum (Mo) is essential for several biological systems since it is required by enzymes that catalyze key reactions in the global carbon, sulfur and nitrogen metabolism [88, 89]. Mo is abundant in oceans in the molybdate anion form (MoO_4^{2-}) and also in soils, where this oxoanion is the only form of Mo is available for plants and microorganisms. In biochemistry, molybdenum belongs to the group of trace elements, which is needed in very minute quantities for the proper development of an organism [88, 90]. However, if an organism takes up high amounts of Mo, toxicity symptoms are observed; nevertheless if Mo is unavailable for uptake, the organism dies [91, 92].

The molybdenum as metal itself is biologically inactive. When complexed with a pterin, it originates a Moco cofactor (**Figure 8**), which is important on the activity of many molybdenum enzymes.

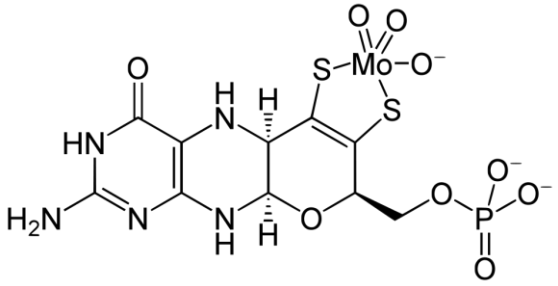

Figure 8 – Molybdenum cofactor, Moco (adapted from [90]).

In humans, molybdenum enzymes include [88 – 90, 92, 93]:

- aldehyde oxidase – enzyme located in the cytosolic compartment of tissues that oxidizes a variety of aldehydes into carboxylic acids. It can also catalyze the oxidation of cytochrome P450 and monoamine oxidase intermediate products;
- sulfite oxidase – mitochondrial enzyme which catalyzes the final step in the degradation of sulfur-containing amino acids (like methionine and cysteine) by oxidizing sulfite to sulfate and is involved in detoxifying excess sulfite;
- xanthine oxidase – is involved in purine catabolism to form uric acid, by catalyzing the oxidation of hypoxanthine to xanthine and xanthine to uric acid.

At low molybdenum levels, xanthine oxidase activity was found to be proportional to the molybdenum concentration; while at higher concentrations, the metal may have an inhibitory effect on the enzymatic activity [93]. The biochemical importance of molybdenum is due to its ability to easily provide electron-transfer pathways and to form bonds with nitrogen, oxygen and sulfur donors. Although Mo can form complexes with numerous physiologically important compounds, this trace element is absorbed, transported and excreted in a simple molybdate form (MoO_4^{2-}) which is structurally similar to phosphate and sulfate, having a low toxicity in humans [78]. In a molybdenum solution (pH > 6.0), the tetrahedral MoO_4^{2-} ion is the most abundant species, while with the pH decrease (5.0 – 6.0) it polymerizes and heptamolybdate ion $Mo_7O_{24}^{6-}$ is formed; at even lower pH values (3.0 – 5.0), octamolybdate ion $Mo_8O_{26}^{4-}$ is produced [93]. These molybdates are chemically similar and the fact that they exist in equilibrium in aqueous medium, indicates that their physiological effects are also alike.

1.4) Aim of this work

Previous research showed that several molybdenum(II) complexes present a remarkable cytotoxic activity [69, 78, 94]. On the other hand, the antitumoral effect of the Copper(II) complexes with α-diimine ligands 1,4-(4-X)phenyl-2,3-naphthalenediazabutadiene was studied in mice with carcinoma [95]. However, the combination of molybdenum(II) and these organic ligands referred above has not yet been studied, and the mechanisms of action of most organometallic complexes of molybdenum are far from being understood, although there is evidence that they interact with the DNA [69].

Starting from these promising results, the present work had the main objective of **evaluating the cytotoxic activity of five molybdenum(II) complexes, [$MoBr(\eta^3$-$C_3H_5)(CO)_2${1,4-(4-X)phenyl-2,3-naphthalenediazabutadiene}] with X = H (C1), Me (C2), OMe (C3), Cl (C4) and COOH (C5), in several cancer cell lines and of studying their possible mechanism of action.**

A colorimetric assay, MTT (3-(4,5-dimethyl-thiazol-2-yl)-2,5-diphenyltetrazolium bromide) was used to study the cytotoxic activity of **C1 – C5** *in vitro* against several cancer cell lines. The interaction with CT DNA was studied, using absorption titration spectroscopy, in order to elucidate the mechanism of action of these molybdenum(II) complexes. Understanding the mechanism of action of the complexes **C1 – C5** can be a valuable tool in cancer chemotherapy research, so that the current limitations in cancer treatment may be overcome.

2) EXPERIMENTAL PROCEDURE

2.1) Materials and instrumentation

Commercially available reagents were purchased from standard chemical suppliers and used without further purification. Hexacarbonylmolybdenum(0) was purchased from *Fluka* and acenaphthoquinone from *Alfa Aesar*. Ethidium bromide (3,8-diamino-5-ethyl-6-phenylphenanthridinium bromide), doxorubicin {(7S,9S)-7-[(2R,4S,5S,6S)-4-amino-5-hydroxy-6-methyloxan-2-yl]oxy-6,9,11-trihydroxy-9-(2-hydroxyacetyl)-4-methoxy-8,10-dihydro-7H-tetracene-5,12-dione} and allyl bromide were purchased from *Sigma-Aldrich*. Dimethyl sulfoxide (DMSO), sodium molybdate dihydrate ($Na_2MoO_4.2H_2O$) and ammonium heptamolybdate [$(NH_4)_6Mo_7O_{24}\cdot 4H_2O$] were purchased from *Merck*. RPMI 1640 (Roswell Park Memorial Institute, without L-glutamine) and DMEM (Dulbecco's Modified Eagle's Medium with 4.5 g/L Glucose, without L-glutamine) cell culture media, fetal bovine serum (FBS), trypsin, L-glutamine and pen-strep were purchased from *Lonza*. Phosphate buffered saline (PBS 10x, 1.7 mM KH_2PO_4, 5 mM Na_2HPO_4, 150 mM NaCl, pH 7.4) was purchased from *AccuGENE™*. MTT (3-(4,5-dimethyl-thiazol-2-yl)-2,5-diphenyltetrazolium bromide) and calf thymus DNA (CT DNA, 0 – 200 μM bp^{-1}) were purchased from *Sigma*.

Solvents were dried under nitrogen using common procedures. Dichloromethane was distilled over CaH_2 and n-hexane over Na/benzophenone. The syntheses of the complexes were carried out under nitrogen atmosphere using *Schlenk* tube techniques.

All cell cultures were maintained in a cell culture incubator kept at 37 °C, in a highly humidified atmosphere of 95% room air / 5% CO_2 (*Shellab* CO_2 Series Sheldon Mfg. Inc.). All cell related procedures were carried out in a cell culture cabinet (*ESCO* Class II Biohazard Safety Cabinet) under sterile conditions, as well as all the materials used in cell culture. The absorbance was measured at 570 nM using a 96-well absorbance reader (*Tecan* Sunrise Absorbance Reader). Infrared spectra were measured on a *Nicolet* 6700 spectrometer. Samples were run as KBr pellets.

NMR spectra were recorded on a *Bruker* Avance-400 spectrometer in $CDCl_3$ or DMF. UV–Vis spectra were recorded on a *Shimadzu* UV-2450 equipped with a Peltier cell for temperature control. All electrochemical measurements were performed using a *CHI* Electrochemical Analyser-620A Model controlled by a computer at room temperature in a one-compartment *Teflon* cell.

2.2) Synthesis and Characterization of Molybdenum(II) Complexes

To study the cytotoxic effect of a family of molybdenum(II) compounds, the complexes (**C1 – C5**), their precursor (**P0**) and the ligands (**L1 – L5**) were synthesized.

The compounds studied were the following:

- **P0** $[MoBr(\eta^3\text{-}C_3H_5)(CO)_2(MeCN_2)]$
- **L1** 1,4-phenyl-2,3-naphthalenediazabutadiene
- **L2** 1,4-(4-methyl)phenyl-2,3-naphthalenediazabutadiene
- **L3** 1,4-(4-methoxy)phenyl-2,3-naphthalenediazabutadiene
- **L4** 1,4-(4-chloro)phenyl-2,3-naphthalenediazabutadiene
- **L5** 1,4-(4-carboxylato)phenyl-2,3-naphthalenediazabutadiene
- **C1** $[MoBr(\eta^3\text{-}C_3H_5)(CO)_2\{1,4\text{-phenyl-2,3-naphthalenediazabutadiene}\}]$
- **C2** $[MoBr(\eta^3\text{-}C_3H_5)(CO)_2\{1,4\text{-(4-methyl)phenyl-2,3-naphthalenediazabutadiene}\}]$
- **C3** $[MoBr(\eta^3\text{-}C_3H_5)(CO)_2\{1,4\text{-(4-methoxy)phenyl-2,3-naphthalenediazabutadiene}\}]$
- **C4** $[MoBr(\eta^3\text{-}C_3H_5)(CO)_2\{1,4\text{-(4-chloro)phenyl-2,3-naphthalenediazabutadiene}\}]$
- **C5** $[MoBr(\eta^3\text{-}C_3H_5)(CO)_2\{1,4\text{-(4-carboxylato)phenyl-2,3-naphthalenediazabutadiene}\}]$

All the synthesis experiments were carried out using standard *Schlenk* techniques in an inert atmosphere, using a vacuum and a nitrogen line, to prevent the oxidation of the molybdenum(II) compounds. All the synthesized compounds were characterized by FTIR and ^1H NMR spectroscopy. The ^1H NMR spectra obtained are defined as s = singlet, d = doublet, t = triplet and m = multiplet and the hydrogen numeration was given according to **Figure 9**.

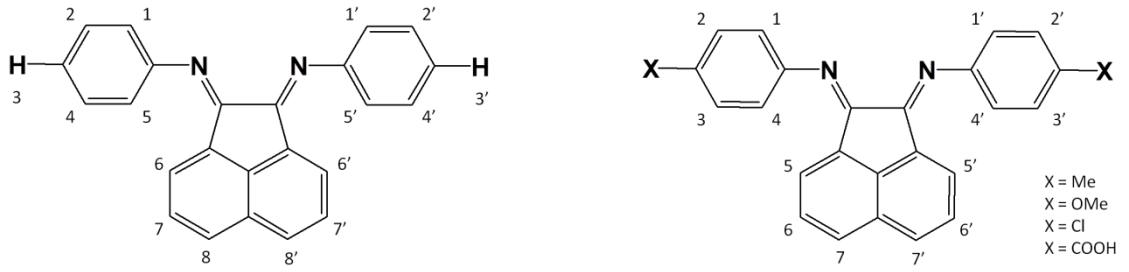

Figure 9 – Numbered hydrogens for the ^{1}H NMR spectra for the ligand **L1** (left) and for the remaining ligands (**L2 – L5**) (right). For the complexes **C1 – C5**, the same numeration was maintained as its respective ligand.

2.2.1) Synthesis of the molybdenum(II) precursor (**P0**) and organic ligands (**L1 – L5**)

[MoBr(η^{3}-C_3H_5)$(CO)_2$($MeCN_2$)] (P0)

Allyl bromide, 1.7 mL, 20 mmol) was added to a solution of hexacarbonylmolybdenum(0) ([$Mo(CO)_6$], 2.47 g, 7 mmol) in acetonitrile (MeCN) [96]. The mixture was refluxed for 12 hours. The red solution was filtered and reduced under vacuum. The solid fraction (yellow color) was filtered, washed and dried.

Yield (η): 69.4% (2.310 g)

IR (KBr pellets, cm^{-1}): 3050, 2985, 2921 (ν_{C-H}), 2321, 2287 ($\nu_{C\equiv N}$), 1942, 1849 ($\nu_{C\equiv O}$)

1,4-phenyl-2,3-naphthalenediazabutadiene (L1)

Acetic acid (5.3 mL) was added to a solution of acenaphthoquinone (0.6 g, 3.3 mmol) in acetonitrile (30 mL). After stirring for 30 minutes, aniline ($C_6H_5NH_2$, 0.437 mL, 7.1 mmol) dissolved in acetonitrile was added and the mixture was refluxed for 4.5 hours. The solution was filtered and reduced under vacuum. The solid fraction (orange/yellow color) was filtered, washed and dried.

Yield (η): 85.6% (0.932 g)

Selected IR (KBr pellets, cm^{-1}): 3050, 2889, 2851 (ν_{C-H}), 1652 ($\nu_{C=N}$), 1399 (ν_{C-N})

^{1}H NMR (400 MHz, $CDCl_3$, room temperature, ppm): δ 8.11 (d, H6/H6', 2H); 7.94 (d, H8/H8', 2H); 7.75 (t, H7/H7', 2H); 7.39 (m, H2/H2'/H4/H4', 4H); 7.23 (m, H3/H3', 2H); 7.02 (d, H1/H1', 2H); 6.90 (d, H5/H5', 2H).

1,4-(4-methyl)phenyl-2,3-naphthalenediazabutadiene (L2)

Acetic acid (5.3 mL) was added to a solution of acenaphthoquinone (0.6 g, 3.3 mmol) in acetonitrile (30 mL). After stirring for 30 minutes, *p*-toluidine ($C_6H_5NH_2Me$, 0.76 g, 7.1 mmol) dissolved in acetonitrile was added and the mixture was refluxed for 4.5 hours. The solution was filtered and reduced under vacuum. The solid fraction (orange color) was filtered, washed and dried.

Yield (η): 74.6% (0.882 g)

Selected IR (KBr pellets, cm^{-1}): 3177, 3055, 3022 (ν_{C-H}), 1653 ($\nu_{C=N}$), 1399 (ν_{C-N})

^1H NMR (400 MHz, $CDCl_3$, room temperature, ppm): δ 8.11 (d, H5, 1H); 7.94 (d, H5', 1H); 7.81 (d, H7, 1H); 7.74 (t, H7', 1H); 7.39 (t, H6, 1H); 7.31 (t, H6', 1H); 7.21 (d, H4/H4', 2H); 7.05 (d, H1, 1H); 6.95 (t, H2/H2'/H3/H3', 4H); 6.86 (d, H1', 1H); 2.38 (s, *Me*, 6H).

1,4-(4-methoxy)phenyl-2,3-naphthalenediazabutadiene (L3)

Acetic acid (5.3 mL) was added to a solution of acenaphthoquinone (0.6 g, 3.3 mmol) in acetonitrile (30 mL). After stirring for 30 minutes, *p*-anisidine ($C_6H_5NH_2OMe$, 0.875 g, 7.1 mmol) dissolved in acetonitrile was added and the mixture was refluxed for 4.5 hours. The solution was filtered and reduced under vacuum. The solid fraction (yellow color) was filtered, washed and dried.

Yield (η): 67.6% (0.723 g)

Selected IR (KBr pellets, cm^{-1}): 3071, 2997, 2934 (ν_{C-H}), 1617 ($\nu_{C=N}$), 1436 (ν_{C-N})

^1H NMR (400 MHz, $CDCl_3$, room temperature, ppm): δ 7.82 (d, H5/H5'/H7/H7', 4H); 7.31 (t, H6/H6', 2H); 7.20 (d, H1/H1'/H4/H4', 4H); 6.90 (m, H2/H2'/H3/H3', 4H); 3.83 (s, *OMe*, 6H).

1,4-(4-chloro)phenyl-2,3-naphthalenediazabutadiene (L4)

Acetic acid (5.3 mL) was added to a solution of acenaphthoquinone (0.6 g, 3.3 mmol) in acetonitrile (30 mL). After stirring for 30 minutes, 4-chloroaniline ($C_6H_5NH_2Cl$, 0.924 g, 7.1 mmol) in acetonitrile (10 mL) was added to the previous solution and the mixture was refluxed for 4.5 hours. The solution was filtered and reduced under vacuum. The solid fraction (orange/yellow color) was filtered, washed and dried.

Yield (η): 87.4% (1.15 g)

Selected IR (KBr pellets, cm^{-1}): 2982, 2925, 2852 (ν_{C-H}), 1731 ($\nu_{C=N}$), 1479 (ν_{C-N})

^1H NMR (400 MHz, $CDCl_3$, room temperature, ppm): δ 7.96 (d, H7/H7', 2H); 7.65 (m, H6/H6'/H5/H5', 4H); 7.24 (m, H2/H2'/H4/H4', 4H); 7.09 (d, H1/H1', 2H); 6.99 (d, H3/H3', 2H).

1,4-(4-carboxylato)phenyl-2,3-naphthalenediazabutadiene (L5)

Acetic acid (5.3 mL) was added to a solution of acenaphthoquinone (0.62 g, 3.3 mmol) in acetonitrile (30 mL). After stirring for 30 minutes, 4-aminobenzoic acid ($C_6H_5NH_2COOH$, 0.91 g, 7.1 mmol) in acetonitrile (10 mL) was added to the previous solution and the mixture was refluxed for 4.5 h. The solution was filtered and reduced under vacuum. The solid fraction (orange color) was filtered, washed and dried.

Yield (η): 61.2% (0.748 g)

Selected IR (KBr pellets, cm^{-1}): 3256 (ν_{O-H}), 2951, 2902, 2853 (ν_{C-H}), 1638 ($\nu_{C=N}$), 1420 (ν_{C-N})

^1H NMR (400 MHz, $CDCl_3$, room temperature, ppm): δ 8.18 (m, H7/H7'/H5/H5', 4H); 7.99 (d, H3/H3', 2H); 7.78 (t, H2/H2', 2H); 7.40 (t, H6/H6', 2H); 7.11 (d, H1/H1', 2H); 6.87 (d, H4/H4', 2H).

2.2.2) Synthesis of the molybdenum(II) complexes (**C1 – C5**)

[MoBr(η^3-C_3H_5)$(CO)_2${1,4-phenyl-2,3-naphthalenediazabutadiene}] (C1)

1,4-phenyl-2,3-naphthalenediazabutadiene (**L1**) (0.5 mmol, 0.233 g) was added to a yellow solution of [MoBr(η^3-C_3H_5)$(CO)_2(MeCN_2)$] (**P0**) (0.5 mmol, 0.178 g) in ethanol (20 mL), and the mixture was stirred for 48 hours. The solution was filtered, reduced under vacuum and a dark green solid precipitated with n-hexane (20 mL, at 4 °C).

Yield (η): 68.1% (0.227 g)

Selected IR (KBr pellets, cm^{-1}): 2943, 2910, 2817 (ν_{C-H}), 1945, 1875 ($\nu_{C\equiv O}$), 1646 ($\nu_{C=N}$), 1399 (ν_{C-N})

^1H NMR (400 MHz, $CDCl_3$, room temperature, ppm): δ 8.16 (d, H6/H6', 2H); 8.11 (d, H8/H8', 2H); 7.99 (d, H7/H7', 2H); 7.78 (t, H4/H4', 2H); 7.66 (d, H1/H1', 2H); 7.54 (d,

H2/H2', 2H); 7.45 (t, H3/H3', 2H); 6.99 (d, H5/H5', 2H); 4.26 (m, H_{meso}); 3.41 (m, H_{syn}); 1.62 (d, H_{anti}); 1.22 (d, H_{anti}).

[MoBr(η^3-C_3H_5)$(CO)_2${1,4-(4-methyl)phenyl-2,3-naphthalenediazabutadiene}] (C2)

1,4-(4-methyl)phenyl-2,3-naphthalenediazabutadiene (**L2**) (0.5 mmol, 0.252 g) was added to a yellow solution of [MoBr(η^3-C_3H_5)$(CO)_2(MeCN_2)$] (**P0**) (0.5 mmol, 0.178 g) in ethanol (20 mL), and the mixture was stirred for 48 hours. The solution was filtered, reduced under vacuum and a dark green solid precipitated with n-hexane (20 mL, at 4 °C). The dark green precipitate was recrystallized by dissolving in dichloromethane (CH_2Cl_2) and adding n-hexane. Green crystals formed after a few days, suitable for single crystal X-ray diffraction.

Yield (η): 94.9% (0.331 g)

IR (KBr pellets, cm^{-1}): 3032, 2923, 2841 (ν_{C-H}), 1933, 1870 ($\nu_{C\equiv O}$), 1639 ($\nu_{C=N}$), 1415 (ν_{C-N})

^{1}H NMR (400 MHz, $CDCl_3$, room temperature, ppm): δ 7.84 (d, H5/H5', 2H); 7.49 (d, H7/H7', 2H); 7.42 (d, H6/H6', 2H); 7.33 (m, H1/H1'/H2/H2'/H3/H3'/H4/H4'/, 8H); 4.21 (m, H_{meso}); 3.39 (m, H_{syn}); 2.42 (s, *Me*, 6H); 1.21 (m, H_{anti}), 0.82 (m, H_{anti})

[MoBr(η^3-C_3H_5)$(CO)_2${1,4-(4- methoxy)phenyl-2,3-naphthalenediazabutadiene}] (C3)

1,4-(4- methoxy)phenyl-2,3-naphthalenediazabutadiene (**L3**) (0.5 mmol, 0.273 g) was added to a yellow solution of [MoBr(η^3-C_3H_5)$(CO)_2(MeCN_2)$] (**P0**) (0.5 mmol, 0.180 g) in ethanol (20 mL), and the mixture was stirred for 48 hours. The solution was filtered, reduced under vacuum and a dark green solid precipitated with n-hexane (20 mL, at 4 °C).

Yield (η): 71.9% (0.251 g)

Selected IR (KBr pellets, cm^{-1}): 2984, 2960, 2879 (ν_{C-H}), 1953, 1860 ($\nu_{C\equiv O}$), 1639 ($\nu_{C=N}$), 1415 (ν_{C-N})

^{1}H NMR (400 MHz, $CDCl_3$, room temperature, ppm): δ 8.16 (d, H5, 1H); 8.09 (d, H5', 1H); 7.99 (d, H7', 1H); 7.85 (d, H7/H3, 2H); 7.76 (t, H6', 1H); 7.55 (d, H3', 1H); 7.47 (t, H6, 1H); 7.34 (t, H2/H2', 2H); 7.13 (d, H4/H1', 2H); 7.05 (d, H4/H1, 2H); 4.41 (m, H_{meso}); 4.23 (m, H_{meso}); 3.89 (s, O*Me*, 6H); 3.65 (m, H_{syn}); 3.42 (m, H_{syn}); 1.58 (d, H_{anti}); 1.17 (m, H_{anti}).

[MoBr(η^3-C_3H_5)$(CO)_2${1,4-(4-chloro)phenyl-2,3-naphthalenediazabutadiene}] (C4)

1,4-(4-chloro)phenyl-2,3-naphthalenediazabutadiene (**L4**) (1 mmol, 0.401 g) was added to a yellow solution of [MoBr(η^3-C_3H_5)$(CO)_2(MeCN_2)$] (**P0**) (1 mmol, 0.355 g) in ethanol (20 mL), and the mixture was refluxed for 48 hours. The solution was filtered, reduced under vacuum and a green yellowish solid precipitated with n-hexane (20 mL, at 4 °C) [97].

Yield (η): 76.1% (0.821 g)

Selected IR (KBr pellets, cm^{-1}): 3024, 2916, 2850 (ν_{C-H}), 1964, 1883 ($\nu_{C\equiv O}$),1639 ($\nu_{C=N}$), 1495 (ν_{C-N})

^{1}H NMR (400 MHz, $CDCl_3$, room temperature, ppm): δ 8.18 (d, H7/H7', 2H); 8.12 (d, H2/H2', 2H); 8.02 (d, H3/H3', 2H); 7.78 (t, H6, 1H); 7.64 (m, H4/H4'/H1/H1', 4H); 7.50 (t, H6', 1H); 7.03 (d, H5/H5', 2H); 4.34 (m, H_{meso}); 3.41 (m, H_{syn}); 1.62 (d, H_{anti}); 1.61 (d, H_{anti}); 1.63 (d, H_{anti}).

[MoBr(η^3-C_3H_5)$(CO)_2${1,4-(4-carboxylato)phenyl-2,3-naphthalenediazabutadiene}] (C5)

1,4-(4-carboxylato)phenyl-2,3-naphthalenediazabutadiene (**L5**) (0.5 mol, 0.269 g) was added to a yellow solution of [MoBr(η^3-C_3H_5)$(CO)_2(MeCN_2)$] (**P0**) (0.5 mol, 0.180 g) in ethanol (20 mL), and the mixture was refluxed for 48 hours. The solution was filtered, reduced under vacuum and a dark greenish blue solid precipitated with n-hexane (20 mL, at 4 °C). The green/blue precipitate was recrystallized by dissolving in dichloromethane (CH_2Cl_2) and adding n-hexane. Green/blue crystals formed after a few days, suitable for single crystal X-ray diffraction.

Yield (η): 64.2% (0.226 g)

Selected IR (KBr pellets, cm^{-1}): 3126 (ν_{O-H}), 2995, 2925, 2852 (ν_{C-H}), 1940, 1869 ($\nu_{C\equiv O}$), 1693 ($\nu_{C=O}$), 1598 ($\nu_{C=N}$), 1420 (ν_{C-N})

^{1}H NMR (400 MHz, DMF, room temperature, ppm): δ 8.39 (d, H2/H2', 2H); 8.35 (d, H3/H3', 2H); 8.31 (d, H5/H5', 2H); 7.96 (d, H7/H7', 2H); 7.70 (t, H6/H6'/H4/H4', 4H); 6.91 (d, H1/H1', 2H); 4.06 (m, H_{meso}); 2.98 (m, H_{syn}); 1.40 (d, H_{anti}).

2.3) Electrochemical Studies

Cyclic voltammetry (CV) is a fundamental electrochemical technique to study the redox behavior of an electroactive species. It consists of cycling the potential of a working electrode in an electrolyte solution (containing electroactive species) and measuring the resulting current intensity (*i*, or peak current, *j*). The potential (E) of the working electrode is controlled *versus* a reference electrode (commonly saturated calomel electrode, SCE) and the measurements are made between two chosen potential values (for example: 0 – 1.2 V) at a constant sweep rate (mV/s). The resulting cyclic voltammogram displays the measured current during a potential scan and is represented in a current peak (*j*) *versus* potential (E) plot [98].

Metal complexes and some organic compounds may undergo electron transfer reactions without making or breaking covalent bonds. Most electrochemical reactions involve one electron transfer step leading to reactive species, which react at the (working) electrode. CV is capable of generating a new oxidation state during the forward scan and following its changes on the reverse scan. The important electrochemical parameters that can be measured from cyclic voltammograms are the oxidation and reduction potentials (E_p^{ox} and E_p^{red}), usually associated with the cathodic and anodic current respectively, and current intensity.

All electrochemical measurements were performed using a *CHI* Electrochemical Analyser-620A Model controlled by a computer at room temperature in an one-compartment electrochemical Teflon cell. A polycrystalline platinum (Pt) working electrode (area 1.28 cm^2), a platinum foil counter electrode (area 2.0 cm^2) and a saturated calomel electrode (SCE) as reference electrode were used. Before each experiment, a mirror-finishing platinum surface was generated by hand-polishing the electrode in an aqueous suspension of successively finer grades of alumina (down to 0.05 μm). All the solutions were deoxygenated directly in the electrochemical cell with nitrogen gas (N_2).

The electrochemical studies were performed at different sweep rates (20, 50, 100, 200, 1000, 2000 mV/s) in the potential range of 0 – 1.2 V, starting with fastest velocities to slower ones, to prevent solution decay.

To minimize solution resistance and promote the flow of electrons, the electrolyte solution used was 0.1 M tetrabutylammonium hexafluorophosphate ($TBAPF_6$) in dichloromethane (CH_2Cl_2). 1 mM solutions of the molybdenum complexes (**C1 – C5**), ligands (**L1**, **L2**, **L4** and **L5**) and precursor (**P0**) were prepared in $TBAPF_6$/ CH_2Cl_2 electrolyte.

2.4) Cell Culture and Cytotoxic Assays *in vitro*

Several human cell lines were used to study the cytotoxic activity of the molybdenum(II) complexes synthesized (**C1 – C5**), as well as their mechanism of action. The human cell lines used were: HeLa (cervical adenocarcinoma), SW480 and Caco-2 (colorectal adenocarcinoma), MCF-7 and MDA-MB-231 (breast adenocarcinoma). HeLa and Caco-2 cell lines were maintained in RPMI 1640 culture medium (Roswell Park Memorial Institute, without L-Glutamine), while SW480, MCF-7 and MDA cells were grown in DMEM culture medium (Dulbecco's Modified Eagle's Medium with 4.5 g/L Glucose without L-Glutamine). Both media were supplemented with 10% of fetal bovine serum (FBS), 1% of penicillin and streptomycin (200 U/mL PEN-STREP) and 1% of L-glutamine (2 mM). These media contain a pH indicator (phenol red) that changes the color to yellow or fuchsia as the pH becomes acidic or alkaline, respectively. When the medium becomes yellow, it indicates that the cells consumed most of the existing nutrients and the medium is not oxygenated enough, so an exchange of the culture medium is necessary to prevent cell death. The FBS enhances cell attachment and provides additional nutrients and growth factors that promote an healthy cell growth and it also contains trypsin inhibitors.

All cell cultures were maintained in a cell culture incubator kept at 37 °C, in a highly humidified atmosphere of 95% room air / 5% CO_2. All cell related procedures were carried out in a cell culture cabinet under sterile conditions, as well as all the materials used in cell culture.

2.4.1) Cryopreservation and resuscitation of frozen cells

Cells can be preserved for later use by freezing stocks in liquid nitrogen – cryopreservation. Cells are harvested, centrifuged at 900 *g* for 10 minutes and the pellet is resuspended in a solution of 90% FBS / 10% DMSO and placed on cryogenic vials. DMSO is a cryoprotective agent used to lower the freezing point of the aliquots and prevent formation of ice crystals inside the cells on the frozen state that might lead to cell inviability. Additionally, the vials are kept in a cryo freezing container ("Mr Frosty", filled with isopropanol) which allows the cells to cool down slowly from room temperature to -80 °C at a rate of 1 °C per minute. After that, the cryogenic vials are placed in a liquid nitrogen storage tank where they can remain for long periods.

When preserved frozen cells are required, they can be revived by removing the cryogenic vial from liquid nitrogen storage and warming it at 37 °C for 1 – 2 minutes or until the ice crystals melt. The cell suspension is then transferred to a culture flask containing fresh growth medium pre-warmed and incubated at 37 °C, 5% CO_2 / 95% air, humidified cell culture incubator.

2.4.2) Cell Subcultures and Quantification

The adherent cells grow in a continuous layer that eventually occupies the whole surface of the culture flask (confluent state). Once this happens, the cells stop dividing, stop growing (senesce) and die. To prevent this occurrence, it is necessary to subculture the cells. In this process, the cells are harvested, diluted in fresh growth medium and replaced in a new culture flask to promote their growth and viability.

While the cells grow into the gaps of the flask and reach confluency (80% - 90%), they need to be subcultured with trypsin, a proteolytic enzyme that is used to detach the cells from each other and the flask (trypsinization). For this, the consumed medium is removed from the flask, the cells are washed with phosphate buffered saline (PBS 1x, pH 7.4), trypsin is added and the flask is incubated at 37 °C for 5 minutes. After trypsinization, PBS is added to the suspended cells and a fraction of this solution is placed in a new flask with fresh supplemented medium.

In order to obtain reproducible experimental results and optimum cell growth it is important to have an appropriate seeding density. The most common method for quantification of cells involves the use of a haemocytometer, a thickened glass slide

with a grid that contains 9 large squares and inside has 16 small squares visible on an optical microscope. Each large square measures 1 mm x 1 mm and is 0.1 mm deep and, with a coverslip in place, has a volume of 0.1 mm^3 (10^{-4} cm^3). It is possible to calculate the total number of cells in the solution per cubic centimeter (or mL) by counting the cells in each large square multiplied by a conversion factor corresponding to the volume of the large square (10^4).

2.4.3) Cytotoxic activity assay *in vitro* using a colorimetric method

To determine the cell viability after exposure to the molybdenum(II) complexes, a colorimetric assay is used: MTT (3-(4,5-dimethyl-thiazol-2-yl)-2,5-diphenyltetrazolium bromide). MTT is a yellow molecule that can be reduced by mitochondrial reductase to purple formazan crystals in viable cells [27]. After quantification, 5 x 10^5 cells were seeded in a 96-well flat-bottomed microplate and incubated for approximately 48 h at 37 °C in a humidified 5% CO_2 / 95% air atmosphere. Afterwards, the consumed medium was removed and the cells were treated with 8 concentrations of the compounds (1, 5, 10, 25, 50, 75, 100 and 200 µM) dissolved in 0.5% DMSO and supplemented medium, and incubated for 48 h. There were also control wells containing only 0.5% DMSO dissolved in supplemented medium (**Figure 10**).

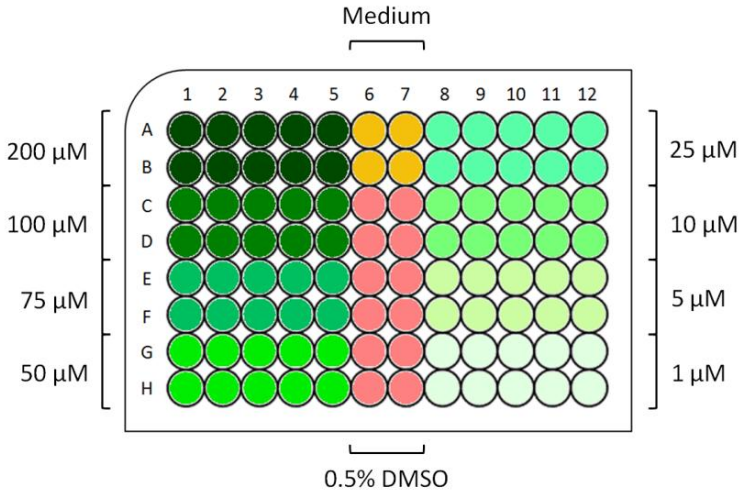

Figure 10 – Representative scheme with the distribution of the 8 concentrations of compound dissolved in 0.5% DMSO (1, 5, 10, 25, 50, 75, 100 and 200 µM) and control wells containing only 0.5% DMSO dissolved in supplemented medium, on a 96-well microplate.

After the 48 h incubation time, the medium was removed and 100 µL of MTT solution (0.5 mg/mL MTT dissolved in medium) was added into each well and incubated for 2 h. Afterwards the medium was removed, and 100 µL of DMSO were added to dissolve the formazan crystals (which are not soluble in an aqueous media). The absorbance was measured at 570 nM using a 96-well absorbance reader.

There is a direct correlation between the absorbance and cell viability. It has been assumed that the absorbance of the control wells (containing 0.5% DMSO dissolved in medium) corresponds to 100% cell viability, which means that all cells in those wells are metabolically active. The cell viability for each compound concentration was calculated based on the ratio of the absorbance for each concentration and the absorbance for the DMSO control wells.

The IC_{50} values (half maximal inhibitory concentration) were determined by non-linear regression fittings (dose-response curves). In this work, the IC_{50} value refers to compound concentration that causes 50% of cell viability. Each experiment had ten replicates for each compound concentration and the results represent an average of three independent experiments.

To determine the influence of the precursor (**P0**) and ligands (**L1 – L5**) on the complexes activity, cytotoxic assays *in vitro* were performed in HeLa using the later MTT assay protocol.

The effect of some molybdates, such as sodium molybdate dihydrate ($Na_2MoO_4.2H_2O$) and ammonium heptamolybdate [$(NH_4)_6Mo_7O_{24}{\cdot}4H_2O$], as well as classical DNA intercalators, such as doxorubicin [(7S,9S)-7-[(2R,4S,5S,6S)-4-amino-5-hydroxy-6-methyloxan-2-yl]oxy-6,9,11-trihydroxy-9-(2-hydroxyacetyl)-4-methoxy-8,10-dihydro-7H-tetracene-5,12-dione] and ethidium bromide (3,8-diamino-5-ethyl-6-phenylphenanthridinium bromide), was also studied in HeLa cells.

To study the variation of IC_{50} values of molybdenum(II) complexes (**C1 – C5**) along the course of time, the MTT assay protocol was followed and the HeLa cells were exposed to the compounds for several periods of time: 1, 4, 8, 12, 24, 48 and 72 hours.

2.5) DNA Binding Studies

The mechanism of action of most antitumor compounds involves the DNA as their primary intracellular target, since interaction with DNA is one of the possible mechanisms which metal compounds can inhibit cell proliferation [30]. Electronic absorption titration spectroscopy is one of the most useful and widely used techniques to study the binding mode of the complexes with DNA.

The mode of interaction between the complex and the DNA can be evaluated by the changes on the absorption spectrum. If the complex intercalates with DNA, a red-shift (bathochromism) of the absorption maximum in the studied region can be observed along with a decrease in the intensity of the complex absorbance (hypochromism). The hypochromism indicates that the DNA-binding mode of the compound may be due to electrostatic effects or intercalation with the DNA, while the bathochromism is indicative of the stabilization of the DNA duplex [99]. The compound-DNA interaction strength can be estimated by the intrinsic binding constant, K_b (binding constant *per* DNA base pair) [100].

To study the possible interaction between the molybdenum(II) complexes and DNA, a DNA binding assay *in vitro* was performed using electronic absorption titration spectroscopy. Calf thymus DNA (CT DNA) was dissolved in buffer Tris NaCl (5 mM Tris, 50 mM NaCl, pH 7.2) and stirred for at least 2 days. Before each experiment, the UV absorbance of the DNA solution was measured and the ratio at 260 and 280 nm, Abs_{260} / Abs_{280}, was between 1.8 – 1.9, indicating that the DNA was sufficiently free of protein contamination [69]. Different concentrations of CT DNA (0 – 200 μM) were added to a constant concentration of 20 μM buffered solutions of the metal complex (5 mM Tris, 50 mM NaCl, pH 7.2). The same amount of CT DNA was added to the reference cell (control with no complex) in order to correct the contribution of the increasing DNA concentration. Absorption spectra of the complexes were generated after 10 min incubation with each CT DNA concentration at 37 °C. The ratio absorbance observed / [complex] (20 μM) gives the apparent absorption coefficient ε_a.

To determine the extinction coefficient for each free compound (ε_f), the absorbance of different concentrations (0, 10, 20, 30, 40, 50 and 60 µM) were measured at the peaks of the spectra for each molybdenum complex, using the Lambert-Beer Law.

The intrinsic binding constant (K_b) was determined according to the following equation [100]:

$$\frac{[\mathrm{DNA}]}{(\varepsilon_a - \varepsilon_f)} = \frac{[\mathrm{DNA}]}{(\varepsilon_b - \varepsilon_f)} + \frac{1}{K_b(\varepsilon_b - \varepsilon_f)}$$

[DNA] is the DNA concentration in base pairs, the apparent absorption coefficients ε_a correspond to absorbance observed / [complex], ε_f the extinction coefficient for the free complex and ε_b the extinction coefficient for the complex in the fully bound form with DNA and the intrinsic binding constant K_b is given by the ratio slope / intercept in the plot [DNA] / (ε_a - ε_f) *versus* [DNA].

3) RESULTS AND DISCUSSION

3.1) Synthesis and Characterization of Molybdenum(II) Complexes

The bidentate nitrogen ligands (**L1 – L5**) were synthesized by the reaction of acenaphthoquinone with the appropriate aniline ($C_6H_5NH_2X$, with X = H, Me, OMe, Cl, COOH) in acetonitrile (MeCN) (**Scheme 1**).

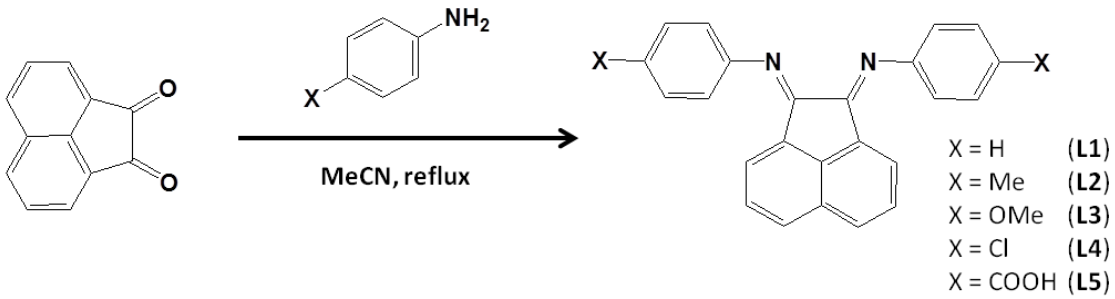

Scheme 1 – Synthesis of the ligands 1,4-(4-X)phenyl-2,3-naphthalenediazabutadiene (**L1 – L5**).

The molybdenum(II) precursor [$MoBr(\eta^3\text{-}C_3H_5)(CO)_2(MeCN_2)$] (**P0**) was synthesized by the reaction of hexacarbonylmolybdenum(0) ([$Mo(CO)_6$]) in acetonitrile (MeCN) with allyl bromide (**Scheme 2**).

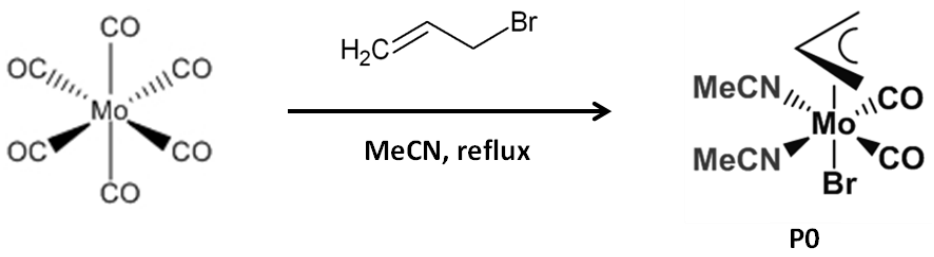

Scheme 2 – Synthesis of the precursor [$MoBr(\eta^3\text{-}C_3H_5)(CO)_2(MeCN_2)$] (**P0**).

The complexes (**C1 – C5**) were synthesized by substitution of acetonitrile ligands (MeCN) from the precursor (**P0**) and subsequent coordination of the bidentate nitrogen ligand (α-diimines, **L1 – L5**) to the molybdenum center [97] (**Scheme 3**).*

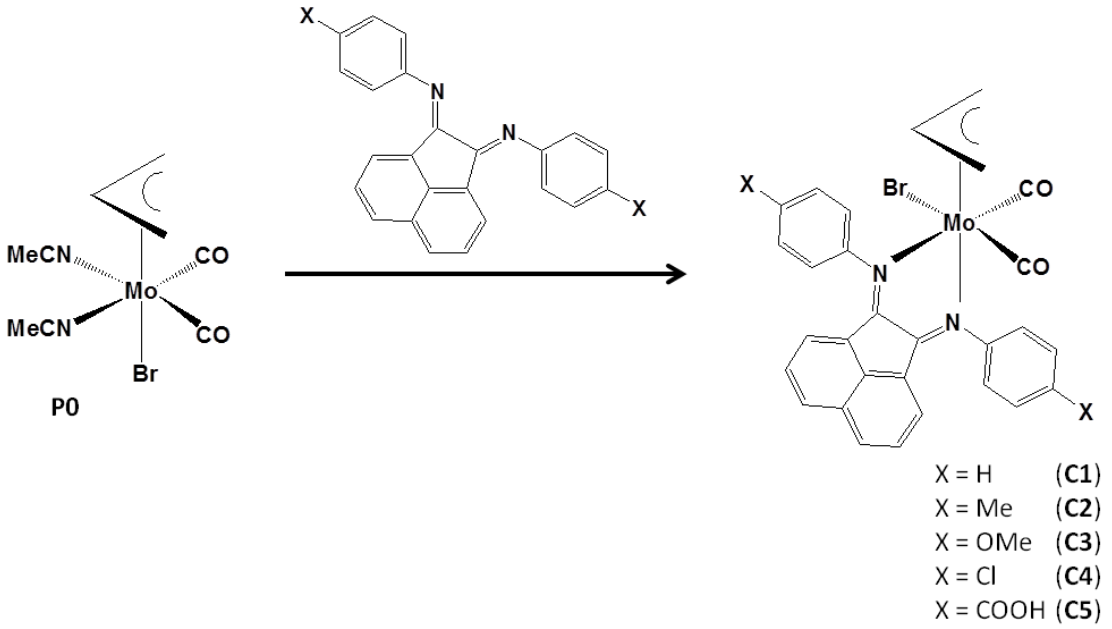

Scheme 3 – Synthesis of the molybdenum(II) complexes [MoBr(η^3-C_3H_5)$(CO)_2${1,4-(4-X)phenyl-2,3-naphthalenediazabutadiene}] (**C1 – C5**).

All the synthesized compounds were characterized by FTIR and ^{1}H NMR spectroscopy.

The FTIR spectrum of the precursor [MoBr(η^3-C_3H_5)$(CO)_2(MeCN_2)$] (**P0**) shows ν_{C-H} bands of the allyl group (η^3-C_3H_5) at 3050, 2985 and 2921 cm^{-1}, the $\nu_{C\equiv N}$ bands assigned to the acetonitrile ligands (MeCN) at 2321 and 2287 cm^{-1} and the $\nu_{C\equiv O}$ stretching modes of the carbonyl group at 1942 and 1849 cm^{-1}.

The infrared spectra of the ligands 1,4-(4-X)phenyl-2,3-naphthalenediazabutadiene (**L1 – L5**) show typical bands of the C–H, C=N and C–N bonds between 3050 to 2850 cm^{-1} (ν_{C-H}), ≈ 1650 cm^{-1} ($\nu_{C=N}$) and ≈ 1400 cm^{-1} (ν_{C-N}). No $\nu_{C=O}$ band corresponding to the C=O bond in acenaphthoquinone was observed, indicating that this group was substituted by the amino group of the aniline.

* All the available ligand **L3** was used in the formation of the complex **C3**.

In the molybdenum(II) complexes [MoBr(η^3-C_3H_5)$(CO)_2${1,4-(4-X)phenyl-2,3-naphthalenediazabutadiene}] (**C1 – C5**), the FTIR spectra show ν_{C-H} bands corresponding to all aromatic C–H bonds at ≈ 3030 to 2800 cm^{-1} and the $\nu_{C\equiv O}$ band assigned to the carbonyl groups at ≈ 1960 to 1860 cm^{-1}. These bands were slightly deviated when compared to those of the **P0** spectrum owing to the coordination of the bidentate nitrogen ligands. The absence of the $\nu_{C\equiv N}$ bands assigned to acetonitrile ligands (MeCN) of **P0** in the complexes spectra, as well as the $\nu_{C=N}$ and ν_{C-N} vibrational modes at ≈ 1645 cm^{-1} and 1400 cm^{-1} (slightly shifted to lower cm^{-1} relative to the free ligands), indicate that the acetonitrile ligands from the precursor where replaced by the bidentate nitrogen ligands in the synthesis.

^{1}H NMR spectra were run and the obtained results support the proposed structures for the synthesized compounds.

The crystal structure of the complexes [MoBr(η^3-C_3H_5)$(CO)_2${1,4-(4-methyl)phenyl-2,3-naphthalenediazabutadiene}] (**C2**) and [MoBr(η^3-C_3H_5)$(CO)_2${1,4-(4-carboxylato)phenyl-2,3-naphthalenediazabutadiene}] (**C5**) was determined by single-crystal X-ray diffraction in University of Aveiro (**Figure 11**) and selected bond distances (Å) and angles (º) are resumed in **Table 1**.

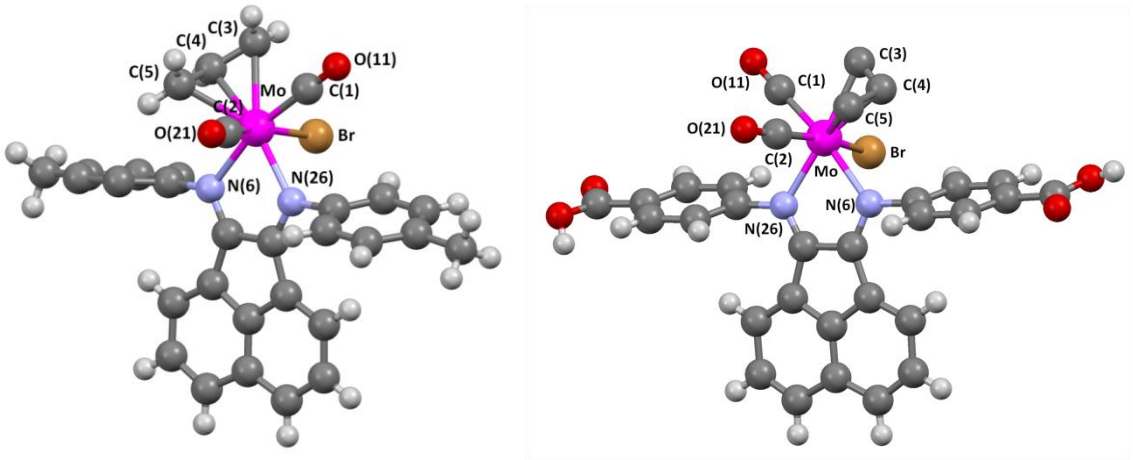

Figure 11 – Molecular structure of the molybdenum(II) complexes **C2** (left) and **C5** (right) obtained by single-crystal X-ray diffraction. Ball and stick representation (using *Mercury 3.0* CDCC®).

Table 1 – Selected bond distances (Å) and angles (º) from the molybdenum(II) coordination sphere in **C2** and **C5**.

Bond Distance (Å)			Bond Angle (º)		
	C2	C5		C2	C5
Mo–C(3)	2.358	2.200	C(1)–Mo–C(2)	80.88	83.84
Mo–C(4)	2.219	2.137	N(6)–Mo–N(26)	73.05	72.42
Mo–C(5)	2.326	2.296	C(1)–Mo–N(6)	116.53	168.29
Mo–C(1)	1.966	1.978	C(2)–Mo–N(6)	100.46	100.67
Mo–C(2)	1.965	1.996	C(1)–Mo–N(26)	93.76	97.29
Mo–N(6)	2.284	2.262	C(2)–Mo–N(26)	85.97	86.22
Mo–N(26)	2.211	2.220	N(6)–Mo–Br	82.71	82.66
Mo–O(21)	3.074	3.062	N(26)–Mo–Br	81.11	82.49
Mo–O(11)	3.120	3.123	C(1)–Mo–Br	92.74	90.57
Mo–Br	2.670	2.613	C(2)–Mo–Br	165.19	166.68

These values fall in the range usually observed for similar complexes [97]. There are two stable isomers, axial and equatorial (**Scheme 4**), associated to this family of complexes [MoBr(η^3-C_3H_5)$(CO)_2$(L-L)]. The ligand **L-L** occupies different positions in each complex.

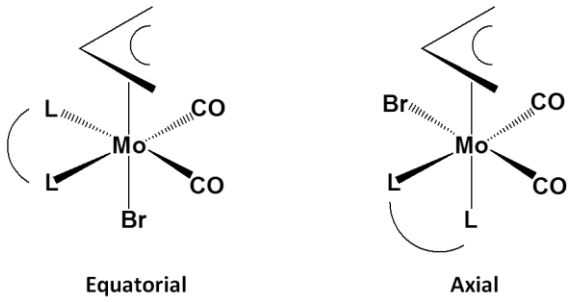

Scheme 4 – Possible isomers for the complexes [MoBr(η^3-C_3H_5)$(CO)_2$(L-L)], equatorial and axial.

The preference between these two isomers is not clear, and they often interconvert in solution [97], but position of the allyl group (η^3-C_3H_5) is more stable when its opening lies over the carbonyl ligands (as in **Scheme 4**). Usually bulky ligands (such as **L1 – L5** synthesized for the complexes **C1 – C5**) tend to favor the formation of axial isomers [97].

3.2) Electrochemical Studies

To determine the redox potential of the molybdenum(II) complexes [MoBr(η^3-C_3H_5)$(CO)_2${1,4-(4-X)phenyl-2,3-naphthalenediazabutadiene}] (**C1 – C5**, **Figure 12**), cyclic voltammetry experiments were performed.

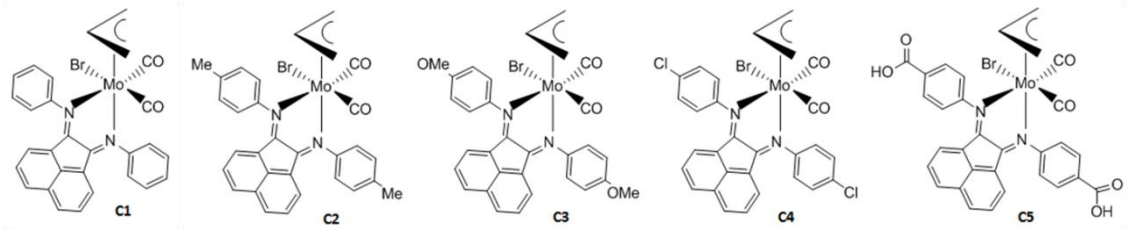

Figure 12 – Schematic structure of the molybdenum(II) complexes studied (**C1 – C5**).

Solutions of the molybdenum complexes (**C1 – C5**), ligands (**L1**, **L2**, **L4** and **L5**) and precursor (**P0**) were prepared in supporting electrolyte ($TBAPF_6/CH_2Cl_2$).

The results obtained at different sweep rates for the complexes studied (**C1 – C5**) are shown in **Figure 13**. At faster sweep rates (200, 1000 and 2000 mV/s), the waves current is enhanced and they occur at higher potential values, as expected, but the response is not well defined (end of the oxidation process) in the potential range under study. At slower sweep rates (20, 50 and 100 mV/s) the oxidation/reduction waves are well defined, which in these conditions allow the full redox reaction to take place, leading to more defined waves, even though the potential peaks shift still occurred.

Typical voltammograms of the complexes (**C1 – C5**), their precursor (**P0**) and the ligands (**L1**, **L2**, **L4** and **L5**), are represented in **Figure 14** for the sweep rate of 50 mV/s.

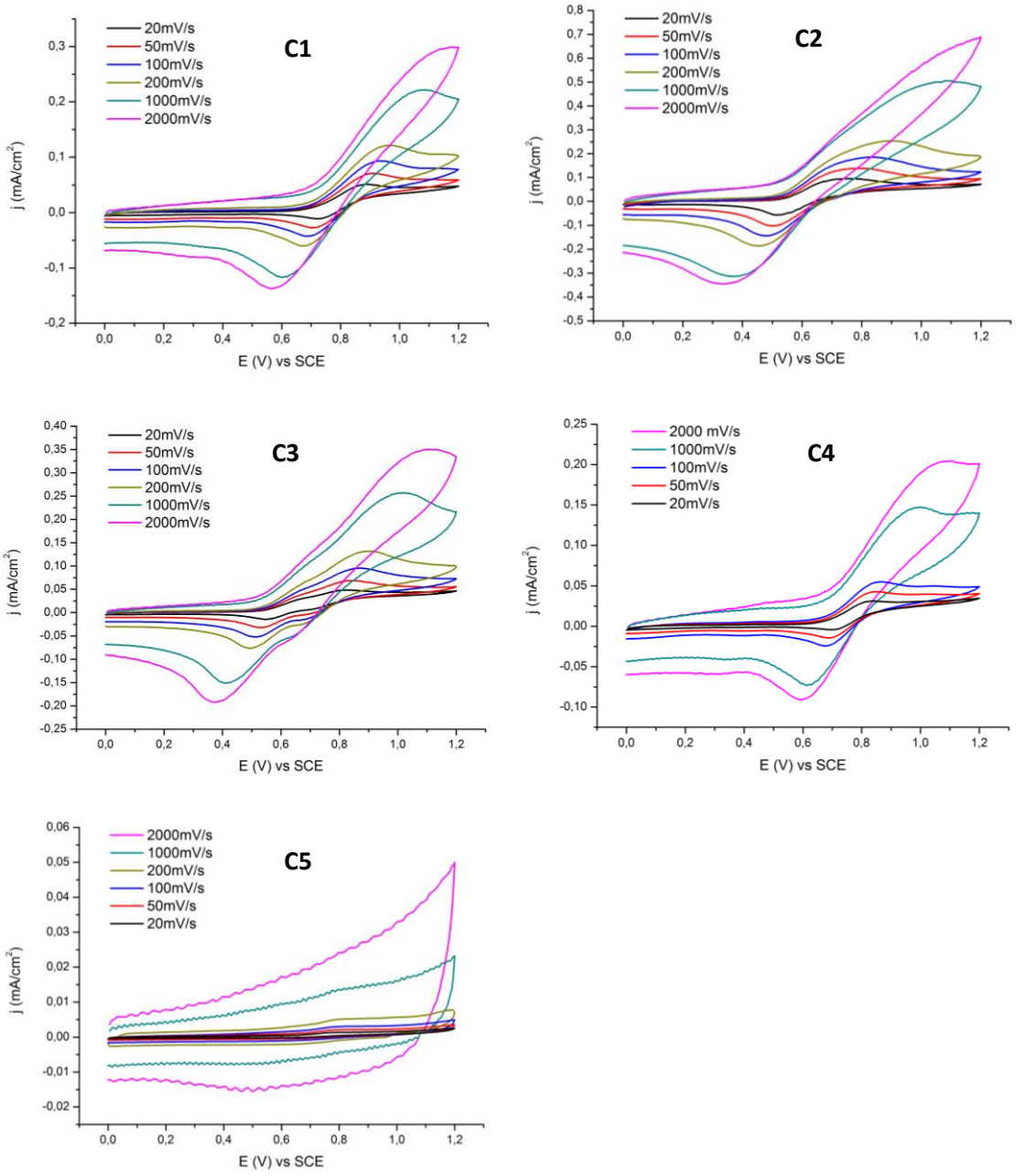

Figure 13 – Cyclic voltammograms of the Pt electrode in presence of 1 mM solutions of the organometalic complexes (**C1 – C5**) in 0.1 M $TBAPF_6/CH_2Cl_2$ in the potential range of 0 – 1.2 V, at sweep rates of 20, 50, 100, 200, 1000 and 2000 mV/s.

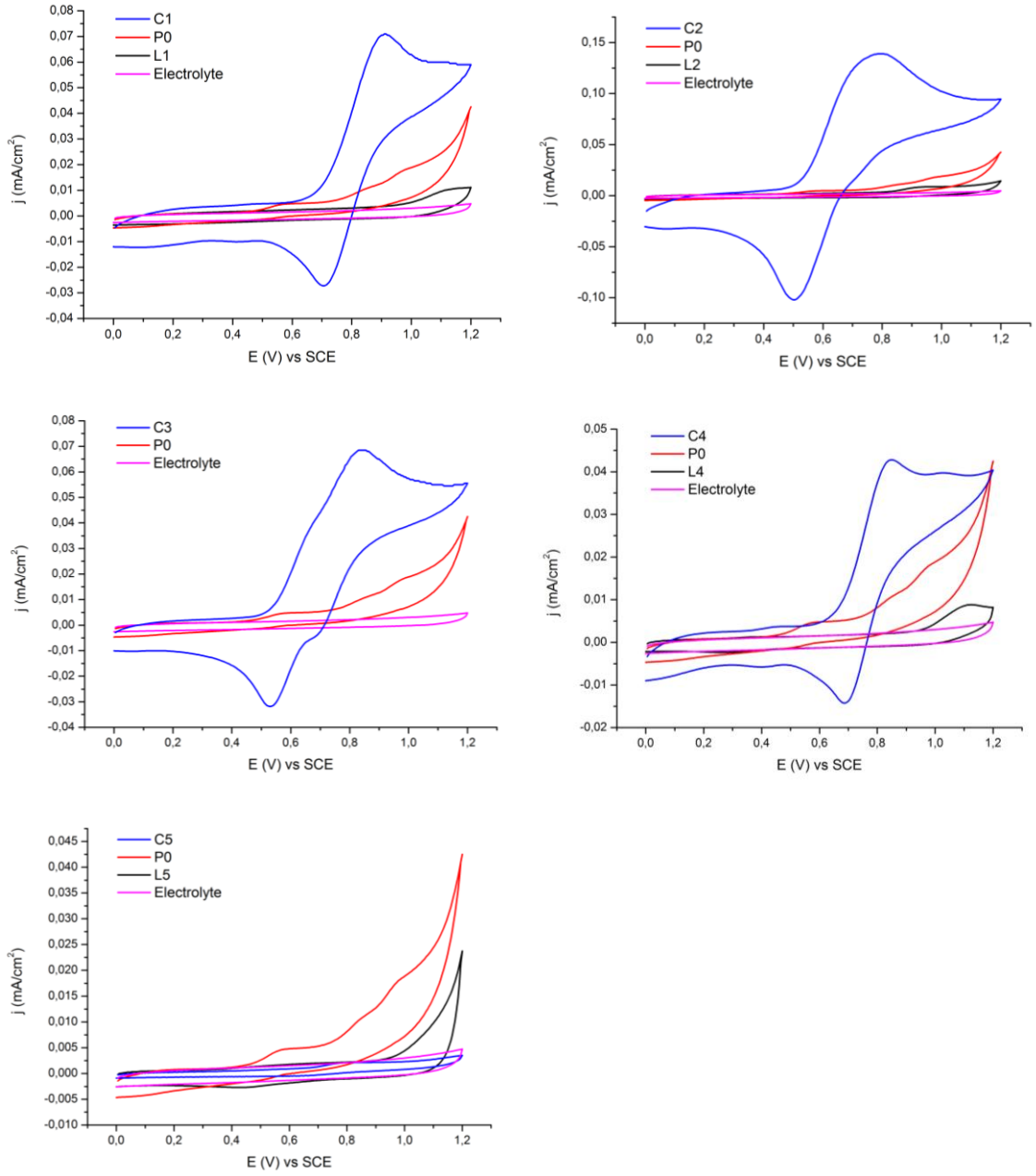

Figure 14 – Cyclic voltammograms of the Pt electrode in presence of 1 mM solutions of the organometalic complexes (**C1 – C5**), their respective ligands (**L1**, **L2**, **L4** and **L5**) and molybdenum(II) precursor (**P0**) in 0.1 M $TBAPF_6/CH_2Cl_2$ in the potential range of 0 – 1.2 V, at 50 mV/s. The electrolyte response is also depicted.

As shown in **Figure 14**, the $TBAPF_6/CH_2Cl_2$ electrolyte does not interfere with the obtained results, since it has a very low current response (near zero). The molybdenum(II) precursor (**P0**) has three oxidation waves and no observable reduction wave in the cyclic voltammetric time scale, indicating that the oxidations of the molybdenum(II) are irreversible in solution. The organic ligands (**L1**, **L2**, **L4** and **L5**) exhibit one irreversible oxidation.

The voltammograms of the complexes (**Figure 14**) show that the complexes **C1**, **C2** and **C5** have one oxidation wave, while complexes **C3** and **C4** have two intense oxidations wave. Complexes **C1**, **C2** and **C4** show one small reduction peak, while complex **C3** has two reduction peaks. There are no visible reduction waves in the voltammogram of complex **C5**. The wave shape of the voltammograms is alike for all the complexes, except for complex **C5** (which has a very low current response).

The voltammograms of the complexes **C1 – C5**, for the sweep rate of 50 mV/s, are all collected in a single figure (**Figure 15**) in order to compare them more easily.

The electrode potential values (E, V) measured from the cyclic voltammograms are presented in **Table 2**.

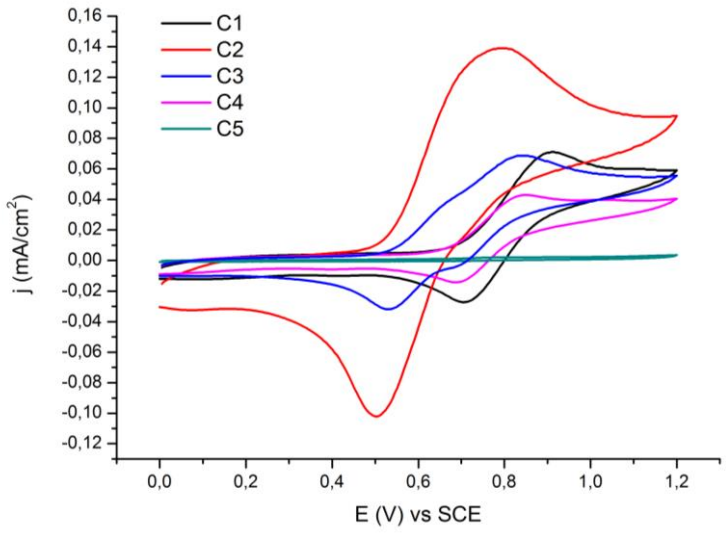

Figure 15 – Cyclic voltammograms of the Pt electrode in presence of 1 mM solutions of the organometalic complexes (**C1 – C5**) in 0.1 M $TBAPF_6/CH_2Cl_2$, with the potential range of 0 – 1.2 V, at 50 mV/s.

Table 2 – Oxidation (E_p^{ox}) and reduction (E_p^{red}) potentials (V *vs* SCE) and **ΔE** (E_p^{ox} - E_p^{red}) for all compounds, at the sweep rate of 50 mV/s. *

Compounds	E_p^{ox} (V)	E_p^{red} (V)	ΔE (V)
P0	0.580	-	0.580
	0.840	-	0.840
	0.973	-	0.973
L1	1.110	-	1.110
L2	0.920	-	0.920
L3	n.t.	n.t.	-
L4	1.120	-	1.120
L5	-	-	-
C1	0.901	0.711	0.190
C2	0.781	0.504	0.277
C3	0.670	0.534	0.136
	0.830	0.690	0.140
C4	0.827	0.692	0.135
	1.030	-	1.030
C5	0.783	-	-

*on a platinum electrode in 0.1 M $TBAPF_6/CH_2Cl_2$ electrolyte

Regarding the values of for the potencial (V *vs* SCE) (**Table 2**) and the cyclic voltammograms for the molybdenum(II) complexes (**C1 – C5**, **Figure 14** and **Figure 15**), one or two intense oxidation peaks and one lower reduction peak are observed.

C3 has the lowest oxidation potential (E_p^{ox} = 0.670 V), which means that this complex is more likely to lose one (or more) electron(s) and become oxidized, than the other complexes. **C1** has the highest first oxidation potential (E_p^{ox} = 0.901 V) and is the most difficult to oxidize. This complex (**C1**) has the highest reduction potential (E_p^{red} = 0.711 V), and is easily reduced. **C5** shows no visible reduction wave, indicating that its oxidation is completely irreversible. Although all five complexes present a tendency to an irreversible oxidation behavior (ΔE > 0.059 V) [98], some complexes, like **C1 – C3** are slightly more reversible (with higher ΔE values) than **C4**.

Tridimensional representation of the highest occupied molecular orbital (HOMO) and lowest unoccupied molecular orbital (LUMO) of the complexes **C1 – C5**, calculated by density functional theory (DFT) are shown in **Figure 16** and **Figure 17**, respectively. The schematic structures of complexes **C1** – **C5** are shown in **Figure 18**.

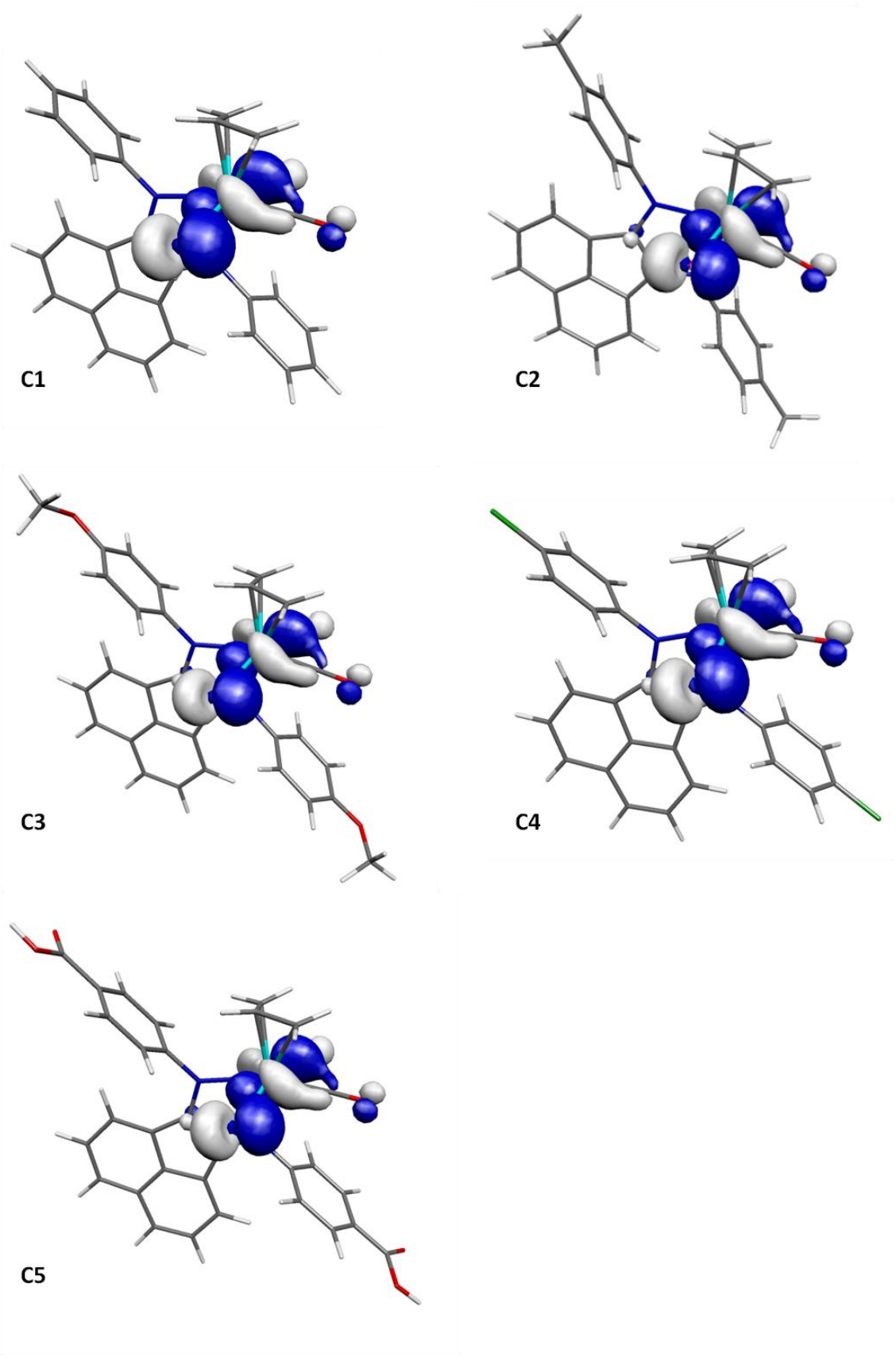

Figure 16 – Tridimensional representation of the HOMO of the complexes **C1 – C5** (using Molekel®).

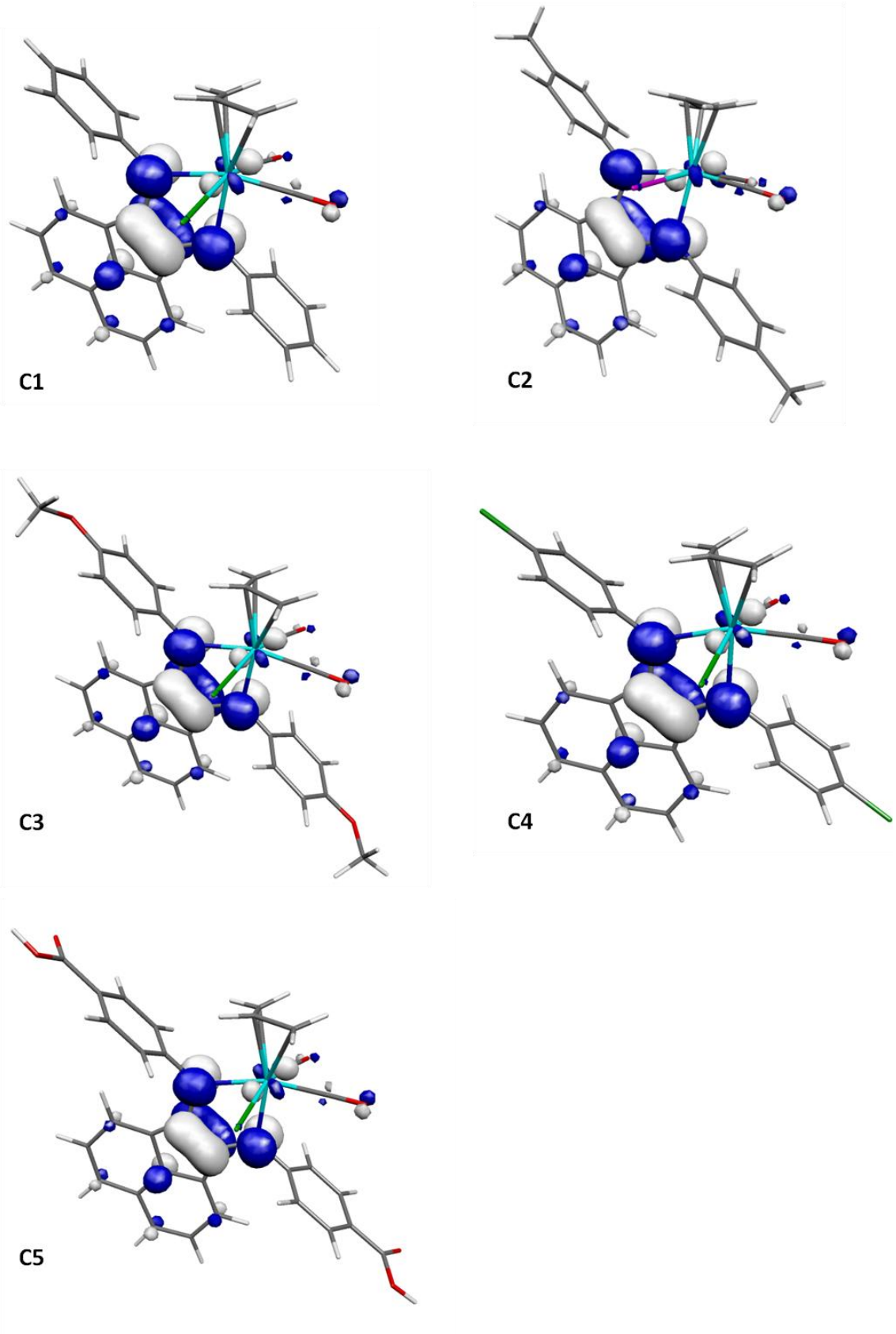

Figure 17 – Tridimensional representation of the LUMO of the complexes **C1 – C5** (using Molekel®).

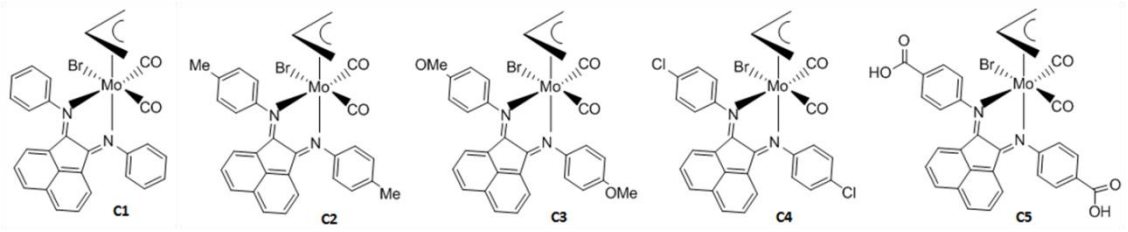

Figure 18 – Schematic structure of the complexes **C1 – C5**.

As shown in **Figure 16**, the oxidation takes place at the Mo(II) center in all complexes and can thus be assigned to a Mo(II) to Mo(III) oxidation, since the HOMO is mainly located in metal center. The second oxidation, when observed (**C3** and **C4**), can probably be an oxidation from Mo(III) to Mo(IV). The complexes **C3** and **C4** have electronegative atoms in the ligand (O and Cl, respectively), but they are also π donors, and it is possible that donation of π electrons from these substituents stabilize the Mo(II) oxidized species. This allows a more stable positive complex and a second oxidation can occur at higher potential values.

The reduction occurs at the ligand, since the LUMO (lowest unoccupied molecular orbital) of all these complexes is almost completely located in the α-diimine (**Figure 17**).

3.3) Cytotoxic Assays *in vitro*

To evaluate the antitumoral activity of the molybdenum(II) complexes synthesized (**C1 – C5**, **Figure 19**), cytotoxic assays *in vitro* were performed in various human cell lines: HeLa (cervical adenocarcinoma), MCF-7 and MDA-MB-231 (breast adenocarcinoma), SW480 and Caco-2 (colorectal adenocarcinoma).

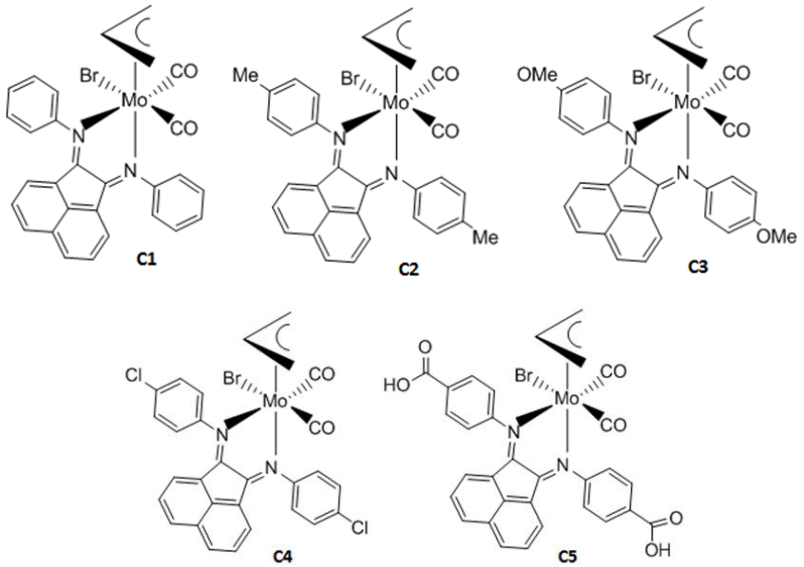

Figure 19 – Schematic structure of the molybdenum(II) complexes studied (**C1 – C5**).

To determine the IC_{50} value (compound concentration that causes 50% of cell viability) of each complex, the cell lines were incubated with several compound concentrations (1, 5, 10, 25, 50, 75, 100 and 200 µM) for 48 h and afterwards the MTT assay was performed. This well known colorimetric assay reflects the number of viable cells and is also used to measure cytotoxicity (loss of viable cells) [27] through the absorbance of purple formazan (reduced form of the yellow MTT).

The relation between cell viability and complex concentration and the dose-response curves obtained by nonlinear regression analysis, in HeLa, are shown in **Figure 20** and **Figure 21**. The given results represent an average of three independent experiments and each experiment includes ten replicates for each compound concentration.

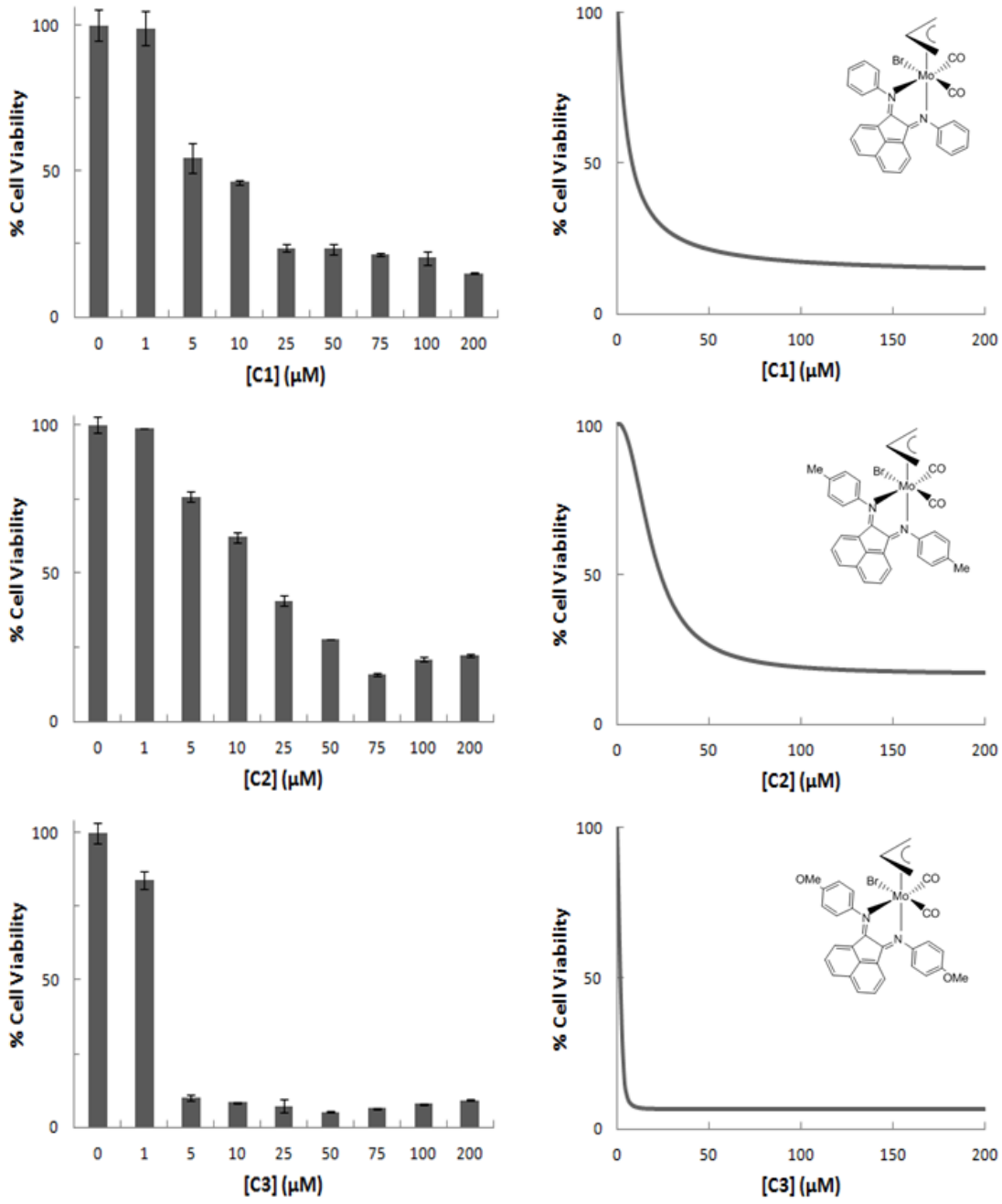

Figure 20 – *In vitro* cytotoxic assays for the complexes **C1 – C3** in HeLa after 48 h incubation. Histogram representing the relation between cell viability and the complex concentrations (1, 5, 10, 25, 50, 75, 100 and 200 µM) and dose-response curves obtained by nonlinear regression analysis for each complex.

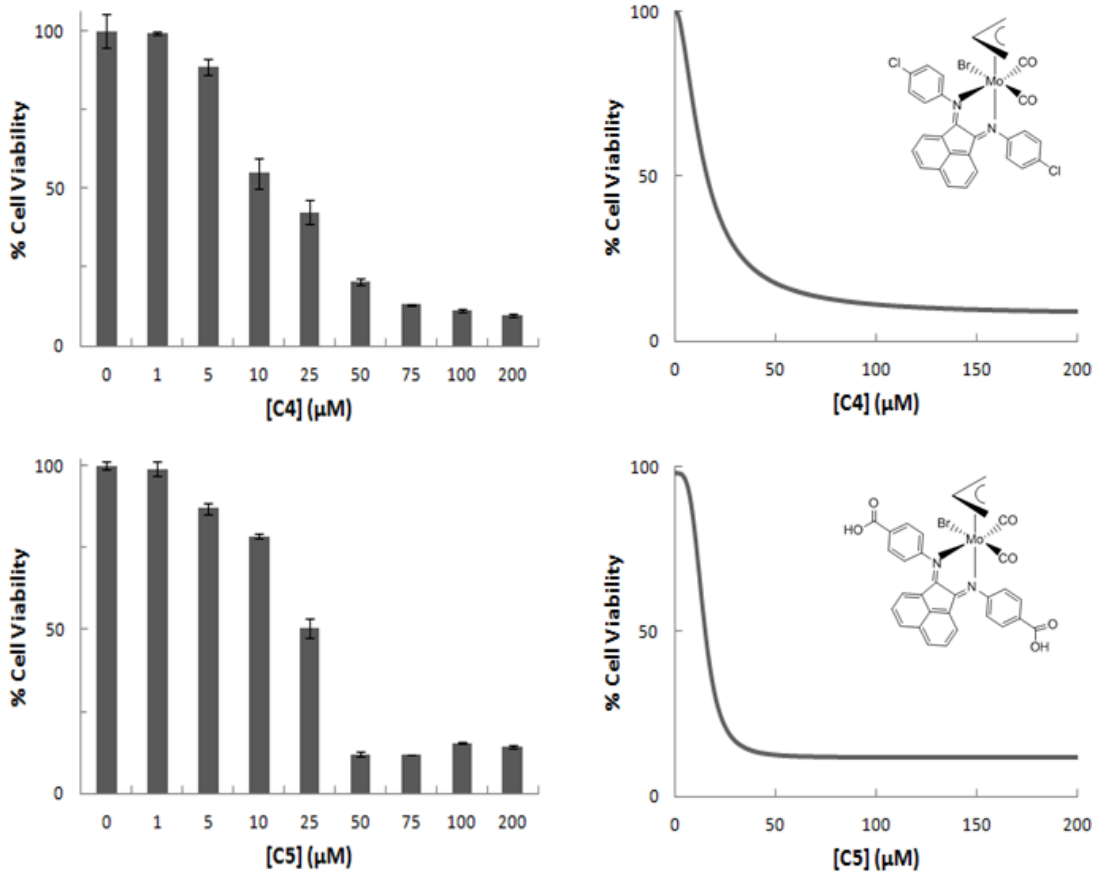

Figure 21 – *In vitro* cytotoxic assays for the complexes **C4** and **C5** in HeLa after 48 h incubation. Histogram representing the relation between cell viability and the complex concentrations (1, 5, 10, 25, 50, 75, 100 and 200 μM) and dose-response curves obtained by nonlinear regression analysis for each complex.

The IC_{50} values for the complexes **C1 – C5** in HeLa cells were calculated through the non linear fitting represented by the dose-response curves. For the other cell lines (MCF-7, MDA-MB-231, SW480 and Caco-2) the same protocol and data analysis for HeLa was followed (histograms and dose-response curves in **Annex** – **Figure 37** to **Figure 42**).

The IC_{50} values for the complexes **C1 – C5** in all the cell lines studied are shown in **Table 3**.

Table 3 – IC_{50} values (mean ± standard deviation) for the complexes **C1 – C5** tested in HeLa, MCF-7, MDA-MB-231, SW480 and Caco-2 cell lines.

IC_{50} (μM) 48 h					
Complex	**HeLa**	**MCF-7**	**MDA-MB-231**	**SW480**	**Caco-2**
C1	5.5 ± 1.18	> 75	> 100	12.7 ± 1.11	> 100
C2	21.5 ± 4.16	29.0 ± 16.36	> 100	10.1 ± 1.09	> 200
C3	3.2 ± 1.39	≈ 25	> 200	0.6 ± 0.11	> 200
C4	17.3 ± 3.49	42.2 ± 19.75	> 100	9.8 ± 4.02	> 100
C5	27.1 ± 3.52	98.4 ± 12.38	> 200	≈ 50	> 200

The results presented in the **Table 3** show that the molybdenum(II) complexes **C1 – C5** display a powerful cytotoxic activity *in vitro* in HeLa, MCF-7 and SW480 cell lines (IC_{50} < 100 μM), while MDA-MB-231 and Caco-2 cells seem to be more resistant to the complexes action (IC_{50} > 100 and 200 μM). All the cells lines studied are derived from adenocarcinomas (epithelial type): HeLa (cervical adenocarcinoma), MCF-7 and MDA-MB-231 (breast carcinoma) and SW480 and Caco-2 (colorectal adenocarcinoma). From previous work with Caco-2 cell subcultures [101], in general, these cells have a slow growth rate and are more resistant to contaminations and antibiotics than the other cell lines handled. It is expected that Caco-2 cells should be more resistant to xenobiotics, resulting in higher IC_{50} values. MDA-MB-231 cell resistance may be related to cell specificity and/or growth rate. This cell line has a fast growth rate (much higher than HeLa cells) which could possibly explain why the complexes action is ineffective.

In the cell lines where the IC_{50} values are below 100 μM, the complexes exhibited a strong cytotoxic effect in SW480 and HeLa cells, but are less toxic towards MCF-7. This behavior of the MCF-7 cells has also been observed in previous works [102, 103]. **C3** has the lowest IC_{50} value of the five complexes analyzed, being the most effective cytotoxic compound (with an IC_{50} of 3.2 μM in HeLa and 0.6 μM in SW480), whereas **C5** has the highest IC_{50} value compared to the other molybdenum(II) complexes (**C1 – C4**), which makes it the less toxic complex against the cell lines studied. Some complexes (**C1** and **C3**) have low IC_{50} values against HeLa (< 6 μM). These values are comparable to the classical chemotherapy drug cisplatin which has an IC_{50} < 10 μM in a wide range of cancer cell lines [104].

To determine the influence of the molybdenum(II) precursor (**P0**) and organic ligands (**L1**, **L2**, **L4** and **L5**) (**Figure 22**) on the complexes activity, cytotoxic assays *in vitro* were performed in HeLa.

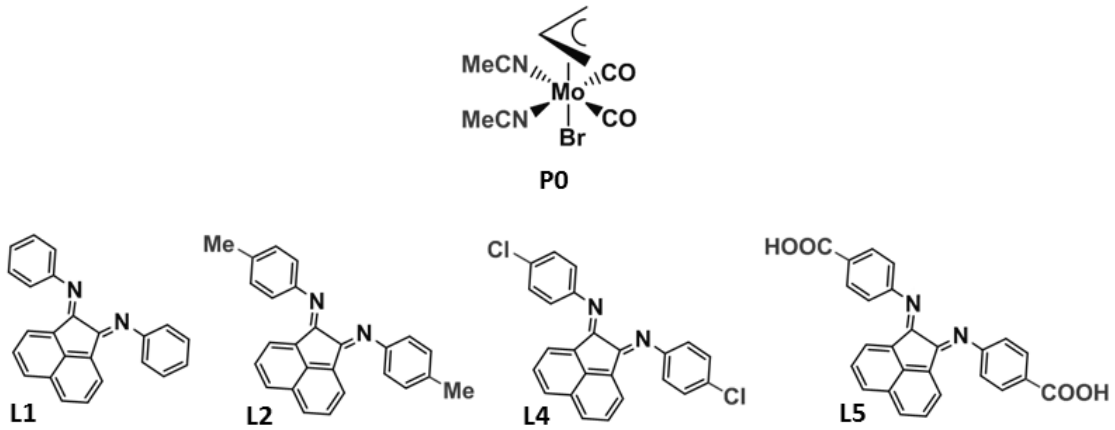

Figure 22 – Schematic structure of the molydenum precursor (**P0**) and organic ligands (**L1**, **L2**, **L4** and **L5**) tested in HeLa.

The relation between the cell viability and precursor (**P0**) concentration (1 – 200 µM) in HeLa is depicted in **Figure 23**. Histogram and dose-response curves obtained by nonlinear regression analysis for the ligands (**L1**, **L2**, **L4** and **L5**) are shown in **Figure 24**. The results represent an average of three independent experiments and each experiment includes ten replicates for each compound concentration.

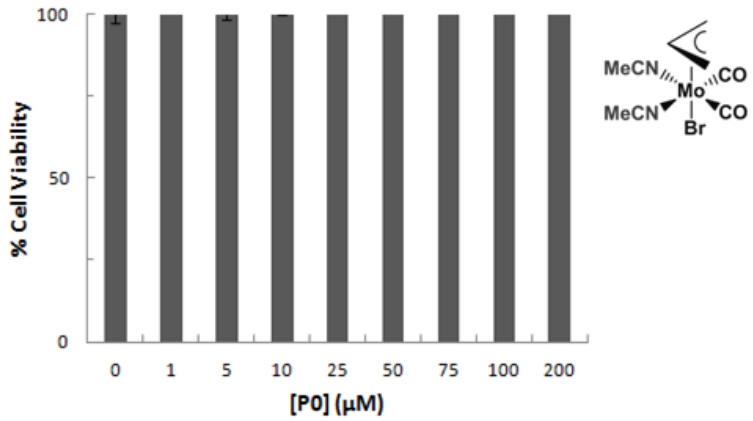

Figure 23 – *In vitro* cytotoxic assay for the precursor (**P0**) in HeLa after 48 h incubation. Histogram representing the relation between percentage of cell viability and the precursor concentrations (1, 5, 10, 25, 50, 75, 100 and 200 µM).

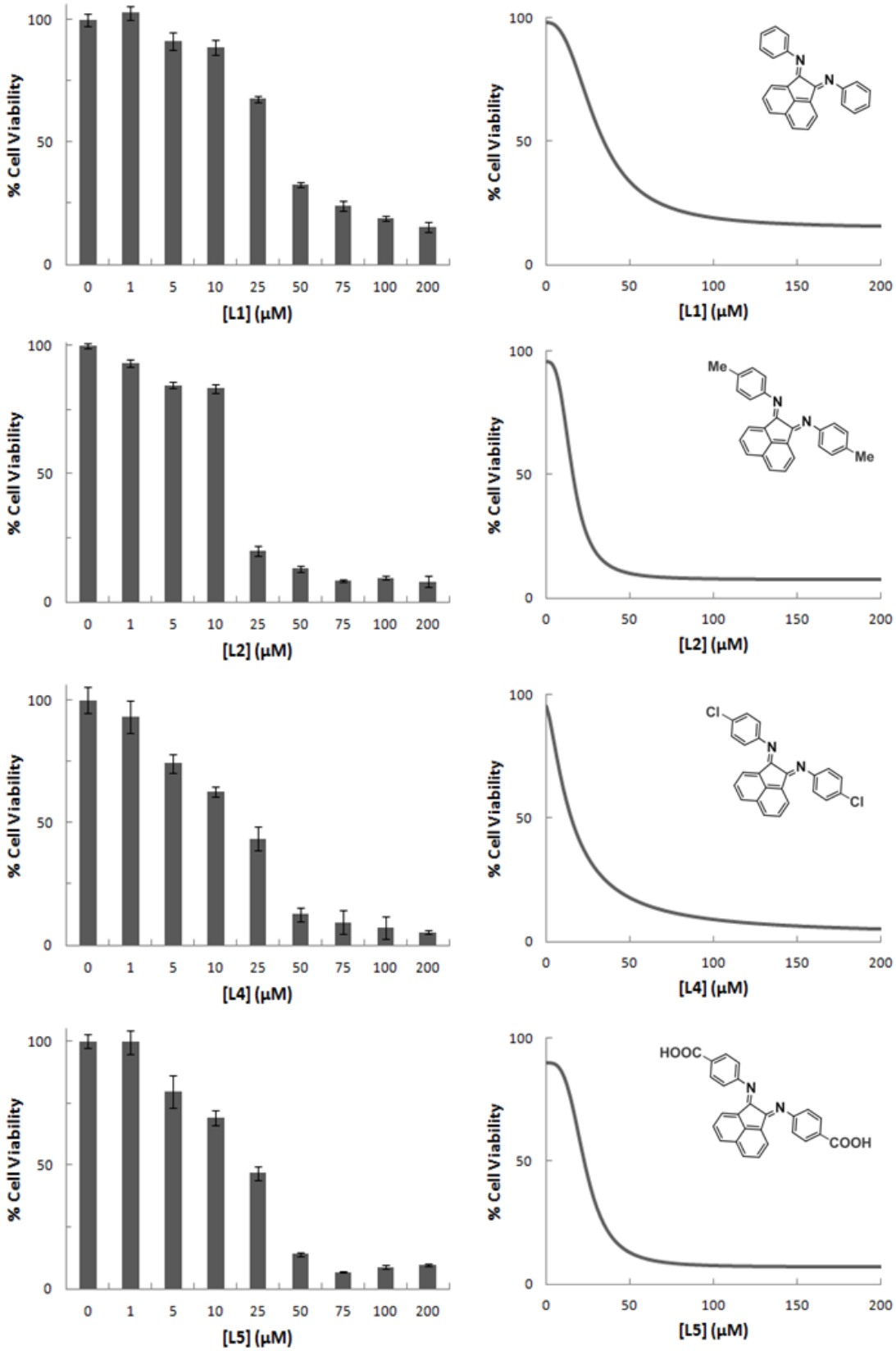

Figure 24 – *In vitro* cytotoxic assays for the ligands (**L1**, **L2**, **L4** and **L5**) in HeLa after 48 h incubation. Histogram representing the relation between cell viability and the complex concentrations (µM) and dose-response curves obtained by nonlinear regression analysis for each ligand.

The IC_{50} values for the ligands and the precursor in HeLa are summarized in **Table 4**.

Table 4 – IC_{50} values (mean ± standard deviation) in HeLa for the ligands (**L1 – L5**) and the molybdenum(II) precursor (**P0**).

IC_{50} (μM) 48h	
Compound	**IC_{50} (μM)**
L1	29.4 ± 1.22
L2	17.1 ± 2.92
L3	n.t.
L4	16.9 ± 1.49
L5	20.3 ± 3.755
P0	> 200

The results presented in the **Table 4** show that all tested ligands (**L1**, **L2**, **L4** and **L5**) have IC_{50} values ranging from 17 to 30 μM (higher IC_{50} values than their respective complex in the same conditions), which indicates a lower cytotoxic activity than the molybdenum(II) complexes. The effect on the cell viability of the precursor **P0** was also tested to determine the contribution of the molybdenum(II) component in the cytotoxic activity of the complex. The IC_{50} value for **P0** was over 200 μM. Since both precursor and ligands have elevated IC_{50} values when compared to their respective complexes, it appears to be the combination of the precursor + ligand that creates a complex with a more powerful cytotoxicity than its components separately.

The use of molybdenum complexes in chemotherapy is related to its expected low toxicity towards human cells. Molybdenum salts are very similar to phosphate salts existent in body fluids and cellular environment. Molybdenum is an important cofactor in several human enzymes such as aldehyde oxidase, sulfite oxidase and xanthine oxidase [89]. Therefore two molybdates (compound containing a molybdenum oxoanion in its highest oxidation state, VI) were tested in HeLa cells: sodium molybdate dihydrate ($Na_2MoO_4.2H_2O$) and ammonium heptamolybdate [$(NH_4)_6Mo_7O_{24}\cdot 4H_2O$]. The histograms obtained containing cell viability *vs* molybdate concentrations are in **Figure 25** and **Figure 26**.

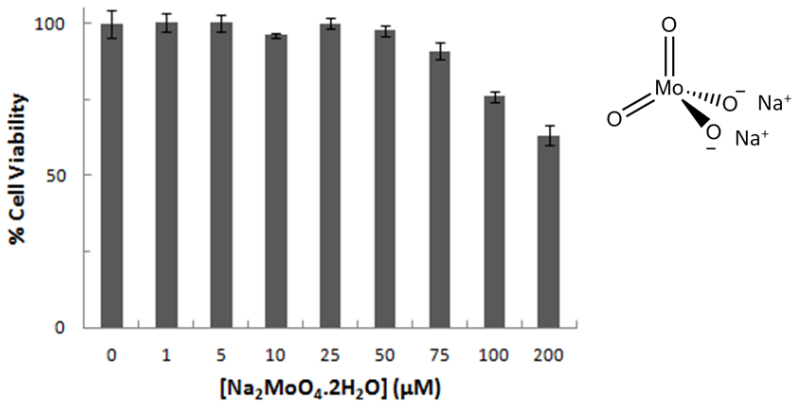

Figure 25 – *In vitro* cytotoxic assay for sodium molybdate dihydrate ($Na_2MoO_4.2H_2O$) in HeLa after 48 h incubation. Histogram representing the relation between percentage of cell viability and the salt concentrations (1, 5, 10, 25, 50, 75, 100 and 200 µM).

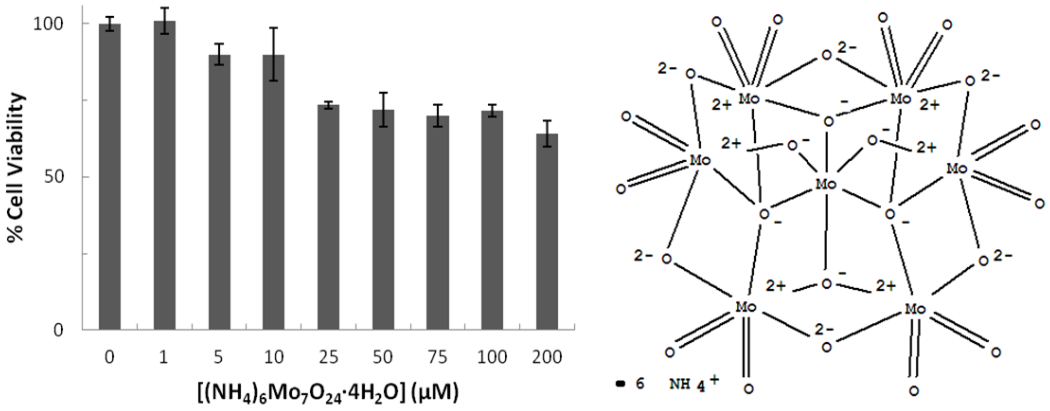

Figure 26 – *In vitro* cytotoxic assay for ammonium heptamolybdate [$(NH_4)_6Mo_7O_{24}\cdot4H_2O$] in HeLa after 48 h incubation. Histogram representing the relation between percentage of cell viability and the salt concentrations (1, 5, 10, 25, 50, 75, 100 and 200 µM).

The histograms shown in the previous figures show that both $Na_2MoO_4.2H_2O$ and $(NH_4)_6Mo_7O_{24}\cdot4H_2O$ have an IC_{50} value > 200 µM, indicating that these molybdenum oxoanions do not affect cellular growth.

The cytotoxic effect *in vitro* of classical DNA intercalators – doxorubicin and ethidium bromide – has also been tested in HeLa using the MTT assay. Doxorubicin is a drug used in chemotherapy that by intercalates with the DNA molecule and inhibits the DNA replication process. Ethidium bromide is a potent mutagen that intercalates with double stranded DNA, therefore is commonly used as a fluorescent dye to detect DNA under ultraviolet light [35].

The histograms with cell viability *vs* compound concentrations (1, 5, 10, 25, 50, 75, 100 and 200 µM) and also the dose-response curves obtained by nonlinear regression analysis in HeLa are shown in **Figure 27**. These results represent an average of two independent experiments and each experiment includes ten replicates for each compound concentration.

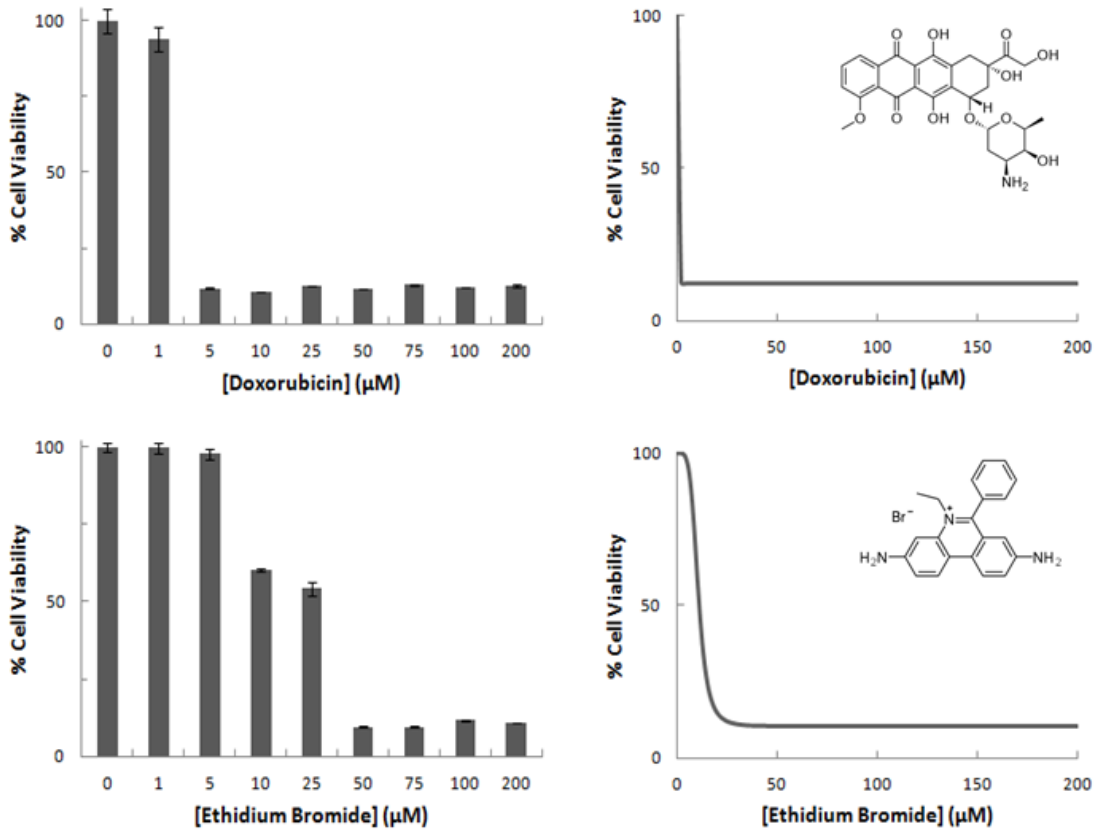

Figure 27 – *In vitro* cytotoxic assays for doxorubicin and ethidium bromide in HeLa cells after 48 h incubation. Histogram representing the relation between cell viability and the compound concentrations (1, 5, 10, 25, 50, 75, 100 and 200 µM) and dose-response curves obtained by nonlinear regression analysis.

The IC_{50} values for doxorubicin and ethidium bromide in HeLa are shown in **Table 5**.

Table 5 – IC_{50} values (mean ± standard deviation) in HeLa for the DNA intercalators: doxorubicin and ethidium bromide.

IC_{50} (μM) 48h	
Compound	**IC_{50} (μM)**
Doxorubicin	1.4 ± 0.49
Ethidium Bromide	10.5 ± 1.12

The results show that doxorubicin has a powerful cytotoxic activity against HeLa cells, with a very low IC_{50} value of 1.4 ± 0.49 μM (comparable to results found in the literature [105]). Ethidium bromide also presents a strong cytotoxic effect in HeLa (IC_{50} = 10.5 ± 1.12 μM) [106], but due to its toxicity and mutagenic characteristics, there are not many studies investigating the potential role of ethidium bromide as a chemotherapeutic agent. These IC_{50} results (1.4 ± 0.49 μM and 10.5 ± 1.12 μM) are comparable to the ones obtained for the molybdenum complexes (**C1 – C5**) in HeLa cells (IC_{50} values ranging from 3.2 ± 1.39 to 27.1 ± 3.52 μM).

Effect of the complexes incubation time on cell viability

To investigate the effect of the molybdenum(II) complexes **C1 – C5** in HeLa cells in more detail, the relation between incubation time and cell viability was also studied. The MTT protocol was performed allowing the cell lines to be exposed to the same compound concentrations (1, 5, 10, 25, 50, 75, 100 and 200 μM) with different incubation times: 1, 4, 8, 24, 48 and 72 hours. The obtained results are represented in **Figure 28**.

The IC_{50} values for each hour were determined through nonlinear regression analysis and are shown in **Table 6** (dose-response curves not shown).

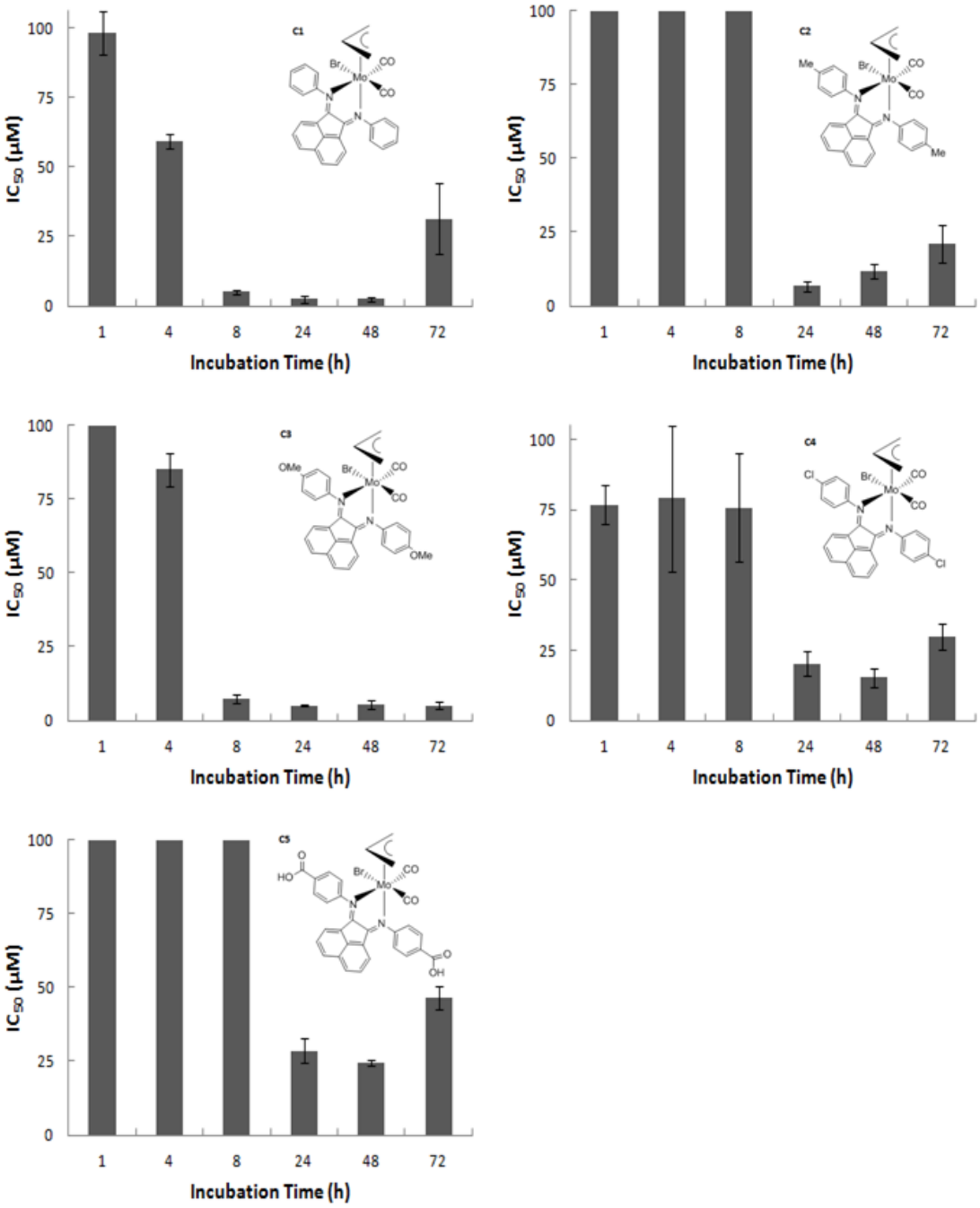

Figure 28 – *In vitro* cytotoxic assays for the complexes **C1 – C5** in HeLa. Histogram representing the relation between IC50 and different incubation times (1, 4, 8, 24, 48 and 72 hours).

Table 6 – IC_{50} values (mean ± standard deviation) for the complexes **C1 – C5** against HeLa with different incubation times (1, 4, 8, 24, 48 and 72 hours).

IC_{50} (μM)						
Complex	**1 h**	**4 h**	**8 h**	**24 h**	**48 h**	**72 h**
C1	98.1 ± 7.80	59.2 ± 2.66	5.1 ± 0.89	2.4 ± 1.39	2.6 ± 0.79	31.4 ± 12.64
C2	> 200	> 100	> 100	6.7 ± 1.73	11.8 ± 2.41	20.9 ± 6.39
C3	> 200	> 75	7.4 ± 1.27	5.1 ± 0.27	5.4 ± 1.42	5.1 ± 1.39
C4	76.8 ± 7.11	81.8 ± 26.13	75.8 ± 19.17	20.2 ± 4.31	15.2 ± 3.18	29.9 ± 4.63
C5	> 200	> 200	> 100	28.6 ± 4.15	24.5 ± 1.15	46.4 ± 3.94

As shown in **Figure 28** and **Table 6**, the molybdenum(II) complexes inhibit cell proliferation in a time-dependent way. The IC_{50} values of the complexes **C1 – C5** decrease until 48 h incubation time (and increase after). All the complexes reach their maximum cytotoxicity at 48 h (although there are no significant differences between 24 h and 48 h values). In the first hours of incubation (1 h and 4 h) there are no considerable changes in the IC_{50} values, which suggest that the complexes take time to penetrate the cell membrane and reach their biological target. At 8 h of incubation, **C1** and **C3** complexes (with the lowest IC_{50} in HeLa) already have IC_{50} values similar to the maximum cytotoxicity (24 h / 48 h), while the other complexes (**C2**, **C4** and **C5**) still have IC_{50} values near 100 μM. After 72 h of incubation, most of the complexes have less cytotoxic activity (higher IC_{50} values) than the optimum values appointed 24 h before. These results may be explained by the decomposition of the complexes in the aqueous medium, preventing their mechanism of action and consequently the antitumoral effect.

3.4) DNA Binding Studies

To study the possible interaction between the molybdenum complexes studied (**C1 – C5**) and DNA, a DNA binding assay *in vitro* was performed using electronic absorption titration spectroscopy.

The absorbance of the CT DNA solution was measured in the beginning of each experiment and the ratio Abs_{260} / Abs_{280} was between 1.8 – 1.9, indicating that the DNA was sufficiently free of protein contamination [69]. The addition of CT DNA (0 – 200 µM) to the 20 µM metal complex solution led to spectral changes (**Figure 29** to **Figure 33**).

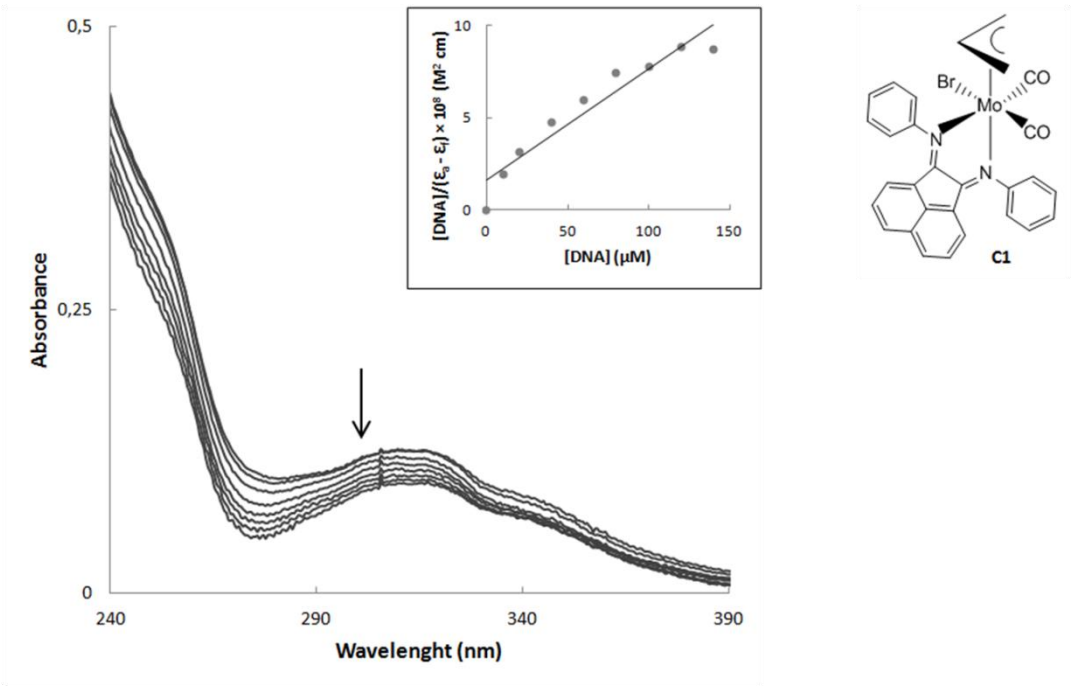

Figure 29 – UV-Vis absorption spectra of **C1** (20 µM) in Tris buffer in the presence of increasing amounts of CT DNA (0 – 150 µM). The inset plot represents [DNA] / (ε_a - ε_f) (M^2 cm) *vs* [DNA] (µM) for the titration. The arrow indicates the absorbance changes monitored at 305 nm upon increasing DNA concentration.

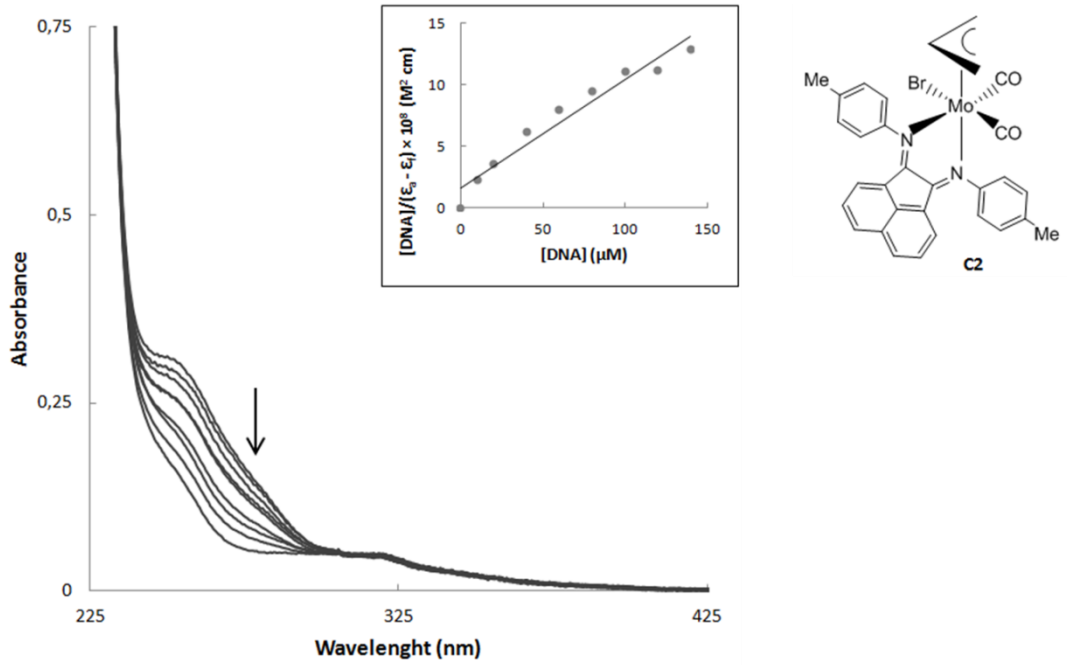

Figure 30 – UV-Vis absorption spectra of **C2** (20 µM) in Tris buffer in the presence of increasing amounts of CT DNA (0 – 150 µM). The inset plot represents [DNA] / (ε_a - ε_f) (M^2 cm) *vs* [DNA] (µM) for the titration. The arrow indicates the absorbance changes monitored at 318 nm upon increasing DNA concentration.

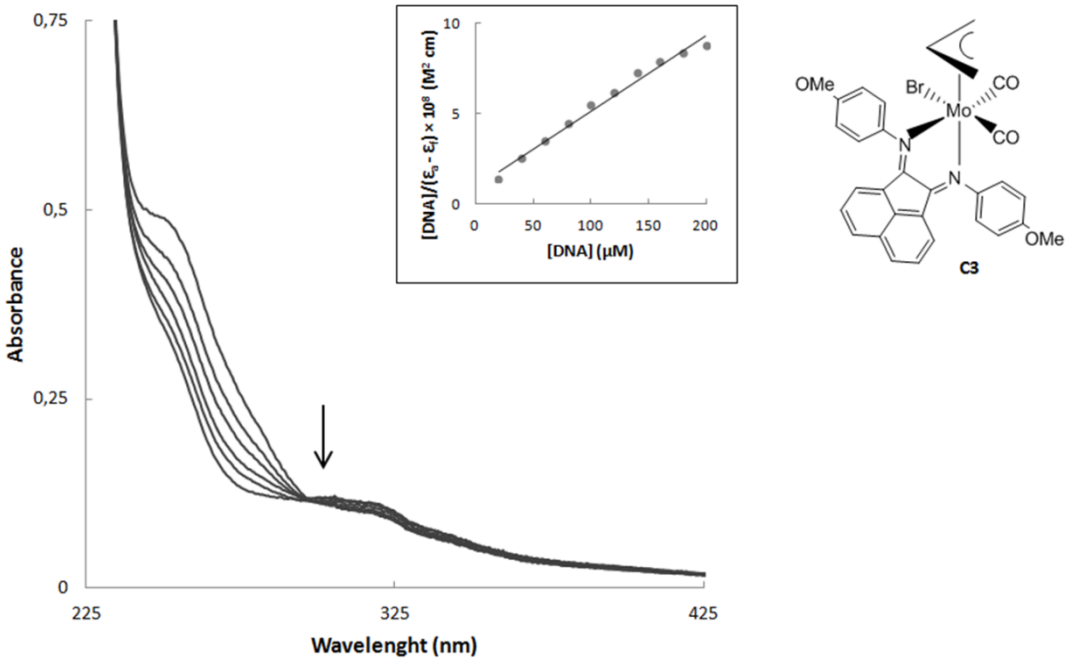

Figure 31 – UV-Vis absorption spectra of **C3** (20 µM) in Tris buffer in the presence of increasing amounts of CT DNA (0 – 200 µM). The inset plot represents [DNA] / (ε_a - ε_f) (M^2 cm) *vs* [DNA] (µM) for the titration. The arrow indicates the absorbance changes monitored at 304 nm upon increasing DNA concentration.

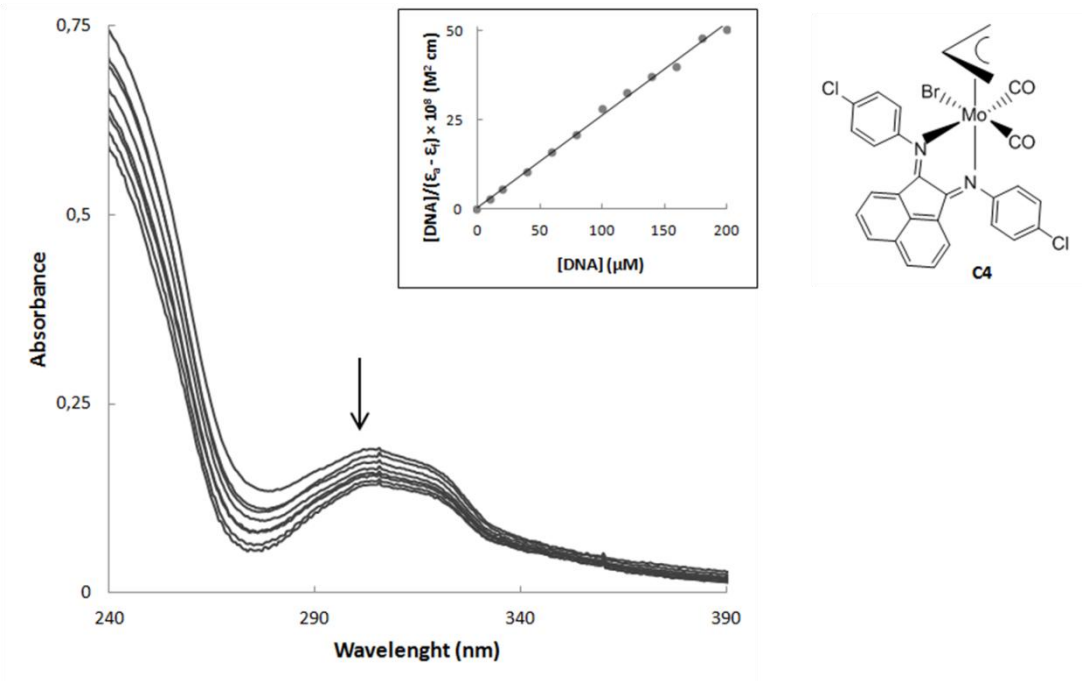

Figure 32 – UV-Vis absorption spectra of **C4** (20 μM) in Tris buffer in the presence of increasing amounts of CT DNA (0 – 200 μM). The inset plot represents [DNA] / (ε_a - ε_f) (M^2 cm) *vs* [DNA] (μM) for the titration. The arrow indicates the absorbance changes monitored at 303 nm upon increasing DNA concentration.

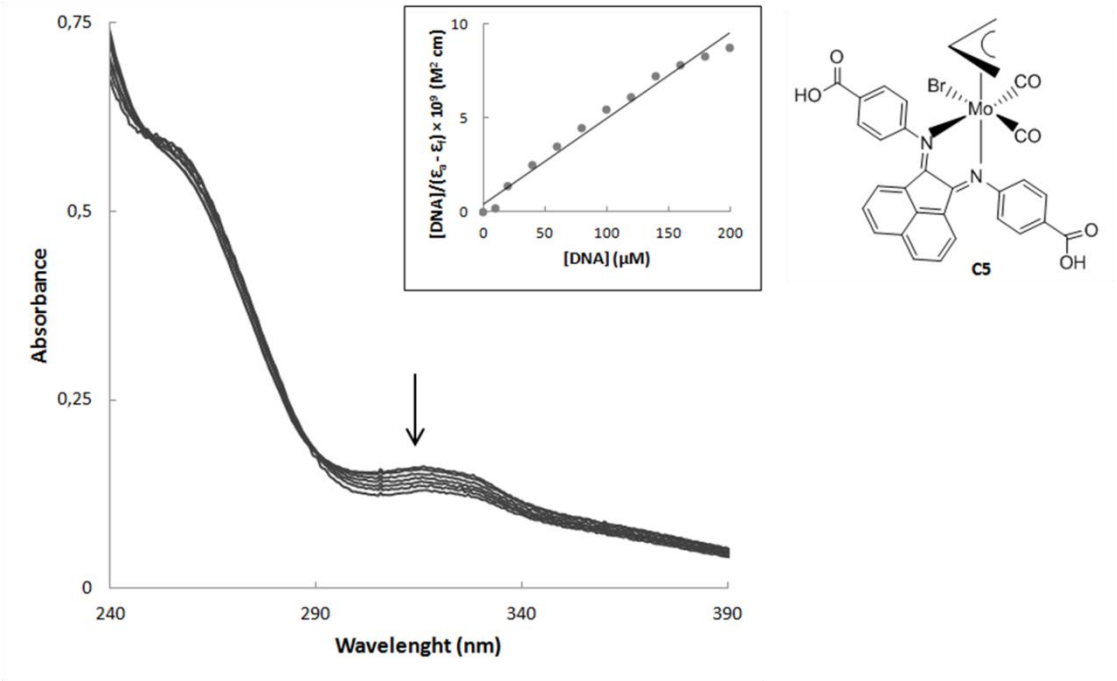

Figure 33 – UV-Vis absorption spectra of **C5** (20 μM) in Tris buffer in the presence of increasing amounts of CT DNA (0 – 200 μM). The inset plot represents [DNA] / (ε_a - ε_f) (M^2 cm) *vs* [DNA] (μM) for the titration. The arrow indicates the absorbance changes monitored at 316 nm upon increasing DNA concentration.

Regarding the absorption spectra of the molybdenum(II) complexes **C1 – C5** (**Figure 29** to **Figure 33**), a decrease in the intensity of the complexes absorbance (hypochromism) is observed, accompanied by a small red-shift (batochromism) of the monitored bands upon increasing CT DNA concentration. This indicates a possible intercalation of the complexes with the DNA [99]. The inset plot of each previous figure represents [DNA] / (ε_a - ε_f) (M^2 cm) *vs* [DNA] (μM) for the respective titration, and by the ratio slope / intercept, it is possible to calculate the intrinsic binding constant (K_b). The obtained values of K_b are summarized in **Table 7**.

Table 7 – Values of intrinsic binding constant (K_b) calculated for the complexes **C1 – C5**.

Complex	K_b (M^{-1})
C1	3.77×10^4
C2	2.11×10^4
C3	4.47×10^4
C4	4.01×10^4
C5	6.53×10^4

The K_b values are very similar for all the complexes with the same order of magnitude (10^4), which could indicate a possible interaction of the compounds with DNA. **C5** and **C3** have higher intrinsic binding constant values ($K_b = 6.53 \times 10^4$ M^{-1} and 4.47×10^4 M^{-1}) comparing to the other complexes, indicating that these complexes bind more strongly to the DNA. **C2** has the lowest K_b value ($K_b = 2.11 \times 10^4$ M^{-1}), which could indicate that this complex has a weaker interaction with DNA. These molybdenum(II) complexes have ligands (nitrogen bidentate α-diimines) with extended π systems which can intercalate with DNA [97, 99].

The tendency of these K_b values is related to the IC_{50} values studied (**Chapter 3.3**) for most of the complexes. **C3** has the highest cytotoxic against HeLa (with the the lowest IC_{50} value of the five complexes: 3.2 ± 1.39 μM) and **C2** and **C5** have higher IC_{50} values (21.5 ± 4.16 μM and 27.1 ± 3.52 μM, respectively), indicating a lower cytotoxic effect in HeLa cells. These tendency could indicate that the antitumoral effect of these molybdenum(II) is due to their interaction with DNA (except for complex **C5**). On one hand, **C5** has the highest K_b value (indicating a strong binding of this complex to the

DNA) but, on the other hand, **C5** also has the highest IC_{50} value comparing with the other complexes (**C1 – C4**), which indicates lower cytotoxicity against cancer cell lines. This suggests that complex **C5** maybe does not reach in its totality to the nucleus (possibly due to its low solubility in aqueous medium) and does not have the chance to bind to DNA.

It is also important to mention that these organometallic complexes can also have a mechanism of action (and consequent antitumoral effect) that is not fully due to interaction with the DNA.

The classical DNA intercalators, doxorubicin and ethidium bromide [35], where also studied and DNA binding assays *in vitro* were performed for electronic absorption titration spectroscopy under the same conditions described for the complexes **C1 – C5**. The obtained spectra are represented in **Figure 34** and **Figure 35** and the K_b values calculated for these classical DNA intercalators are in **Table 8**.

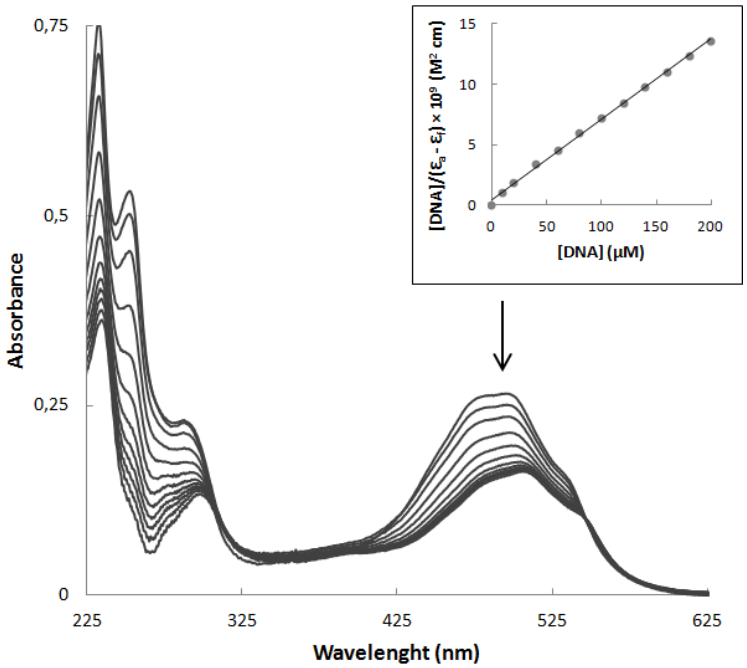

Figure 34 – UV-Vis absorption spectra of **Doxorubicin** (20 μM) in Tris buffer in the presence of increasing amounts of CT DNA (0 – 200 μM). The arrow indicates the absorbance changes monitored at 495 nm upon increasing DNA concentration. The inset plot represents [DNA] / (ε_a - ε_f) (M^2 cm) *vs* [DNA] (μM) for the titration.

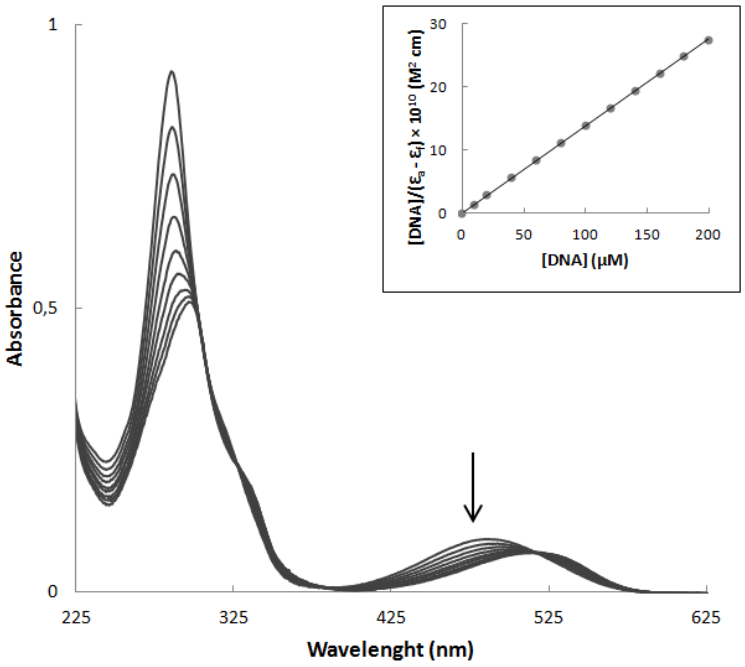

Figure 35 – UV-Vis absorption spectra of **Ethidium Bromide** (20 μM) in Tris buffer in the presence of increasing amounts of CT DNA (0 – 200 μM). The arrow indicates the absorbance changes monitored at 479 nm upon increasing DNA concentration. The inset plot represents [DNA] / (ε_a - ε_f) (M^2 cm) *vs* [DNA] (μM) for the titration.

Table 8 – Values of intrinsic binding constant (K_b) calculated for the intercalators: doxorubicin and ethidium bromide.

Compound	K_b (M^{-1})
Doxorubicin	1.52×10^5
Ethidium Bromide	1.02×10^6

In the absorption spectra for doxorubicin and ethidium bromide, a decrease in the intensity of the compound absorbance (hypochromism) and an evident red-shift (batochromism) of the monitored bands are observed upon increasing CT DNA concentration. This indicates DNA binding by intercalation and is confirmed by the K_b values obtained [99].

The K_b values of the complexes (**C1 – C5**) are similar to those obtained for the classical intercalators studied, although more studies are necessary to understand the exact interaction between these metal complexes and DNA.

In order to complement the obtained DNA binding results, and in addition to previous studies, cyclic voltammetry of the complexes **C1** – **C5** with increasing concentrations of CT DNA were attempted. However, these molybdenum complexes would not dissolve in the buffer solution necessary for the experiment and these studies could not be continued. DNA thermal denaturation studies were also attempted, for the calculation of melting temperatures (T_m) of the DNA and DNA + molybdenum(II) complex, using absorption UV-VIS spectroscopy. However, none of the UV-Vis spectrophotometers available reached temperatures high enough to denature the CT DNA and the melting transition curves could not be observed. As a result, neither of these studies was completed.

4) CONCLUSIONS AND PERSPECTIVES

The increasing number of metal complexes that have a cytotoxic activity against cancer cells contributed to a general comprehension that the mechanism of action of these organometallic compounds could be adjusted by an appropriate choice of the metal, its oxidation state and of the ligands [82, 83], providing almost unlimited combinations.

Five molybdenum(II) complexes, [MoBr(η^3-C_3H_5)(CO)$_2${1,4-(4-**X**)phenyl-2,3-naphthalenediazabutadiene}] (X = H (**C1**), Me (**C2**), OMe (**C3**), Cl (**C4**) and COOH (**C5**), **Figure 36**) were studied with the aim of elucidating their cytotoxic activity in several tumoral cell lines, possible mechanism of action and their potential for use in chemotherapy.

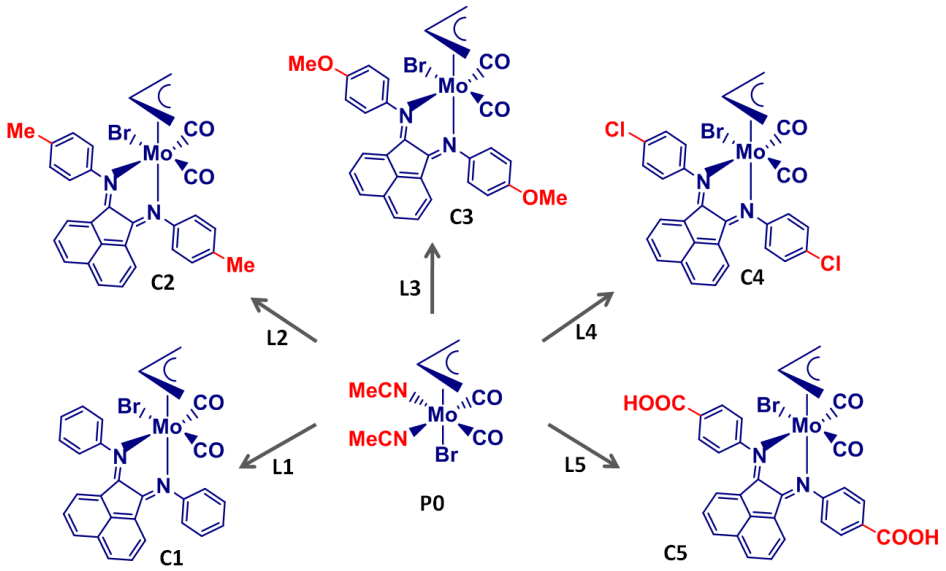

Figure 36 – Schematic structure of the molydenum complexes studied (**C1 – C5**) and their precursor (**P0**).

The cyclic voltammetry experiments showed that complexes **C1 – C5** have intense oxidation waves and a lower reduction wave and the difference between the oxidation and reduction potentials ($\Delta E = E_p^{ox} - E_p^{red} > 0.059$) indicates that these complexes have an irreversible oxidation behavior. Oxidations are associated with the Mo(II) to Mo(III) conversion while reductions occur at the α-diimine ligand.

The IC_{50} values (compound concentration that causes 50% of cell viability) obtained from the cytotoxic activity studies *in vitro*, at 48 h are summarized in **Table 9**.

Table 9 – IC_{50} values (mean ± SD) for all the compounds tested in HeLa cells in this work.

IC_{50} (μM) 48h	
Compound	**HeLa**
C1	5.5 ± 1.18
C2	21.5 ± 4.16
C3	3.2 ± 1.39
C4	17.3 ± 3.49
C5	27.1 ± 3.52
L1	29.4 ± 1.22
L2	17.1 ± 2.92
L3	n.t.
L4	16.9 ± 1.49
L5	20.3 ± 3.755
P0	> 200
$Na_2MoO_4.2H_2O$	> 200
$[(NH_4)_6Mo_7O_{24}\cdot 4H_2O]$	> 200
Doxorubicin	1.4 ± 0.49
Ethidium Bromide	10.5 ± 1.12

Complexes **C1 – C5** have a powerful cytotoxic activity in these conditions against several cell lines (HeLa, SW480 and MCF-7) and a smaller antitumoral effect in other cells (MDA-MB-231 and Caco-2). **C3** is the most cytotoxic complex, with lowest IC_{50}, while **C5** has the highest IC_{50} value of all cell lines tested. The cytotoxicity of these organometallic complexes is mainly due to the α-diimine ligands (**L1 – L5**), since the precursor (**P0**) does not kill cancer cells (IC_{50} > 200 μM, in Hela cells). Although both precursor and ligands have elevated IC_{50} values when compared to their respective complexes, the ligands exhibit some activity. Therefore, it seems that the combination of the precursor + ligand creates a complex with a more powerful cytotoxicity than its components separately. **C1** and **C3** have low IC_{50} values against HeLa (IC_{50} < 6 μM), which are comparable to the classical chemotherapy drug, cisplatin (IC_{50} < 10 μM in a wide range of cancer cell lines) [104]. Therefore, these two complexes can possibly be good candidates to chemotherapeutical drugs, since molybdenum is less toxic metal *in vivo* than, for example, platinum. These IC_{50} values are also comparable to the ones obtained for the DNA intercalators, doxorubicin (IC_{50} = 1.4 ± 0.49 μM) and ethidium bromide (IC_{50} = 10.5 ± 1.12 μM) obtained in HeLa cells, which may indicate that the molybdenum(II) organometallic complexes may intercalate with the DNA.

Absorption titration spectroscopy studies addressed the DNA-complexes interaction and the results showed that complexes **C1 – C5** interact with CT DNA, possibly through intercalation, with intrinsic binding constant (K_b) values ranging from 2.11 x 10^4 M^{-1} to 6.53 x 10^4 M^{-1}. These K_b values are not too much lower than to the ones obtained for the classical intercalators, doxorubicin (K_b = 1.52 x 10^5 M^{-1}) and ethidium bromide (K_b = 1.02 x 10^6 M^{-1}) (**Table 10**).

Table 10 – Values of intrinsic binding constant (K_b) for all the compounds tested in this work.

Complex	K_b (M^{-1})
C1	3.77 x 10^4
C2	2.11 x 10^4
C3	4.47 x 10^4
C4	4.01 x 10^4
C5	6.53 x 10^4
Doxorubicin	1.52 x 10^5
Ethidium Bromide	1.02 x 10^6

If the complexes **C1 – C5** interact with CT DNA *in vitro*, it is possible that this process may also occur *in vivo*, however more studies are necessary to understand the exact interaction between these metal complexes and DNA and to elucidate the remaining mechanisms involved in the activity of these molybdenum(II) complexes.

Cellular molybdenum uptake assays and fluorescence microscopy (with binding of an adequate chromophore) could indicate the localization of the organometallic complexes inside the cell, elucidating their biological targets. Techniques, such as circular dichroism and atomic force microscopy (AFM) can be used to observe structural changes in the DNA, in the presence of the complexes and complement the absorption titration spectroscopy studies. Interaction of the organometallic complexes with molybdenum cofactor dependant enzymes, such as aldehyde oxidase, sulfite oxidase and xanthine oxidase, could also evidence the possible interaction of these molybdenum complexes with other biological targets, revealing other mechanisms of action not involving DNA intercalation. In long-term investigations, the effect of these molybdenum complexes should be studied *in vivo*, as chemotherapeutical agents.

5) ACKNOWLEDGEMENTS

Gostaria de começar por agradecer às minhas orientadoras, Dra. Margarida Meireles e Dra. Maria José Calhorda, por me aceitarem neste fantástico projeto de Mestrado e um obrigado especial por toda a ajuda, ânimo e orientação prestados ao longo destes anos.

Queria também agradecer a todos os membros do grupo de Química Inorgânica e Teórica que, de uma forma ou de outra, me ajudaram neste projeto. Um muito obrigado em especial à Marta Saraiva, pelo apoio constante e imprescindível na síntese e caracterização química dos complexos estudados e pela motivação, tanto dentro do laboratório como fora dele. Agradeço também à Dra. Carla Nunes e Cristina Fernandes, pela disponibilização do laboratório, para as sínteses químicas e ensaios de espectrofotometria do UV-Vis e à Dra. Ana Mourato pela colaboração e ajuda, que foram essenciais, nos ensaios eletroquímicos.

Um agradecimento em geral à Faculdade de Ciências da Universidade de Lisboa, particularmente ao Departamento de Química e Bioquímica, pelo fornecimento das condições necessárias para este projeto e para todas as pessoas que colaboraram para tal, incluindo todos os professores que tive ao longo da Licenciatura e Mestrado em Bioquímica, e todos os outros que fui conhecendo de outros grupos, pelos ensinamentos que me deram.

Queria também agradecer ao Daniel Bandarra e ao Miguel Lopes por me terem apresentado e aliciado para este projeto, de modo a tentar continuar a fazer o excelente trabalho deixado por eles, embora o tempo com a vossa companhia no laboratório tenha sido curto, aprendi várias abordagens e técnicas experimentais essenciais para esta Dissertação. À Ana Cristina Silva, Gonçalo Covas, Pedro Falé, Ana Morna, Hugo Santos e Fátima Cardoso, obrigado pela vossa companhia e troca de ideias (e ocasional troca de linhas celulares) dentro da faculdade e pela amizade fora dela.

Um obrigado à Maria João Lima e ao Carlos Neves por me terem convidado a passar um Verão na Escócia e pela oportunidade de estagiar brevemente com eles no Institute of Medical Sciences da Universidade de Aberdeen. Aprendi imensas coisas novas nessa curta temporada no laboratório, que me ajudaram neste projeto.

Gostaria de agradecer de um modo geral a todos os meus amigos, tanto aos da ilha: Ana Cristina Borges, Joana Costa, Loíde Soares, Marisa Raposo e Pedro Valadão, como os que conheci aqui no “contenante”, com ênfase para: Ana Filipa Ribeiro, Armando Cruz, Bruno Moraes, Carlos Neves, Daniel Bandarra, Maria João Lima, Mariana Oliveira, Miguel Lopes e Sara Carvalhal, como ainda aos que vivem longe fisicamente, mas não longe do coração: Leornan Melo e Verônica Brito. Um muito obrigado pela vossa amizade e pelo tempo que passamos juntos.

Por fim, quero deixar um sincero e o maior agradecimento à minha família. Aos meus pais e avós, madrinhas, tios e primos, um muitíssimo obrigado por tudo e por sempre terem acreditado em mim e me terem apoiado em todas as situações.

Gostaria ainda de agradecer a todos os que dedicaram um bocadinho do seu tempo a ler esta Dissertação. Obrigado pela vossa atenção!

6) REFERENCES

[1] World Health Organization website – http://www.who.int/cancer/en/

[2] Abbott RG, Forrest S, Pienta KJ. Simulating the hallmarks of cancer. *Artif Life*, 12(4): 617-634, 2006.

[3] Schulz WA. Molecular Biology of Human Cancers – An Advanced Student's Textbook. *Springer*, 2007.

[4] Garrett MD. Cell cycle control and cancer. *Current Science*, 81(5): 515-522, 2001.

[5] Hanahan D, Weinberg RA. The Hallmarks of Cancer. *Cell*, 100: 57-70, 2000.

[6] Colotta F, Allavena P, Sica A, Garlanda C, Mantovani A. Cancer-related inflammation, the seventh hallmark of cancer: links to genetic instability. *Carcinogenesis*, 30(7): 1073-1081, 2009.

[7] Cavallo F, De Giovanni C, Nanni P, Forni G, Lollini PL. 2011: the immune hallmarks of cancer. *Cancer Immunology, Immunotherapy*, 60(3): 319-26, 2011.

[8] Hanahan D, Weinberg RA. The Hallmarks of Cancer: The Next Generation. *Cell*, 144: 646-674, 2011.

[9] Jemal A, Siegel R, Ward E. Cancer Facts & Figures 2012. *American Cancer Society*, 2012.

[10] McKnight JA. Principles of Chemotherapy. *Clinical Techniques in Small Animal Practice*, 18(2): 67-72, 2003.

[11] Knowles MA, Selby PJ. Introduction to the Cellular and Molecular Biology of Cancer. *Oxford University Press*, 2005.

[12] Chabner BA, Roberts TG Jr. Timeline: Chemotherapy and the war on cancer. *Nature Reviews Cancer*, 5(1): 65-72, 2005.

[13] Papac RJ. Origins of cancer therapy. *Yale Journal of Biology and Medicine*, 74(6): 391–398, 2001.

[14] Diehl V. Advanced Hodgkin's disease: ABVD is better, yet is not good enough! *Journal of Clinical Oncology*, 21(4): 583-585, 2003.

[15] Kaplan HS. Hodgkin's disease: biology, treatment, prognosis. *Blood*, 57(5): 813-822, 1981.

[16] Gilman A. The initial clinical trial of nitrogen mustard. *American Journal of Surgery*, 105: 574-578, 1963.

[17] Farber S, Diamond LK, Mercer RD, Sylvester RF Jr, Wolff JA. Temporary Remissions in Acute Leukemia in Children Produced by Folic Acid Antagonist, 4-Aminopteroyl-Glutamic Acid (Aminopterin). *The New England Journal of Medicine*, 238: 787-793, 1984.

[18] Hitchings GH, Elion GB. The chemistry and biochemistry of purine analogs. *Annals of the New York Academy of Sciences*, 60(2): 195-199, 1954.

[19] Frei E 3rd, Karon M, Levin RH, Freireich EJ. The effectiveness of combinations of antileukemic agents in inducing and maintaining remission in children with acute leukemia. *Blood*, (5):642-656, 1965.

[20] Rosenberg B, Van Camp L, Krigas T. Inhibition of Cell Division in Escherichia coli by Electrolysis Products from a Platinum Electrode. *Nature* 205, 698-699, 1965.

[21] Ho YP, Au-Yeung SC, To KK. Platinum-based anticancer agents: innovative design strategies and biological perspectives. *Medicinal Research Reviews*, 23(5): 633-655, 2003.

[22] Köpf-Maier P. Complexes of metals other than platinum as antitumour agents. *European Journal of Clinical Pharmacology***,** 47(1): 1-16, 1994.

[23] Ott I, Gust R. Non platinum metal complexes as anti-cancer drugs. *Archiv der Pharmazie*, 340(3): 117-126, 2007.

[24] Tancini G, Bonadonna G, Valagussa P, Marchini S, Veronesi U. Adjuvant CMF in breast cancer: comparative 5-year results of 12 versus 6 cycles. *Journal of Clinical Oncology*, 1(1): 2-10, 1983.

[25] Bonadonna G, Moliterni A, Zambetti M, Daidone MG, Pilotti S, Gianni L, Valagussa P. 30 years' follow up of randomised studies of adjuvant CMF in operable breast cancer: cohort study. *BMJ*, 330(7485): 217, 2005.

[26] Chan DA, Giaccia AJ. Harnessing synthetic lethal interactions in anticancer drug discovery. *Nature Reviews Drug Discovery*, 10(5): 351-64, 2011.

[27] Mossman T. Rapid colorimetric assay for cellular growth and survival: application to proliferation and cytotoxicity assays. *Journal of Immunological Methods*, 65(1-2): 55-63, 1983.

[28] Brunton L, Parker K, Blumenthal D, Buxton I. Goodman and Gilman's Manual of Pharmacology and Therapeutics. *McGraw-Hill*, 2008.

[29] Neuse EW. Synthetic Polymers as Drug-Delivery Vehicles in Medicine. *Metal Based Drugs*, 469531, 2008.

[30] Pizarro AM, Sadler PJ. Unusual DNA binding modes for metal anticancer complexes. *Biochimie*, 91(10): 1198-1211, 2009.

[31] Cepeda V, Fuertes MA, Castilla J, Alonso C, Quevedo C, Pérez JM. Biochemical mechanisms of cisplatin cytotoxicity. *Anticancer Agents in Medicinal Chemistry*, 7(1):3-18, 2007.

[32] Damsma GE, Alt A, Brueckner F, Carell T, Cramer P. Mechanism of transcriptional stalling at cisplatin-damaged DNA. *Nature Structural & Molecular Biology*, 14(12): 1127-1133, 2007.

[33] Masters JR, Köberle B. Curing metastatic cancer: lessons from testicular germ-cell tumours. *Nature Reviews Cancer*, 3(7): 517-525, 2003.

[34] Boulikas T, Pantos A, Bellis E, Christofis P. Designing platinum compounds in cancer: structures and mechanisms. *Cancer Therapy*, 5: 537-583, 2007.

[35] Martínez R, Chacón-García L. The search of DNA-intercalators as antitumoral drugs: what it worked and what did not work. *Current Medicinal Chemistry*, 12(2): 127-151, 2005.

[36] Frederick CA, Williams LD, Ughetto G, van der Marel GA, van Boom JH, Rich A, Wang AH. Structural comparison of anticancer drug-DNA complexes: adriamycin and daunomycin. *Biochemistry*, 29(10): 2538-2549, 1990.

[37] Pigram WJ, Fuller W, Hamilton LD. Stereochemistry of intercalation: interaction of daunomycin with DNA. *Nature New Biology*, 235(53): 17-19, 1972.

[38] Zhang R, Wu X, Guziec LJ, Guziec FS, Chee GL, Yalowich JC, Hasinoff BB. Design, synthesis and biological evaluation of a novel series of anthrapyrazoles linked with netropsin-like oligopyrrole carboxamides as anticancer agents. *Bioorganic and Medicinal Chemistry*, 18(11): 3974-3984, 2010.

[39] Cullinane C, Phillips DR. Induction of stable transcriptional blockage sites by Adriamycin: GpC specificity of apparent Adriamycin-DNA adducts and dependence on iron(III) ions. *Biochemistry*, 29: 5638–5646, 1990.

[40] Cullinane C, van Rosmalen A, Phillips DR. Does Adriamycin induce interstrand cross-links in DNA? *Biochemistry*, 33: 4632–4638, 1994.

[41] Skladanowski A, Konopa J. Interstrand DNA crosslinking induced by anthracyclines in tumour cells. *Biochemical Pharmacology*, 47: 2269–2278, 1994.

[42] Swift LP, Rephaeli A, Nudelman A, Phillips DR, Cutts SM. Doxorubicin-DNA adducts induce a non-topoisomerase II-mediated form of cell death. *Cancer Research*, 66(9): 4863-4871, 2006.

[43] Hollander DH, Litton LE, Liang YW. Ethidium bromide counterstain for differentiation of quinacrine stained interphase bodies and brilliant metaphase bands. *Experimental Cell Research*, 99(1): 174-175, 1976.

[44] Crissman HA, Oka MS, Steinkamp JA. Rapid staining methods for analysis of deoxyribonucleic acid and protein in mammalian cells. *Journal of Histochemistry and Cytochemistry*, 24(1): 64-71, 1976.

[45] The-Crankshaft Publishing's Staff. What-when-how. In Depth Tutorials and Information: Ethidium Bromide (Molecular Biology). *The-Crankshaft Publishing's*, 2012.

[46] Lerman LS. Structural considerations in the interaction of DNA and acridines. *Journal of Molecular Biology*. 3: 18-30, 1961.

[47] Lerman LS. The Structure of the DNA-Acridine Complex. *Proceedings of the National Academy of Sciences*, 49(1): 94–102, 1963.

[48] Long E, Barton JK. On demonstrating DNA intercalation. *Journal: Accounts of Chemical Research*, 23(9): 271-273, 1990.

[49] Waring MJ. Complex formation between ethidium bromide and nucleic acids. *Journal of Molecular Biology*, 13(1): 269-282, 1965.

[50] Goodman LS, Wintrobe MM, Dameshek W, Goodman M, Gilman A, McLennan M. NITROGEN MUSTARD THERAPY – Use of Methyl-Bis(Beta-Chloroethyl)amine Hydrochloride and Tris(Beta-Chloroethyl)amine Hydrochloride for Hodgkin's Disease, Lymphosarcoma, Leukemia and Certain Allied and Miscellaneous Disorders. *Journal of the American Medical Association*, 132(3): 126-132, 1946.

[51] Raguz S, Yagüe E. Resistance to chemotherapy: new treatments and novel insights into an old problem. *British Journal of Cancer*, 99(3): 387–391, 2008.

[52] Stewart DJ. Mechanisms of resistance to cisplatin and carboplatin. *Critical Reviews in Oncology and Hematology*, 63(1): 12-31, 2007.

[53] Stewart DJ, Raaphorst GP, Yau J, Beaubien AR. Active vs. passive resistance, dose-response relationships, high dose chemotherapy, and resistance modulation: a hypothesis. *Investigational New Drugs*, 14(2): 115-30, 1996.

[54] Liu FS. Mechanisms of chemotherapeutic drug resistance in cancer therapy – a quick review. *Taiwan Journal of Obstetetrics & Gynecology*, 48(3): 239-44, 2009.

[55] Nobili S, Landini I, Giglioni B, Mini E. Pharmacological strategies for overcoming multidrug resistance. *Current Drug Targets*, 7(7): 861-79, 2006.

[56] Gillet JP, Gottesman MM. Mechanisms of multidrug resistance in cancer. *Methods Molecular Biology*, 596: 47-76, 2010.

[57] Harris AL, Hochhauser D. Mechanisms of multidrug resistance in cancer treatment. *Acta Oncologica*, 31(2): 205-213, 1992.

[58] Fojo T, Bates S. Strategies for reversing drug resistance. *Oncogene*, 22(47): 7512-7523, 2003.

[59] Riddick DS, Lee C, Ramji S, Chinje EC, Cowen RL, Williams KJ, Patterson AV, Stratford IJ, Morrow CS, Townsend AJ, Jounaidi Y, Chen CS, Su T, Lu H, Schwartz PS, Waxman DJ. Cancer chemotherapy and drug metabolism. *Drug Metabolism and Disposition*, 33(8): 1083-1096, 2005.

[60] Heffeter P, Jungwirth U, Jakupec M, Hartinger C, Galanski M, Elbling L, Micksche M, Keppler B, Berger W. Resistance against novel anticancer metal compounds: differences and similarities. *Drug Resistance Update*, 11(1-2): 1-16, 2008.

[61] Baguley BC. Multidrug resistance in cancer. *Methods in Molecular Biology*, 596: 1-14, 2010.

[62] Garattini S. Pharmacokinetics in cancer chemotherapy. *European Journal of Cancer*, 43(2): 271-282, 2007.

[63] Mansilla S, Bataller M, Portugal J. Mitotic catastrophe as a consequence of chemotherapy. *Anticancer Agents in Medicinal Chemistry*. 6(6): 589-602, 2006.

[64] Dimri G. What has senescence got to do with cancer? *Cancer Cell*, 7(6): 505-512, 2005.

[65] Huang Y, Anderle P, Bussey KJ, Barbacioru C, Shankavaram U, Dai Z, Reinhold WC, Papp A, Weinstein JN, Sadée W. Membrane transporters and channels: role of the transportome in cancer chemosensitivity and chemoresistance. *Cancer Research*, 64(12): 4294-4301, 2004.

[66] Orvig C, Abrams MJ. Medicinal inorganic chemistry: introduction. *Chemical Reviews*, 99(9): 2201-2204, 1999.

[67] Rafique S, Idrees M, Nasim A, Akbar H, Athar A. Transition metal complexes as potential therapeutic agents. *Biotechnology and Molecular Biology Reviews*, 5(2): 38-45, 2010.

[68] Wang Y, Chiu J. Proteomic Approaches in Understanding Action Mechanisms of Metal-Based Anticancer Drugs. *Metal Based Drugs*, 2008: 716329, 2008.

[69] Bandarra D, Lopes M, Lopes T, Almeida J, Saraiva MS, Vasconcellos-Dias M, Nunes CD, Félix V, Brandão P, Vaz PD, Meireles M, Calhorda MJ. Mo(II) complexes: a new family of cytotoxic agents? *Journal of Inorganic Biochemistry*. 104(11): 1171-1177, 2010.

[70] Periodic Table. Wikipedia website – http://en.wikipedia.org/wiki/Periodic_table

[71] Kostova I. Ruthenium complexes as anticancer agents. *Current Medicinal Chemistry*, 13(9): 1085-1107, 2006.

[72] Louie AY, Meade TJ. Metal complexes as enzyme inhibitors. *Chemical Reviews*, 99(9): 2711-2734, 1999.

[73] Barnard PJ, Berners-Price SJ. Targeting the mitochondrial cell death pathway with gold compounds. *Coordination Chemistry Reviews*, 251(13–14): 1889-1902, 2007.

[74] Robertson JD, Orrenius S. Role of mitochondria in toxic cell death. *Toxicology*. 181-182: 491-496, 2002.

[75] Köpf-Maier P, Köpf H, Neuse EW. Ferricenium complexes: a new type of water-soluble antitumor agent. *Journal of Cancer Research and Clinical Oncology*,108(3): 336-340, 1984.

[76] Osella D, Zanello P, Laschi F, Fontani M, Nervi C, Cavigiolio G. On the mechanism of the antitumor activity of ferrocenium derivates. *Inorganic Chimica Acta*, 306: 42-48, 2000.

[77] Köpf H, Köpf-Maier P. Titanocene dichloride – the first metallocene with cancerostatic activity. *Angewandte Chemie International Edition England*, 18(6): 477-478, 1979.

[78] Matos MR, Romão CC, Pereira CL, Rodrigues SS, Mora M, Silva MP, Alves PM, Reis CA. Patent nº WO/087783, 2005.

[79] Chen ZF, Mao L, Liu LM, Liu YC, Peng Y, Hong X, Wang HH, Liu HG, Liang H. Potential new inorganic antitumour agents from combining the anticancer traditional Chinese medicine (TCM) matrine with Ga(III), Au(III), Sn(IV) ions, and DNA binding studies. *Journal of Inorganic Biochemistry*, 105(2): 171-180, 2010.

[80] Chen D, Milacic V, Frezza M, Dou QP. Metal complexes, their cellular targets and potential for cancer therapy. *Current Pharmacological Design*, 15(7): 777-791, 2009.

[81] Gianferrara T, Bratsos I, Alessio E. A categorization of metal anticancer compounds based on their mode of action. *Dalton Transactions*, (37): 7588-7598, 2009.

[82] Ronconi L, Sadler PJ. Using coordination chemistry to design new medicines. *Coordination Chemistry Reviews*, 251(13–14): 1633-1648, 2007.

[83] Hambley TW. Developing new metal-based therapeutics: challenges and opportunities. *Dalton Transactions*, (43): 4929-4937, 2007.

[84] Bruijnincx PC, Sadler PJ. New trends for metal complexes with anticancer activity.

Current Opinion in Chemical Biology, 12(2): 197-206, 2008.

[85] Nguyen A, Vessieres A, Hillard EA, Top S, Pigeon P, Jaouen G. Ferrocifens and ferrocifenols as new potential weapons against breast cancer. *Chimia*, 61: 716–724, 2007.

[86] Sepúlveda C. Estudo da Citotoxicidade e Mecanismo de Acção de Complexos Binucleares de Ferro e Ouro em Linhas Tumorais. Tese de Mestrado, Faculdade de Ciências da Universidade de Lisboa, 2009.

[87] Dougan SJ, Habtemariam A, McHale SE, Parsons S, Sadler PJ. Catalytic organometallic anticancer complexes. *Proceedings of the National Academy of Sciences*, 105(33): 11628–11633, 2008.

[88] Coughlan MP. The role of molybdenum in human biology. *Journal of Inherited Metabolic Disease*, 1: 70-7, 1983.

[89] Kisker C, Schindelin H, Rees DC. Molybdenum-cofactor-containing enzymes: structure and mechanism. *Annual Review of Biochemistry*, 66: 233-67, 1997.

[90] Williams RJ, Fraústo da Silva JJ. The involvement of molybdenum in life. *Biochemical and Biophysical Research Community*, 292(2): 293-299, 2002.

[91] Turnlund JR. Molybdenum metabolism and requirements in humans. *Metal ions in biological systems*, 39:727-39, 2002.

[92] Mendel RR, Bittner F. Cell biology of molybdenum. *Biochimica et Biophysica Acta*, 1763(7): 621-635, 2006.

[93] Jelikić-Stankov M, Uskoković-Marković S, Holclajtner-Antunović I, Todorović M, Djurdjević P. Compounds of Mo, V and W in biochemistry and their biomedical activity. *Journal of Trace Elements in Medicine and Biology*, 21(1): 8-16, 2007.

[94] Saraiva MS, Quintal S, Portugal FCM, Lopes TA, Felix V, Nogueira JMF, Meireles M, Drew MGB, Calhorda MJ. Nitrogen donor ligands bearing N-H groups: Effect on catalytic and cytotoxic activity of molybdenum η^3-allyldicarbonyl complexes. *Journal of organometallic chemistry*, 693: 3411-3418, 2008.

[95] El-Ayaan U, Abdel-Aziz AA, Al-Shihry S. Solvatochromism, DNA binding, antitumor activity and molecular modeling study of mixed-ligand copper(II) complexes containing the bulky

ligand: bis[N-(p-tolyl)imino]acenaphthene. *European Journal of Medicinal Chemistry*, 42(11-12): 1325-1333, 2007.

[96] Hayter RG. A new route to π-allyl complexes of molybdenum and tungsten. *Journal of Inorganometallic Chemistry*, 13: 1-3, 1968.

[97] Alonso JC, Neves P, Silva MJP, Quintal S, Vaz PD, Silva C, Valente A, Ferreira P, Calhorda MJ, Félix V, Drew MGB. Molybdenum η^3-Allyl Dicarbonyl Complexes as a New Class of Precursors for Highly Reactive Epoxidation Catalysts with tert-Butyl Hydroperoxide. *Organometallics*, 26: 5548-5556, 2007.

[98] Bard AJ, Faulkner LR. Electrochemical Methods – Fundamentals and Applications. *John Willey & Sons*, 2001.

[99] Palchaudhuri R, Hergenrother PJ. DNA as a target for anticancer compounds: methods to determine the mode of binding and the mechanism of action. *Current Opinion in Biotechnology*, 18(6): 497-503, 2007.

[100] Wolfe A, Shimer GH Jr, Meehan T. Polycyclic aromatic hydrocarbons physically intercalate into duplex regions of denatured DNA. *Biochemistry*, 26(20): 6392-6396, 1987.

[101] Lopes TA. Estudo da Actividade Antitumoral de Complexos Organometálicos de Molibdénio. Tese de Mestrado, Faculdade de Ciências da Universidade de Lisboa, 2008.

[102] Bandarra D. Cytotoxic Activity and Mechanism of Action of Organometallic Complexes. Tese de Mestrado, Faculdade de Ciências da Universidade de Lisboa, 2010.

[103] Lopes M. Estudo da Actividade Antitumoral de Complexos de Molibdénio(II). Tese de Mestrado, Faculdade de Ciências da Universidade de Lisboa, 2010.

[104] Ma DL, Che CM. A bifunctional platinum(II) complex capable of intercalation and hydrogen-bonding interactions with DNA: binding studies and cytotoxicity. *Chemistry*, 9(24): 6133-6144, 2003.

[105] Draganov A. Novel Rhein Analogues as Potential Anticancer Agents and a Novel Metal Free Synthesis of 6HISOINDOLO[2,1-A]INDOL-6-ONE. Chemistry Theses, Georgia State University, 2011.

[106] Harrison RJ, Reszka AP, Haider SM, Romagnoli B, Morrell J, Read MA, Gowan SM, Incles CM, Kelland LR, Neidle S. Evaluation of by disubstituted acridone derivatives as telomerase inhibitors: the importance of G-quadruplex binding. *Bioorganic & Medicinal Chemistry Letters*, 14(23): 5845-5849, 2004.

7) ANNEX

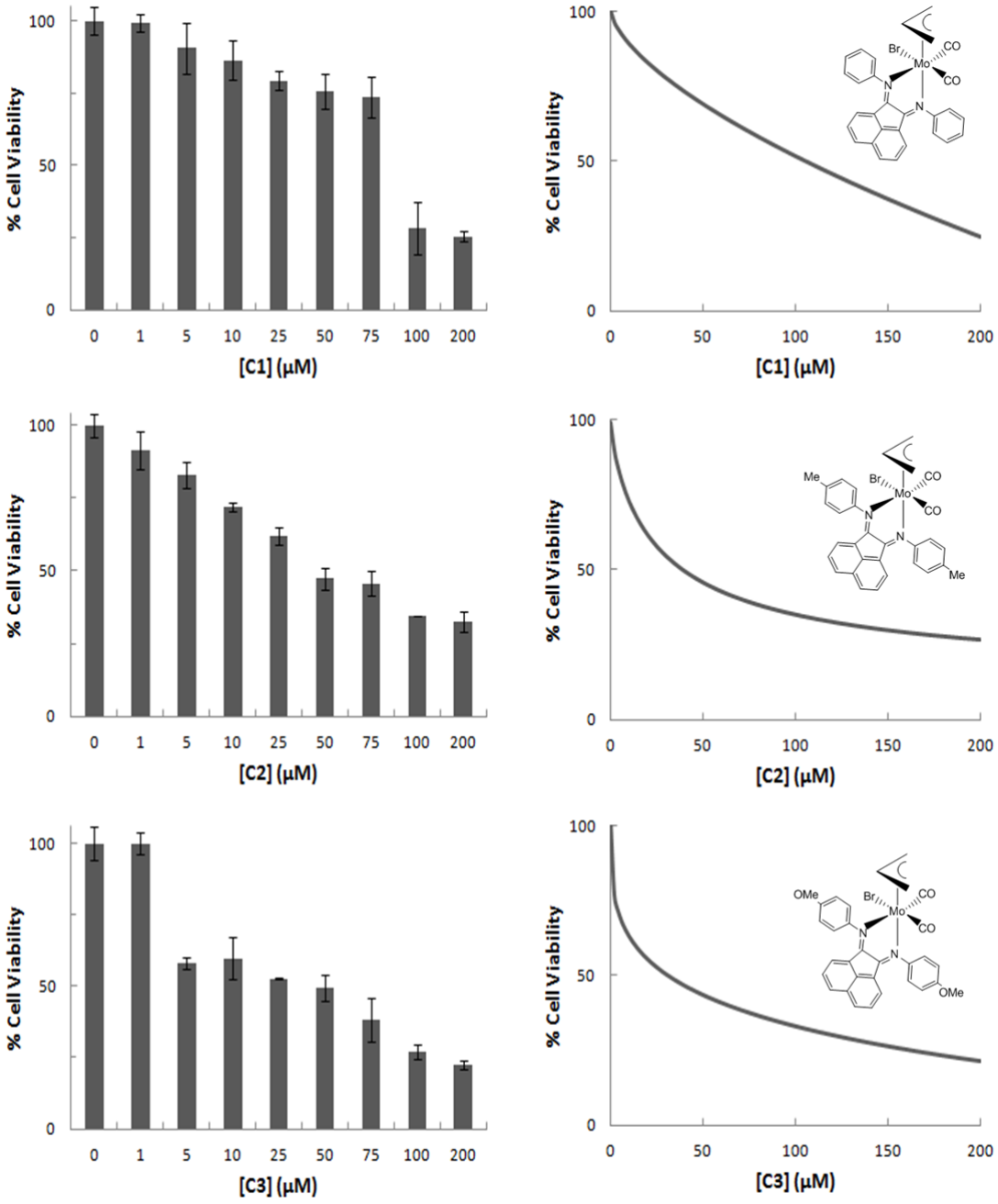

Figure 37 – *In vitro* cytotoxic assays for the complexes **C1 – C3** in MCF-7 after 48 h incubation. Histograms representing the relation between cell viability and the complex concentrations (1, 5, 10, 25, 50, 75, 100 and 200 µM) and dose-response curves obtained by nonlinear regression analysis for each complex.

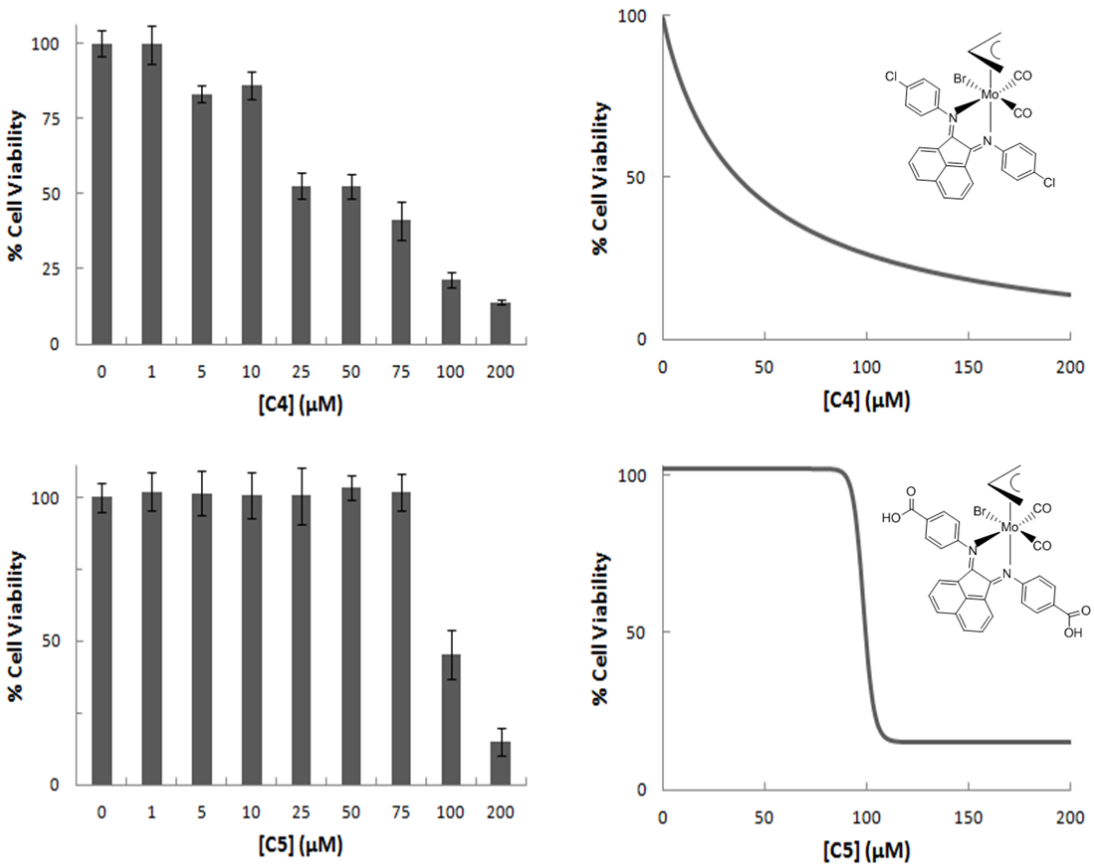

Figure 38 – *In vitro* cytotoxic assays for the complexes **C4** and **C5** in MCF-7 after 48 h incubation. Histograms representing the relation between cell viability and the complex concentrations (1, 5, 10, 25, 50, 75, 100 and 200 µM) and dose-response curves obtained by nonlinear regression analysis for each complex.

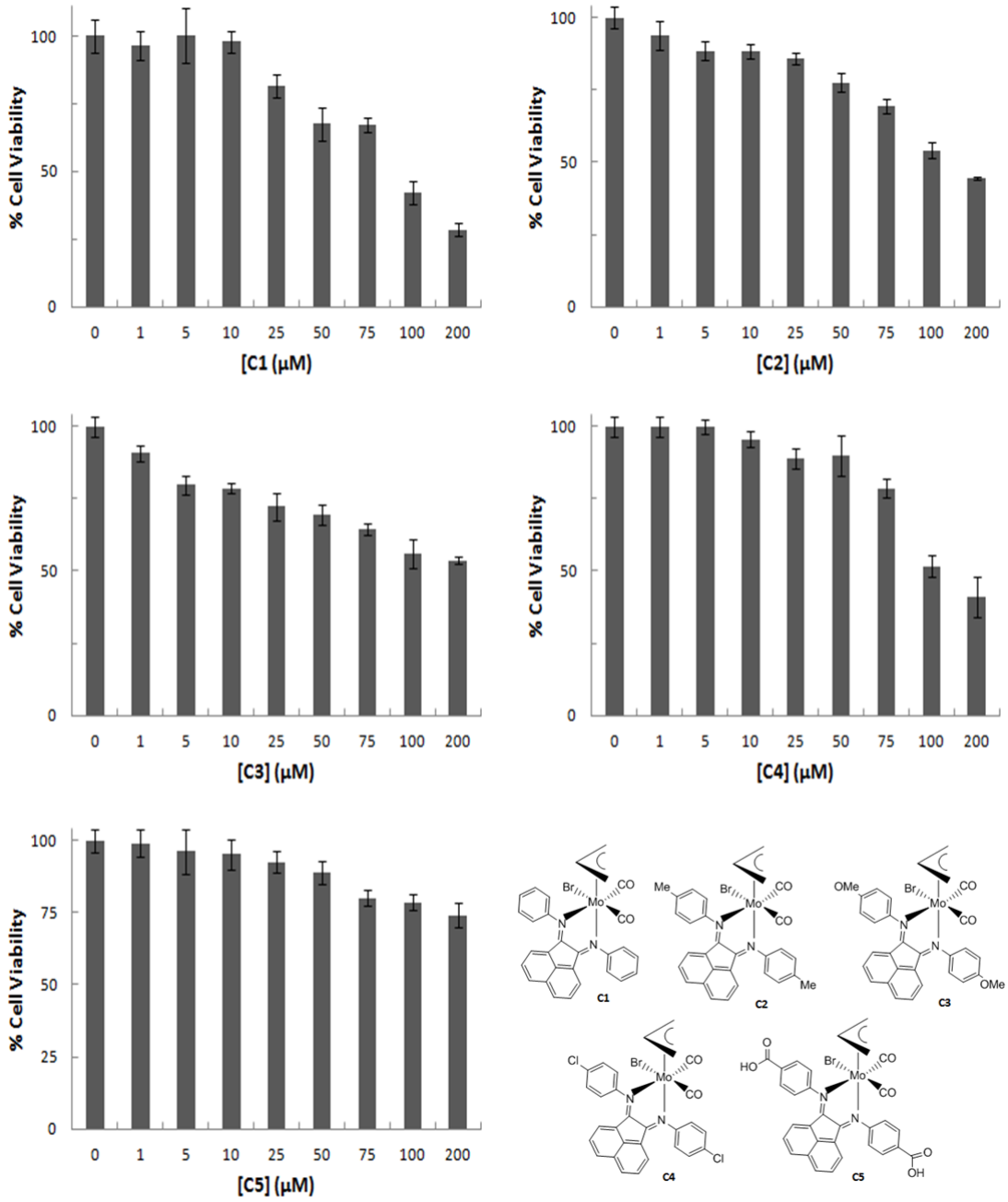

Figure 39 – *In vitro* cytotoxic assays for the complexes **C1 – C5** in MDA-MB-231 after 48 h incubation. Histograms representing the relation between cell viability and the complex concentrations (1, 5, 10, 25, 50, 75, 100 and 200 µM) for each complex.

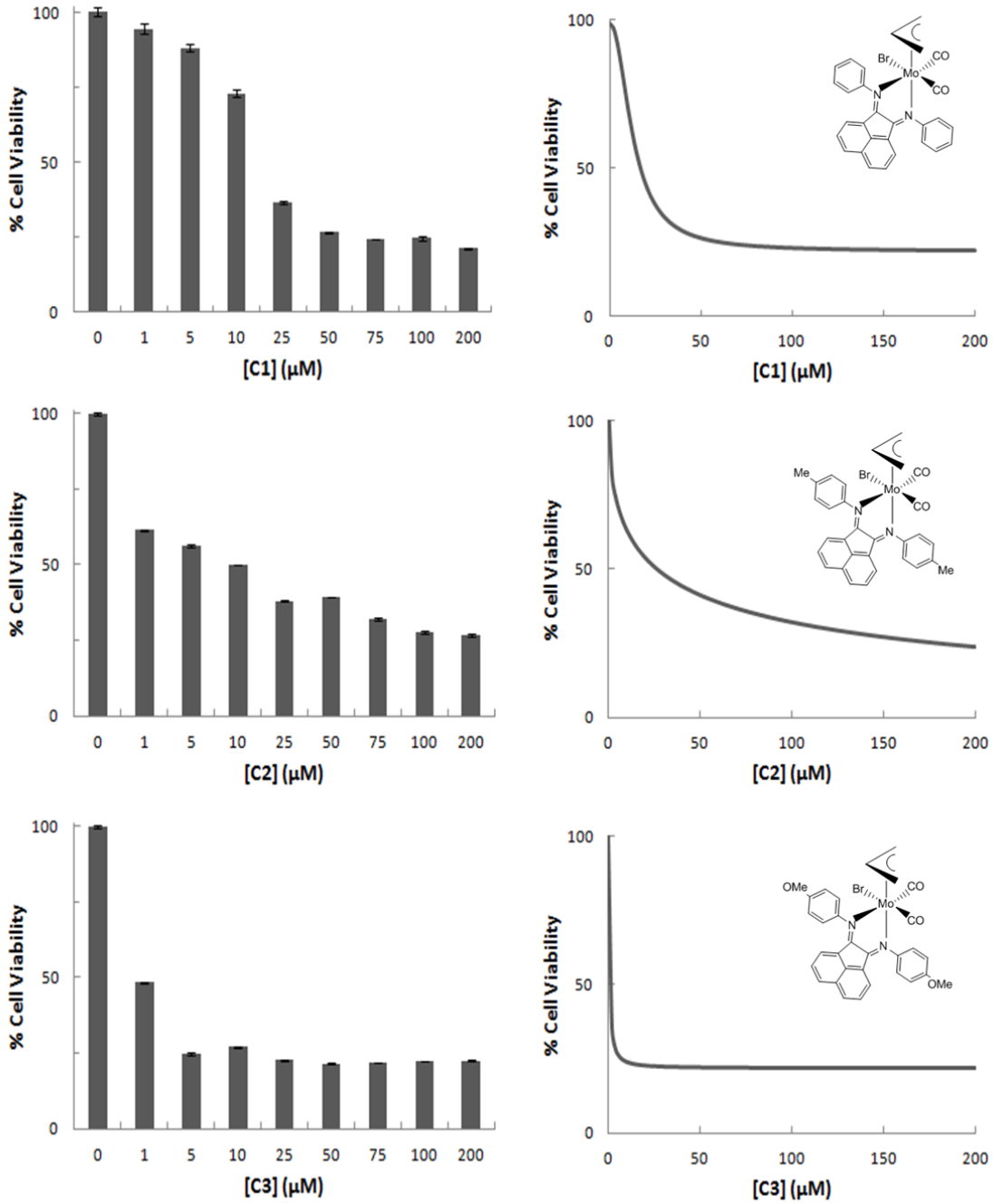

Figure 40 – *In vitro* cytotoxic assays for the complexes **C1 – C3** in SW480 cells after 48 h incubation. Histograms representing the relation between cell viability and the complex concentrations (1, 5, 10, 25, 50, 75, 100 and 200 µM) and dose-response curves obtained by nonlinear regression analysis for each complex.

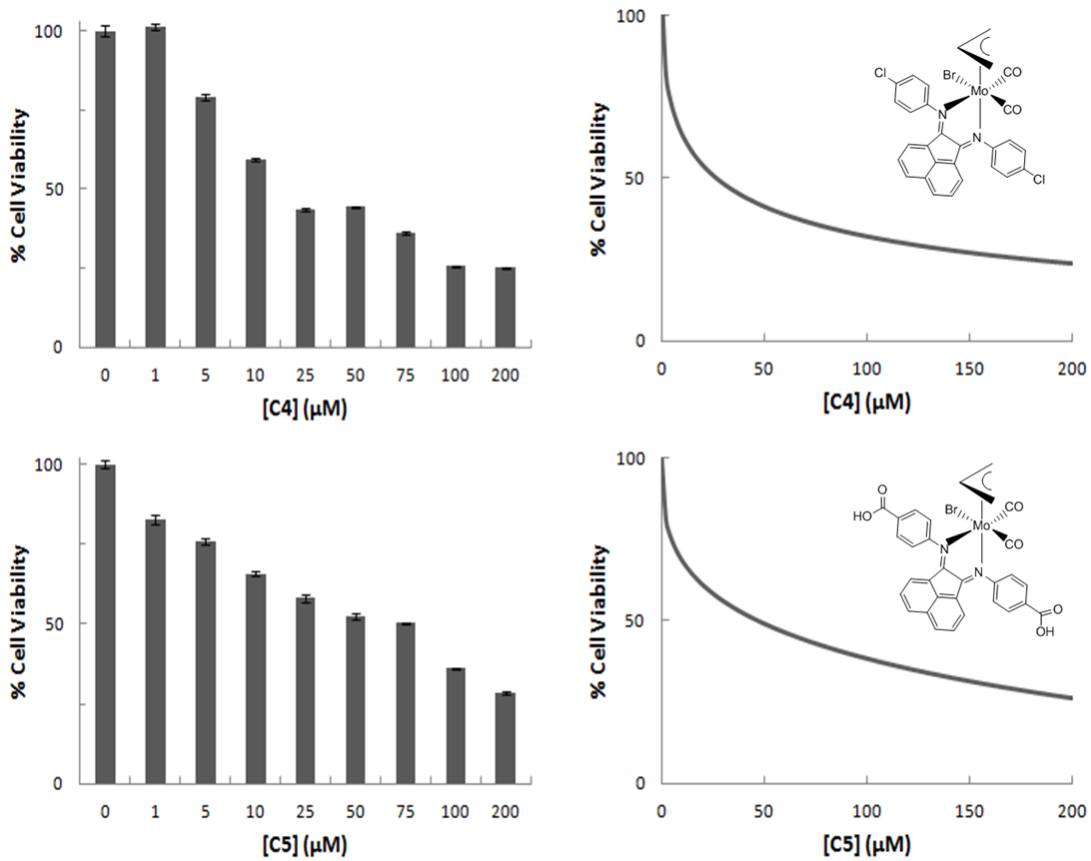

Figure 41 – *In vitro* cytotoxic assays for the complexes **C4** and **C5** in SW480 cells after 48 h incubation. Histograms representing the relation between cell viability and the complex concentrations (1, 5, 10, 25, 50, 75, 100 and 200 µM) and dose-response curves obtained by nonlinear regression analysis for each complex.

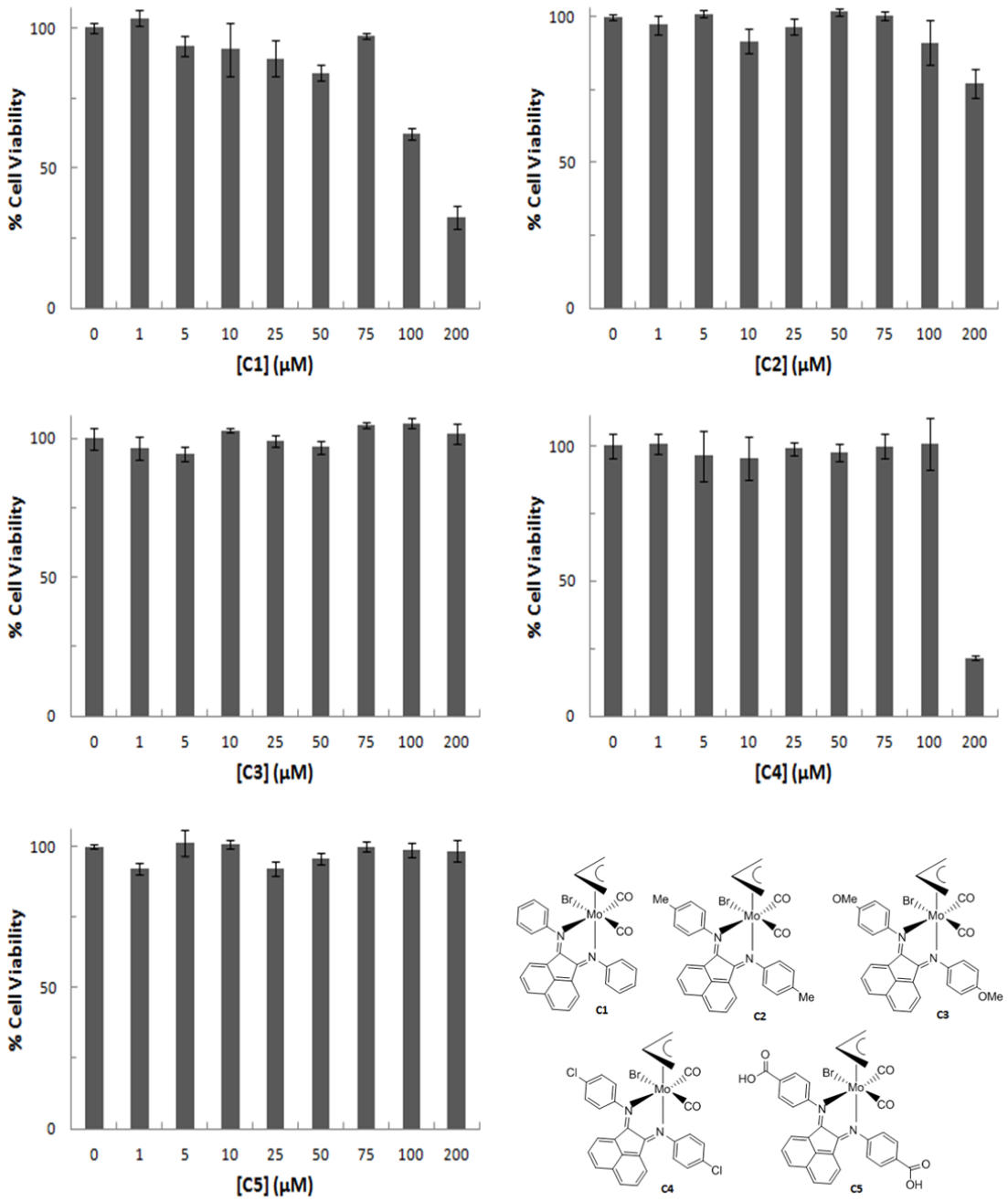

Figure 42 – *In vitro* cytotoxic assays for the complexes **C1 – C5** in Caco-2 cells after 48 h incubation. Histograms representing the relation between cell viability and the complex concentrations (1, 5, 10, 25, 50, 75, 100 and 200 µM) for each complex.